学位論文 (要約)

Role of ocean carbon cycle in glacial reduction of atmospheric carbon dioxide concentration

(氷期の大気中二酸化炭素濃度低下における海洋炭素循環の役割)

平成 29 年 12 月博士 (理学) 申請

東京大学大学院理学系研究科
地球惑星科学専攻

小林 英貴

Doctoral Dissertation

Role of ocean carbon cycle in glacial reduction of atmospheric carbon dioxide concentration

by

Hidetaka Kobayashi

Department of Earth and Planetary Science

Graduate School of Science

The University of Tokyo

December, 2017

Abstract

From climate reconstructions using ice core records, it is shown that atmospheric carbon dioxide concentration ($p\mathrm{CO_2}$) at the Last Glacial Maximum (LGM) is about $100\,\mathrm{ppm}$ lower than that at the pre-industrial period. Since carbon isotope data from ocean sediment records indicates that carbon storage in the terrestrial biosphere was reduced at the LGM, this atmospheric $p\mathrm{CO_2}$ reduction must have arose from changes in the ocean carbon cycle. Paleo-ocean reconstructions recently show that high-salinity and old water mass occupied the deep Southern Ocean at the LGM. These reconstructions suggest a hypothesis that carbon storage in the deep Southern Ocean increased at the LGM as a result of enhanced salinity stratification and caused a decline in atmospheric $p\mathrm{CO_2}$ ("Southern Ocean hypothesis"). However, previous studies using an ocean general circulation model (OGCM) underestimate the $p\mathrm{CO_2}$ change between the LGM and pre-industrial. One of the causes of this underestimation in OGCM studies is that the enhanced stratification in the glacial Southern Ocean suggested by the Southern Ocean hypothesis may not be appropriately represented by OGCMs. In this study, I focus on the Southern Ocean hypothesis and attempt to explain the mechanism of ocean carbon cycle change which contributes to the $100\text{-}\mathrm{ppm}$ decline of atmospheric $p\mathrm{CO_2}$ at the LGM.

In Chapter 2, I first try to improve the insufficient reproducibility of the high-salinity and old water mass in the glacial deep Southern Ocean, and then investigate its influence on the ocean carbon cycle and atmospheric $p\mathrm{CO_2}$. For this purpose, a LGM simulation is conducted, in which salinity in the ocean deepest layer in the Southern Ocean is restored toward high salinity reported from paleo-ocean proxy data and small vertical diffusion coefficient is prescribed to reproduce the enhanced stratification in the Southern Ocean. In the simulated glacial Southern Ocean, salinity stratification is strengthened, and the residence time of deep water gets longer. As a consequence, the concentration of dissolved inorganic carbon (DIC) increases in the Southern Ocean and decreases in the surface ocean through ocean biological process, which lowers atmospheric $p\mathrm{CO_2}$. However, the

glacial decline in atmospheric $p\mathrm{CO_2}$ is only about $47\,\mathrm{ppm}$.

In Chapter 3, in addition to results of OGCM simulations reported in Chapter 2, the role of carbonate compensation process in the glacial reduction of atmospheric $p\mathrm{CO_2}$ is investigated with a newly created ocean sediment model. As a result of carbonate compensation, atmospheric $p\mathrm{CO_2}$ decreases due to an increase in whole ocean alkalinity as previous studies suggested. It is newly found that this carbonate compensation process works more effectively by the enhanced stratification in the Southern Ocean. Owing to this contribution, the glacial reduction of atmospheric $p\mathrm{CO_2}$ reaches about $73\,\mathrm{ppm}$, which is much larger response than that obtained in previous OGCM studies.

In Chapter 4, I attempt to reproduce the physical ocean fields at the LGM by introducing parameterizations of brine rejection during sea ice production and stratification-dependent vertical diffusion coefficient. By using the brine parameterization, I confirm that the high bottom-water salinity in the glacial Southern Ocean obtained in Chapter 2 and 3 is similarly reproduced. Furthermore, when the parameterization of stratification-dependent vertical diffusion coefficient is introduced to the LGM simulation, it results in a more pronounced increase in the vertical gradient of DIC compared with the case of Chapter 2 and 3 in which the vertical diffusion coefficient is reduced only in the Southern Ocean. As a consequence, the difference in atmospheric $p\mathrm{CO_2}$ between the LGM and pre-industrial simulation becomes larger than $90\,\mathrm{ppm}$; therefore, in this study, most of the glacial atmospheric $p\mathrm{CO_2}$ reduction reported from ice core records can be successfully explained under the constraints of paleo-ocean reconstructions.

This study quantitatively demonstrates that changes in the ocean carbon cycle due to the enhanced salinity stratification in the glacial Southern Ocean and carbonate compensation process are essential for explaining the glacial reduction of atmospheric $p\mathrm{CO_2}$ by about $100\,\mathrm{ppm}$.

Acknowledgment

I would like to show my greatest appreciation to Prof. Akira Oka whose critical but hearty advice and continuous encouragements helped this study. Without his guidance and persistent help, this study would not have been possible. I would also like to express my gratitude to Prof. Ichiro Yasuda, Prof. Masahide Kimoto, Prof. Yukio Masumoto, and Prof. Hiroyasu Hasumi for their striking comments and warm encouragements. Discussions and comments given by Prof. Ayako Abe-Ouchi also contribute a lot to this study. I also appreciate to Drs. Takao Kawasaki, Takashi Sakamoto, Noriaki Kimura, Yasuhiro Hoshiba, Ryu Saiki, Shota Katsura, Ms. Yuki Nakamura, Mr. Kazuki Togawa, and all of the members in Division of Climate System Research for their useful comments. Especially, my colleague Sam Sherriff-Tadano and Takashi Obase always encouraged and entertained me. I am particularly grateful for the support and assistance given by Ms. Hiroko Kitajima. Finally, I would like to thank my family Hideaki, Keiko and Ami for their support and warm encouragements.

Contents

Chapter 1

General introduction

1.1 Ocean carbon cycle

Carbon dioxide (CO_2) is one of the major greenhouse gases of the earth. The concentration of atmospheric carbon dioxide (pCO_2) is an important factor for climate state and is highly related to the past and future climate change. Therefore, it is important to investigate factors of changes in atmospheric pCO_2 for understanding mechanisms of climate change. Atmospheric pCO_2 is determined as a result of carbon exchange between carbon reservoirs (atmosphere, ocean, terrestrial, and sediments). Estimated inventory of each carbon reservoir at the pre-industrial is about $600\,\mathrm{PgC}$ in the atmosphere, $2,100\,\mathrm{PgC}$ in the terrestrial, and $39,000\,\mathrm{PgC}$ in the ocean (including the surface and deep ocean) (*Sigman and Boyle*, 2000). Since the stored carbon in the ocean is more than 60 times than that in the atmosphere, changes in the ocean carbon cycle largely affect atmospheric pCO_2.

1.1.1 Ocean surface process

Unlike other gases, CO_2 dissolved in water dissociates to produce a weak acid. After the air-sea exchange of CO_2, dissolved free carbon dioxide ($CO_2(\mathrm{aq})$) reacts with water and forms carbonic acid (H_2CO_3), which further changes to bicarbonate ion (HCO_3^-) or carbonate ion (CO_3^{2-}) as below.

$$CO_2(\mathrm{gas}) + H_2O \rightleftharpoons H_2CO_3^* \rightleftharpoons H^+ + HCO_3^- \rightleftharpoons H^{2+} + CO_3^{2-}, \tag{1.1}$$

where $CO_2(\mathrm{gas})$ is gaseous CO_2. Because it is difficult to analytically distinguish between the two species of $CO_2(\mathrm{aq})$ and H_2CO_3, the sum of these two concentrations is usually expressed as the concentration of a hypothetical species of $H_2CO_3^*$ (*Sarmiento and Gruber*, 2006). Here I introduce two important parameters in this carbon system: dissolved inorganic carbon (DIC) and alkalinity. Dissolved inorganic carbon is the sum

of dissolved CO_2, carbonic acid, bicarbonate ion, and carbonate ion:

$$\mathrm{DIC} = [\mathrm{H_2CO_3^*}] + [\mathrm{HCO_3^-}] + [\mathrm{CO_3^{2-}}]. \tag{1.2}$$

Brackets indicate the concentration of each dissolved material. Alkalinity indicates acid buffer capacity. It is written as bellow (*Sarmiento and Gruber*, 2006):

$$\begin{aligned}\mathrm{Alkalinity} = {} & [\mathrm{Na^+}] + [\mathrm{K^+}] + 2\,[\mathrm{Mg^{2+}}] + 2\,[\mathrm{Ca^{2+}}] + \mathrm{minor\,cations} \\ & -[\mathrm{Cl^-}] - 2\,[\mathrm{SO_4^{2-}}] - [\mathrm{Br^-}] - [\mathrm{NO_3^-}] - \mathrm{minor\,anions}.\end{aligned} \tag{1.3}$$

The partial pressure of CO_2 and pH in water can be calculated from using DIC and alkalinity. The oceanic $p\mathrm{CO_2}$ is approximated from DIC and alkalinity as in the following relationship:

$$p\mathrm{CO_2} = \frac{[\mathrm{H_2CO_3^*}]}{K_0} \approx \frac{K_2}{K_0 \cdot K_1} \frac{(2 \cdot \mathrm{DIC} - \mathrm{Alkalinity})^2}{\mathrm{Alkalinity} - \mathrm{DIC}}, \tag{1.4}$$

where K_0 is the CO_2 solubility, and K_1 and K_2 are dissociation constants of carbonate acid (*Sarmiento and Gruber*, 2006).

The exchange of CO_2 between the atmosphere and ocean depends on the difference in the partial pressure of CO_2 at the sea surface as

$$\Phi = k\,S \cdot (p\mathrm{CO_2}^{os} - p\mathrm{CO_2}^{atm}), \tag{1.5}$$

where Φ is sea-air CO_2 flux, k is piston velocity, S is the solubility of CO_2, $p\mathrm{CO_2}^{os}$ is $p\mathrm{CO_2}$ at the ocean surface, and $p\mathrm{CO_2}^{atm}$ is atmospheric $p\mathrm{CO_2}$ (*Takahashi et al.*, 2009). The piston velocity k depends on wind speed above the sea surface. Partial pressure of CO_2 in the ocean depends on temperature, salinity, DIC and alkalinity. The solubility of CO_2 is inversely related to ocean temperature and salinity. As seawater gets colder and

fresher, the gas solubility of CO_2 increases. Cold and fresh water can store more carbon than warm and saline water. Oceanic pCO_2 also depends on DIC and alkalinity: it is increased as DIC increases, whereas it is decreased as ocean alkalinity increases. The oceanic pCO_2 becomes higher for larger DIC and lower alkalinity.

1.1.2 Biological pumps

The spatial distribution of DIC and alkalinity in the ocean interior is formed by ocean biological process and ocean circulation. In general, biological process sequester carbon from the surface to deep ocean. On the other hand, the stored inorganic carbon is eventually returned to the surface ocean again by deep ocean circulation (*Schmitz*, 1995; *Lumpkin and Speer*, 2007; *Talley*, 2013). The vertical transport of carbon from the surface to deep ocean by ocean biological process is referred to as "biological pumps" (*Volk and Hoffert*, 1985). In the biological pumps, carbon is transported downward in the form of both organic carbon and calcium carbonate ($CaCO_3$) particles. The process associated with the biological pumps will be described below.

Soft-tissue pump

Phytoplankton produces organic materials through its photosynthesis by using dissolved inorganic carbon and nutrients (e.g. nitrate, nitrite, phosphate, etc.) in the surface ocean. The empirical reaction of photosynthesis proposed in *Redfield et al.* (1963) is

$$\begin{aligned} &106\,CO_2 + 16\,HNO_3 + H_3PO_4 + 122\,H_2O \\ &\rightleftharpoons (CH_2O)_{106}(NH_3)_{16}(H_3PO_4) + 138\,O_2. \end{aligned} \tag{1.6}$$

The stoichiometric ratios of $106\,C : 16\,N : P : -138\,O$ are referred to as redfield ratios. The net production of organic carbon by phytoplankton is called primary production. Part of the organic carbon produced by photosynthesis is precipitated from the surface ocean

in the form of particulate organic carbon (POC). The organic carbon that sinks from the surface ocean is referred to as export production. Most of the sinking POC is subject to oxic degradation by bacterial respiration using dissolved oxygen in the deep ocean. As a result, DIC and nutrients are increased in the deep ocean. This vertical transport process of organic carbon is called soft-tissue pump. The soft-tissue pump acts to lower ${p\mathrm{CO_2}}^{os}$ by decreasing DIC in the surface ocean.

Nutrients in the surface ocean are nearly depleted by phytoplankton photosynthesis; therefore, nutrient supply is needed for sustaining photosynthesis. Important processes for nutrient supply to the euphotic zone, where phytoplankton receives enough sunlight for photosynthesis, are ocean upwelling and vertical mixing. Therefore, the distribution of primary production in the surface ocean is controlled by ocean circulation. It is known that there is an area called HNLC (high-nutrient and low-chlorophyll) regions, where photosynthesis is suppressed despite high nutrient concentrations. Typical HNLC regions include the North Pacific, the Equatorial Pacific, and the Southern Ocean. One of the reasons for the limited photosynthesis in the HNLC regions is thought to be the lack of iron supply (*Martin*, 1990).

Carbonate pump

There are some plankton species that produce shells of $\mathrm{CaCO_3}$ like coccolithophore and foraminifera. As with organic matter, the generated $\mathrm{CaCO_3}$ particles eventually sink and part of them is dissolved in the deep ocean. When the sinking $\mathrm{CaCO_3}$ particles are in a state of undersaturation, it is dissolved as

$$\mathrm{CaCO_3} \rightarrow \mathrm{Ca^{2+}} + \mathrm{CO_3^{2-}}. \tag{1.7}$$

The dissolution of $\mathrm{CaCO_3}$ particles hence increases DIC and alkalinity of in situ seawater. The globally averaged rain ratio, which is the ratio of $\mathrm{CaCO_3}$ particles to POC settling

from the surface ocean, is about $0.06\,(\pm\,0.03)$ (*Sarmiento et al.*, 2002). The vertical transport of carbon related to the $\mathrm{CaCO_3}$ production and dissolution is called carbonate pump (or alkalinity pump). The carbonate pump decreases alkalinity as well as DIC in the surface ocean. Therefore, it works in the direction to raise oceanic $p\mathrm{CO_2}$ in the surface ocean, contrary to the soft-tissue pump.

1.1.3 Carbonate compensation process

Sinking particles that are not decomposed or dissolved in water columns reach the ocean floor and accumulate as ocean sediments. In the upper part of ocean sediments, the decomposition or dissolution of such solid particles also occurs. These processes affect concentrations of dissolved materials in the pore water, which is seawater contained in ocean sediments. The interaction between the upper part of ocean sediments and ocean biogeochemical cycles alters the whole ocean inventory of dissolved materials. Therefore, the sedimentation process is important for ocean biogeochemical cycles.

"Carbonate compensation process" is one of such interaction process (*Broecker and Peng*, 1987). Carbonate compensation process acts to stabilize ocean alkalinity budget on a timescale of tens of thousands of years due to the interaction between carbonate sediments and the ocean carbon cycle (*Broecker and Takahashi*, 1977; *Archer et al.*, 1997). Observational-based estimates show that half of the $\mathrm{CaCO_3}$ particles produced in the surface ocean reach the ocean floor and one third of them are buried (*Sarmiento and Gruber*, 2006). In other words, the burial fraction of $\mathrm{CaCO_3}$ is $13\,\%$. It is much higher than the burial fraction of organic matter (the $95\,\%$ of exported organic carbon from the surface ocean is remineralized in water columns and about $0.3\,\%$ is buried). The long-term burial of $\mathrm{CaCO_3}$ in ocean sediments means the loss of alkalinity from the ocean. On the other hand, river inflow of alkalinity from continental weathering increases ocean alkalinity. Generally, whole ocean alkalinity changes depending on the $\mathrm{CaCO_3}$ balance between the river inflow and burial removal into ocean sediments. In a state of non-equilibrium be-

tween the riverine and burial flux, carbonate compensation acts as a negative feedback process to keep its equilibrium as described below. Calcium carbonate particles reaching the ocean floor dissolve in ocean sediments, or are buried without being dissolved. The burial flux of $\mathrm{CaCO_3}$ depends on the undersaturation of $\mathrm{CaCO_3}$ above the seabed. The saturation degree of $\mathrm{CaCO_3}$ (Ω) is defined as

$$\Omega = \frac{[\mathrm{CO_3^{2-}}][\mathrm{Ca^{2+}}]}{[\mathrm{CO_3^{2-}}]_{sat}[\mathrm{Ca^{2+}}]_{sat}}, \tag{1.8}$$

where $[\mathrm{CO_3^{2-}}]$ and $[\mathrm{Ca^{2+}}]$ are concentrations of carbonate and dissolved calcium ions, and the subscript sat indicates the saturation concentration. Seawater is supersaturated when $\Omega > 1$ and is undersaturated when $\Omega < 1$. In the process of the production and dissolution of $\mathrm{CaCO_3}$ particles, changes in $[\mathrm{Ca^{2+}}]$ can be regarded as very small relative to that in $[\mathrm{CO_3^{2-}}]$. Equation (1.8) is thus simply approximated as

$$\Omega \approx \frac{[\mathrm{CO_3^{2-}}]}{[\mathrm{CO_3^{2-}}]_{sat}}. \tag{1.9}$$

The saturation concentration of carbonate ion $[\mathrm{CO_3^{2-}}]_{sat}$ is mainly determined by ocean pressure (depth), and becomes larger as it gets deeper. Because $[\mathrm{CO_3^{2-}}]$ is approximately represented by the difference between alkalinity and DIC as

$$[\mathrm{CO_3^{2-}}] \approx \mathrm{Alkalinity} - \mathrm{DIC}, \tag{1.10}$$

carbonate ion concentration generally decreases with depth as DIC increases due to the decomposition of organic carbon. For this reason, $\mathrm{CaCO_3}$ particles are generally supersaturated in the shallow ocean but are undersaturated in the deep ocean. In addition, the $\mathrm{CaCO_3}$ particles are more soluble in the North Pacific than the North Atlantic because DIC is larger in the Pacific due to deep ocean circulation. Organic matter that reaches the ocean floor also promotes the dissolution of $\mathrm{CaCO_3}$ because the remineralization of POC

increases DIC and decreases $[CO_3^{2-}]$. As these factors change, the upper part of sediments responds so that the burial removal of $CaCO_3$ is balanced with the river inflow of $CaCO_3$. The residence time of ocean alkalinity is of the order of $10,000$ years because these alkalinity fluxes are really small (*Sundquist*, 1991; *Sarmiento and Gruber*, 2006). However, carbonate compensation process is important for long-term changes in the ocean carbon cycle.

1.2 Glacial ocean carbon cycle

Atmospheric pCO_2 in glacial periods is known to be reduced from interglacial periods by 80–$100\,\mathrm{ppm}$, associated with glacial-interglacial cycles from reconstructions using air trapped in ice cores (*Petit et al.*, 1999; *Siegenthaler et al.*, 2005; *Jouzel et al.*, 2007; *Lüthi et al.*, 2008). Changes in carbon reservoirs of the atmosphere, ocean, and terrestrial biosphere are important for changes in the carbon cycle on the glacial-interglacial time scale. The Last Glacial Maximum (LGM), which was about $20,000$ years before present, is referred to as a timing when continental ice sheets reached their maximum volume during the glacial period closest to the present (*Clark et al.*, 2009). Continental ice sheets at the LGM expanded in the North American continent and the Scandinavian peninsula in addition to the Antarctica and the Greenland (*Bird et al.*, 1994; *Crowley*, 1995; *Yokoyama et al.*, 2000). The globally averaged sea surface temperature (SST) was reduced by about 2–$3\,^{\circ}\mathrm{C}$ compared with the pre-industrial (*MARGO Project Members*, 2009; *Elderfield et al.*, 2012; *Bereiter et al.*, 2018). *Anan and Hargrievs* (2013) estimate the average cooling of surface temperature to be about $4\,^{\circ}\mathrm{C}$ by using proxy data of SST anomalies (*MARGO Project Members*, 2009) and surface air temperature anomalies (*Bartlein*, 2011; *Shakun et al.*, 2012). In a study attempting to clarify the mechanism of climate change on the glacial-interglacial scale, the climate state of the LGM is often discussed comparing with that in the pre-industrial. Since the LGM was a cold and dry climate compared with the

present, it is suggested that the shrinkage of terrestrial carbon storage is 330–$694\,\mathrm{PgC}$ (*Bird et al.*, 1994; *Ciais et al.*, 2012; *Peterson et al.*, 2014). Therefore, it is recognized that the excess $\mathrm{CO_2}$ was taken in the ocean. The shift of globally averaged stable carbon isotope ratios ($\delta^{13}\mathrm{C}$) in the ocean also supports the ocean uptake of terrestrial carbon (*Duplessy et al.*, 1988). This means that the about 100-ppm decline in atmospheric $p\mathrm{CO_2}$ at the LGM compared with the pre-industrial is considered to be caused by changes in the ocean carbon cycle (*Broecker*, 1982; *Sigman and Boyle*, 2000; *Kohfeld and Ridgwell*, 2009).

For the reasons mentioned above, the contribution of ocean processes to the low atmospheric $p\mathrm{CO_2}$ at the LGM has been quantitatively evaluated by many numerical modeling studies (*IPCC*, 2013). The top panel of Figure 1.1, which is cited from Figure 6.5 in *Ciais et al.* (2013), shows mechanisms contributing the atmospheric $p\mathrm{CO_2}$ change from the LGM to late Holocene. The yellow bar means the difference of atmospheric $p\mathrm{CO_2}$ between the two time intervals. Filled black circles indicate the contribution of each process to the glacial reduction of atmospheric $p\mathrm{CO_2}$ obtained from individual model-based estimates. The red and blue bars indicate the conceivable contributions determined from the model-based estimates. The contribution of the gas exchange of $\mathrm{CO_2}$ at the sea surface to the atmospheric $p\mathrm{CO_2}$ change is almost unequivocal. The cooling of SST contributes to the increase in the solubility of $\mathrm{CO_2}$ in the surface ocean and reduces atmospheric $p\mathrm{CO_2}$ by about $25\,\mathrm{ppm}$. Meanwhile, the drop of about $135\,\mathrm{m}$ in sea level due to the expansion of continental ice sheets (*Yokoyama et al.*, 2000, 2001) and the accompanying increase in sea surface salinity by about $1\,\mathrm{psu}$ decrease the solubility of $\mathrm{CO_2}$. From these considerations, changes in the gas exchange of $\mathrm{CO_2}$ can contribute to the decline of atmospheric $p\mathrm{CO_2}$ by about $10\,\mathrm{ppm}$ (*Sigman and Boyle*, 2000; *Kohfeld and Ridgwell*, 2009). The remaining glacial reduction of atmospheric $p\mathrm{CO_2}$ is explained by the decrease in $p\mathrm{CO_2}$ in the surface ocean due to changes in the surface ocean DIC and alkalinity. They originate from two factors: (i) redistribution of DIC and alkalinity in the ocean interior caused by changes

in ocean biological process and deep ocean circulation ("closed-system" response) and/or (ii) a change in the whole ocean inventory of DIC and alkalinity induced by carbonate compensation process ("open-system" response) (*Broecker and Peng*, 1987; *Archer et al.*, 2000; *Sigman and Boyle*, 2000; *Kohfeld and Ridgwell*, 2009). Since the variation in quantitative estimates obtained from each numerical study is large, the detailed mechanism of changes in DIC and alkalinity at the LGM have not been clarified.

In addition to modeling studies, the glacial carbon cycle is reconstructed by interpreting geological data. I will introduce changes in ocean biological processes and ocean circulation at the LGM suggested from such paleo-ocean reconstructions. The strength and structure of deep ocean circulation during glacial times are reconstructed from paleo-ocean proxy data such as $\delta^{13}\mathrm{C}$, nutrient-related cadmium-calcium ratios ($\mathrm{Cd/Ca}$), and protactinium-thorium ratios ($^{231}\mathrm{Pa}/^{230}\mathrm{Th}$). The glacial Atlantic meridional overturning circulation (AMOC) is recognized to be shallower and weaker than the preindustrial: a water mass associated with the North Atlantic Deep Water (NADW) flowed at shallower depth than the present, and a water mass associated with the Antarctic Bottom Water (AABW) became saltier and heavier than the NADW flow and occupied the entire deep ocean (*Duplessy et al.*, 1988; *Curry and Oppo*, 2005; *Marchitto and Broecker*, 2006; *Lynch-Stieglitz et al.*, 2007; *Negre et al.*, 2010). From reconstructions using $\delta^{13}\mathrm{C}$, in the glacial Atlantic Ocean, the low-$\delta^{13}\mathrm{C}$ AABW is estimated to expand northward, and the high-$\delta^{13}\mathrm{C}$ NADW is estimated to shift to a shallower depth (*Duplessy et al.*, 1988; *Curry and Oppo*, 2005). This is thought to be due to reduced ventilation and/or active biological productivity. Reconstructions using $\mathrm{Cd/Ca}$ also support the ocean circulation change (*Boyle and Keigwin*, 1987; *Marchitto and Broecker*, 2006). It is recognized that this ocean circulation change led to the sequestration of carbon into the deep ocean, which contributed to the reduction of atmospheric $p\mathrm{CO_2}$ at the LGM.

Changes in biological pumps at the LGM are recognized to contribute the glacial reduction of atmospheric $p\mathrm{CO_2}$. Conceivable processes are iron fertilization of plankton,

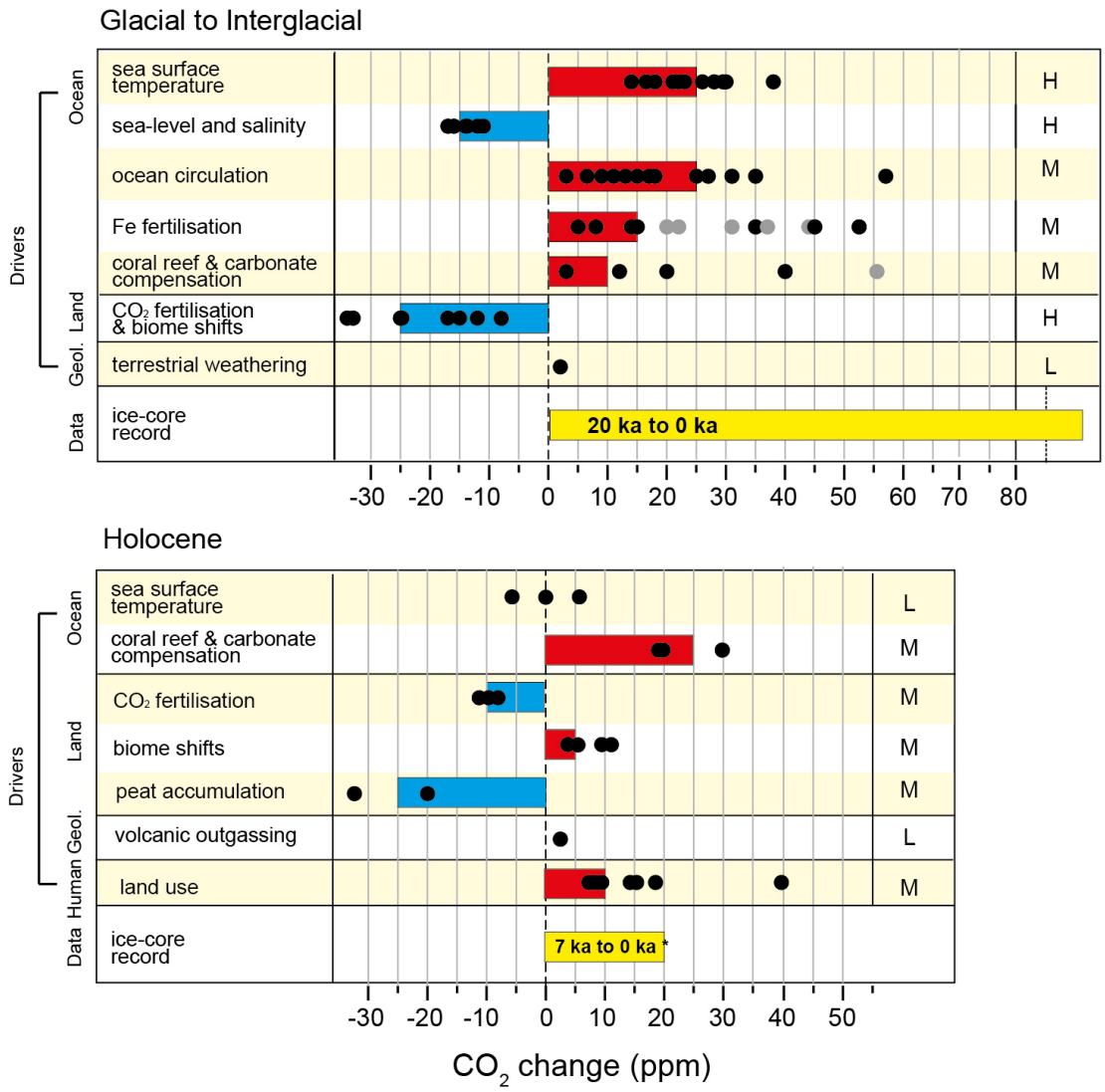

Figure 1.1: Mechanisms contributing to carbon dioxide concentrations changes from Last Glacial Maximum (LGM) to late Holocene (top) and from early/mid Holocene (7 ka) to late Holocene (bottom). Filled black circles represent individual model-based estimates for individual ocean, land, geological or human mechanisms. Solid colour bars represent expert judgment (to the nearest $5\,\mathrm{ppm}$) rather than a formal statistical average. References for the different model results used for explaining CO_2 changes from LGM to late Holocene are as per (*Kohfeld and Ridgwell*, 2009) with excluded model projections in grey. References for the different model results used for explaining CO_2 changes during the Holocene are: *Joos et al.* (2004), *Brovkin et al.* (2002, 2008), *Kleinen et al.* (2010, 2012), *Broecker et al.* (1999), *Ridgwell et al.* (2003), *Schurgers et al.* (2006), *Yu* (2011), *Ruddiman* (2003, 2007), *Strassmann et al.* (2008), *Olofsson and Hickler* (2008), *Pongratz et al.* (2009), *Kaplan et al.* (2011), *Lemmen* (2009), *Stocker et al.* (2011), *Roth and Joos* (2012). Confidence levels for each mechanism are indicated in the left column — H for *high confidence*, M for *medium confidence* and L for *low confidence*. This figure is cited from Figure 6.5 of *Ciais et al.* (2013).

increased inventory or utilization of ocean nutrients, and/or changes in dominant phytoplankton species (*Kohfeld et al.*, 2005). *Kohfeld et al.* (2005) analyze ocean sediment records and argue that the iron fertilization is the most responsible process for changes in biological pumps. The globally averaged iron supply from the atmosphere is estimated to be 3–4 times larger at the LGM than the late Holocene (*Kohfeld and Harrison*, 2001; *Maher et al.*, 2010; *Lambert et al.*, 2015). It was more than 10 times larger especially in polar regions (*Petit et al.*, 1999; *Lambert et al.*, 2008). *Martin* (1990) proposes a hypothesis that the increase in the dust-derived iron supply enlarges ocean productivity and subsequent downward carbon flux. The effect of the iron hypothesis on the glacial atmospheric $p\mathrm{CO_2}$ is evaluated by in situ experiments (*Watson et al.*, 2000) and modeling studies (*Bopp et al.*, 2003; *Gaspari et al.*, 2006). At the LGM, $\delta^{13}\mathrm{C}$ was smaller in the deep Southern Ocean, and its vertical gradient between the surface and deep ocean was larger than that at the pre-industrial (*Duplessy et al.*, 1988; *Hodell et al.*, 2003; *Curry and Oppo*, 2005). In addition, by their multi-proxy reconstructions, *Jaccard et al.* (2009) report that the deep water in the subarctic region was depleted in oxygen at the LGM. This means that the storage of respired biogenic organic carbon was increased in the glacial North Pacific Ocean. These studies suggest that efficient utilization of surface ocean nutrients and/or increased consumption of nutrients occurred at the LGM compared with the pre-industrial. Moreover, it is suggested that the surface ocean cooling at the LGM suppressed the decomposition of organic carbon in the euphotic zone, so that the fraction of organic carbon exported from the surface ocean might have increased (*Matsumoto et al.*, 2007; *Kwon et al.*, 2009).

The process accompanied by a change in the whole ocean inventory of ocean biogeochemical properties includes carbonate compensation process. It is recognized that carbonate compensation process amplifies changes in the ocean carbon cycle owing to the redistribution of DIC and alkalinity in the ocean interior resulting from changes in the gas exchange of $\mathrm{CO_2}$ at the ocean surface, ocean circulation, and biological pumps, and

contributes to the glacial decline in atmospheric $p\mathrm{CO_2}$ (*Broecker and Peng*, 1987; *Archer and Maier-Reimer*, 1994). *Farrell and Prell* (1989) present the calcite lysocline depth, which is the ocean depth where the content of deposited $\mathrm{CaCO_3}$ changes dramatically, has moved by at least 400 to $800\,\mathrm{m}$ in past $800,000$ years at the Central Equatorial Pacific. This is attributed to changes in bottom-water carbonate ion concentration. *Catubig et al.* (1998) estimate burial rate of $\mathrm{CaCO_3}$ at the LGM and Holocene by using global ocean sediment records of the content and mass accumulation rate of $\mathrm{CaCO_3}$. They show that the burial rate between the two time intervals is almost the same. Changes in the ocean carbon cycle associated with carbonate compensation process occur within these observational constraints. In order to evaluate changes in the ocean carbon cycle including carbonate compensation process, an ocean sediment model, which determines whether particles reaching the ocean floor are decomposed or dissolved in the upper part of sediments or buried over a long period, is required to calculate the burial of $\mathrm{CaCO_3}$. In this study, I newly create a sediment model and couple it to an OGCM with an ocean tracer model to investigate the impact of carbonate compensation process to the glacial reduction of atmospheric $p\mathrm{CO_2}$.

1.2.1 Modeling study of the glacial ocean carbon cycle

Numerical modeling is useful for quantitatively evaluating the effect of changes in ocean processes on changes in atmospheric $p\mathrm{CO_2}$. There are many modeling studies approaching the glacial atmospheric $p\mathrm{CO_2}$ using ocean box models (*Knox and McElroy*, 1984; *Sarmiento and Toggweiler*, 1984; *Siegenthaler and Wenk*, 1984; *Toggweiler*, 1999; *Sigman and Boyle*, 2000; *Köhler et al.*, 2005; *Peacock et al.*, 2006; *Hain et al.*, 2010), earth system models of intermediate complexity (EMICs) (*Brovkin et al.*, 2007; *Bouttes et al.*, 2010, 2011; *Menviel et al.*, 2012), ocean general circulation models (OGCMs) (*Archer et al.*, 2000; *Bopp et al.*, 2003; *Kurahashi-Nakamura et al.*, 2007; *Tagliabue et al.*, 2009), and atmosphere-ocean coupled general circulation models (AOGCMs). (*Oka et al.*, 2011;

Chikamoto et al., 2012).

First, I will review the past numerical studies using ocean box models and EMICs. By using an ocean box model, *Toggweiler* (1999) presents that the glacial reduction of atmospheric $p\mathrm{CO_2}$ is about $21\,\mathrm{ppm}$ due to the reduced ventilation, $36\,\mathrm{ppm}$ due to carbonate compensation process, and $23\,\mathrm{ppm}$ due to the SST cooling. They also indicate that $\delta^{13}\mathrm{C}$ in the deep ocean reduces consistent with the proxy data due to the reduced ventilation. *Sigman and Boyle* (2000) show the response of atmospheric $p\mathrm{CO_2}$ when the rain ratio of $\mathrm{CaCO_3}$ to organic carbon particles is halved in a numerical simulation using an ocean box model including an ocean sediment layer. The decrease in atmospheric $p\mathrm{CO_2}$ caused by the open-system ocean carbon cycle response including carbonate compensation process is about $35\,\mathrm{ppm}$ greater than that in the closed-system response. Considering the changes in SST, ocean circulation, biological pump efficiency owing to changes in dust-derived iron supply, carbonate compensation, sea level, and carbon storage in the terrestrial biosphere, *Brovkin et al.* (2007) report that about $65\,\mathrm{ppm}$ of the glacial decline in atmospheric $p\mathrm{CO_2}$ can be explained by simulations using a simple climate model with a two-dimensional ocean model.

Contrary to the simulations conducted by box models and EMICs, previous studies using GCMs show smaller decrease in atmospheric $p\mathrm{CO_2}$. *Archer et al.* (2000) use an OGCM to verify hypotheses regarding the glacial ocean carbon cycle change. In their LGM simulation, atmospheric $p\mathrm{CO_2}$ is reduced by $8\,\mathrm{ppm}$ from their pre-industrial simulation and reaches about $268\,\mathrm{ppm}$. The drop in SST and high iron availability contribute the glacial reduction of atmospheric $p\mathrm{CO_2}$. *Tagliabue et al.* (2009) successfully reproduce the glacial oceanic distribution of $\delta^{13}\mathrm{C}$; however, the derived reduction of atmospheric $p\mathrm{CO_2}$ is only $3.5\,\mathrm{ppm}$. The reason for their underestimation is that the supply of nutrients to the surface ocean decreases owing to the weakening of deep ocean circulation, which decreases the carbon sequestration by biological pumps. Numerical simulations using an AOGCM in *Oka et al.* (2011) and *Chikamoto et al.* (2012) show that atmospheric $p\mathrm{CO_2}$

in their LGM simulation is reduced by about $40\,\mathrm{ppm}$ from that in their pre-industrial simulation. They show that about 20–$23\,\mathrm{ppm}$ of the reduction is caused by the increased gas solubility of $\mathrm{CO_2}$ resulting from the SST cooling, changes in ocean circulation, and the expansion of sea ice coverage (*Chikamoto et al.*, 2012), and about $15\,\mathrm{ppm}$ of the reduction arises from the difference in iron supply (*Oka et al.*, 2011). The contribution to the atmospheric $p\mathrm{CO_2}$ change due to changes in ocean circulation is small in OGCM studies compared with that indicated by box models and EMICs. Since previous studies using GCMs cannot sufficiently explain the amplitude reported from ice core records, the detailed mechanism of the glacial reduction of atmospheric $p\mathrm{CO_2}$ has not been elucidated.

1.2.2 Southern Ocean hypothesis

Past ocean temperature and salinity have been reconstructed using paleo-ocean proxy data included in ocean sediments. *Adkins et al.* (2002) reconstruct bottom-water salinity using oxygen isotope ratios ($\delta^{18}\mathrm{O}$) and chloride ion concentrations contained in the pore water of ocean sediments. At a site in the deep South Atlantic (Ocean Drilling Program site 1093, Shona Rise, $49°58.588'\,\mathrm{S}$, $5°51.935'\,\mathrm{E}$, $3,626\,\mathrm{m}$), the reconstructed glacial bottom-water salinity is suggested to increase by more than $2\,\mathrm{psu}$ compared with the pre-industrial, and becomes beyond $37\,\mathrm{psu}$. The salinity rise in the deep Southern Ocean is much larger than the global average of $1\,\mathrm{psu}$ associated with sea level change. The bottom-water salinity higher than $1\,\mathrm{psu}$ compared with the pre-industrial is also reported in the Pacific Ocean (*Insua et al.*, 2014). Furthermore, bottom-water temperature is shown to be near the freezing point in the glacial Southern Ocean (*Waelbroeck et al.*, 2002; *Elderfield et al.*, 2012; *Schrag et al.*, 2002; *Adkins et al.*, 2002). If these paleo-ocean reconstructions are correct, it is conceivable that low-temperature and high-salinity water occupied the glacial deep Southern Ocean (*Duplessy et al.*, 2002; *Adkins*, 2013).

Water mass ages in the glacial Southern Ocean are estimated to be very old compared with the pre-industrial from reconstructions using radiocarbon isotope ratios ($\Delta^{14}\mathrm{C}$) in-

cluded in foraminifera and deep corals (*Skinner et al.*, 2010; *Burke and Robinson*, 2012). From the analysis of $\Delta^{14}\mathrm{C}$ using samples of planktonic and benthic foraminifera from a core in the South Atlantic (MD07-3076 CQ, $44°4.46'\,\mathrm{S}$, $14°12.47'\,\mathrm{W}$, $3,770\,\mathrm{m}$), ventilation ages in the South Atlantic are suggested to be older than $3,000$ years (*Skinner et al.*, 2010). These studies show that the diapycnal mixing between the $^{14}\mathrm{C}$-depleted dense AABW flow and Circumpolar Deep Water was suppressed at the LGM. *Robinson et al.* (2005) show that water mass ages in the glacial North Atlantic become old because the southern-sourced AABW flow occupied the glacial deep Atlantic. These paleo-ocean reconstructions provide that ocean stratification is enhanced in the glacial Southern Ocean and deep ocean is isolated from the surface ocean compared with the pre-industrial.

From these paleo-ocean reconstructions, it is expected that the strongly stratified and isolated glacial deep Southern Ocean may have accumulated more carbon than the present (*Fischer et al.*, 2010; *Sigman et al.*, 2010; *Skinner et al.*, 2010). This hypothesis is referred to as "Southern Ocean hypothesis" (*Sigman and Boyle*, 2000). In the modern Southern Ocean, ocean surface nutrients and DIC are high compared with the other regions because strong upwelling transports nutrients and carbon to the surface ocean. In addition, the fraction of ocean nutrients that sinks without biological uptake is high (*Ito and Follows*, 2005). This means that the sequestration of carbon by biological pumps is insufficient in the modern Southern Ocean. On the other hand, the Southern Ocean hypothesis suggests that carbon stored in the glacial deep Southern Ocean is increased due to efficient carbon vertical transport through ocean biological pumps and/or the decrease in water mass exchange between the surface and deep ocean. The processes that is assumed to produce such an ocean state is described below.

As mentioned above, the iron fertilization in the Southern Ocean at the LGM has a potential to increase the sequestration of carbon in the deep ocean, which decreases atmospheric $p\mathrm{CO}_2$. *Kohfeld et al.* (2005) estimate the difference of organic carbon export production between the LGM and the late Holocene from ocean sediment records. They

show that export production is decreased in the glacial Antarctic region due to the expansion of sea ice coverage, but increased in the subantarctic region. The high productivity in the subantarctic region may be related to the iron fertilization. *Martínez-Garcia et al.* (2009) present from ocean sediment records in the South Atlantic that there is a good correlation between the iron supply, ocean productivity, SST, and Antarctic temperature in glacial-interglacial climate changes.

The decrease in water mass exchange between the surface and deep ocean in the Southern Ocean also contributes to the increase in the storage of carbon in the deep ocean. Ocean circulation and the associated ocean carbon cycle in the Southern Ocean are significantly altered by glacial changes in winds (*Toggweiler et al.*, 2006; *Menviel et al.*, 2008; *Tschumi et al.*, 2008; *Völker and Köhler*, 2013), sea ice (*Stephens and Keeling*, 2000; *Kurahashi-Nakamura et al.*, 2007; *Sun and Matsumoto*, 2010), brine rejection (*Bouttes et al.*, 2011), sea surface buoyancy (*Watson et al.*, 2015; *Sun et al.*, 2016), and stratification of water columns (*Francois et al.*, 1997; *Schmittner and Galbraith*, 2008; *Hain et al.*, 2010).

The intensity and position of westerly wind in the southern hemisphere influences carbon storage in the Southern Ocean through changes in the strength of deep-water upwelling along the Antarctic Circumpolar Current. *Toggweiler et al.* (2006) use an idealized general circulation model and argue that weakening and/or northward shift of the westerlies is a major factor for changes in the ocean carbon cycle during glacial periods. On the other hand, *Rojas et al.* (2009) analyze simulation results conducted in the second phase of Palaeoclimate Modelling Intercomparison Project and show that there is no clear shift in the westerlies in the LGM simulations, but suggest a decrease in surface wind speeds in the Southern Ocean and subantarctic region. Furthermore, contrary to *Toggweiler et al.* (2006), some previous modeling studies show that atmospheric $p\mathrm{CO_2}$ increases with weakening and northward shift of westerlies (*Menviel et al.*, 2008; *Tschumi et al.*, 2008). From sea salt and mineral dust aerosol records, *Fischer et al.* (2007) present

that the intensity of the glacial westerly wind was almost the same or slightly stronger compared with that in the present day, but they also indicate that the response of the ocean carbon cycle to changes in the westerlies has high uncertainty because the response is different between numerical simulations.

Gersonde et al. (2005) report that winter sea ice spreads off the coast by about 10 degrees in the glacial Southern Ocean compared with the pre-industrial. It means that the glacial sea ice coverage expands to the latitude of modern Polar Front. They also show that the sea ice coverage around the Weddell Sea in the summer at the LGM is the same extent as that in the modern winter season. Due to the expansion of sea ice coverage, $\mathrm{CO_2}$ emitted to the atmosphere is considered to be decreased in the glacial Southern Ocean (*Stephens and Keeling*, 2000). Their box model study suggests that the expansion of sea ice coverage and accompanying changes in ocean stratification bring about a large decline in atmospheric $p\mathrm{CO_2}$.

Watson and Garabato (2006) propose that ocean upwelling in the glacial Southern Ocean is weakened because the obtained buoyancy flux at the sea surface around the Polar Front is decreased from the present day as a consequence of the low sea above temperature. From an analysis of box model simulations, they present that the weakening of upwelling contributes to reduce atmospheric $p\mathrm{CO_2}$ by about $35\,\mathrm{ppm}$.

It is considered that the enhanced ocean stratification and the accompanying weakening of vertical mixing may isolate the deep ocean from the surface ocean at the LGM (*Francois et al.*, 1997; *Toggweiler*, 1999; *Köhler et al.*, 2005; *Marinov et al.*, 2008; *Schmittner and Galbraith*, 2008; *Bouttes et al.*, 2011). *Köhler et al.* (2005) use an ocean-atmosphere-biosphere box model and show that the isolated deep Southern Ocean contributes to reduce atmospheric $p\mathrm{CO_2}$ by about $35\,\mathrm{ppm}$. *Bouttes et al.* (2010), who use the same model of *Brovkin et al.* (2007), focus on brine rejection in the Southern Ocean by incorporating its parameterization into their model to improve its salt transport process to the ocean bottom layer. *Bouttes et al.* (2011) argue that the glacial atmospheric $p\mathrm{CO_2}$

and $\delta^{13}\mathrm{C}$ distribution can be reproduced by considering the brine rejection parameterization suggested in *Bouttes et al.* (2010), stratification-dependent vertical diffusivity, iron fertilization, and carbonate compensation process.

The Southern Ocean hypothesis is also supported by proxy data during the last deglaciation period, which is the transition period from the LGM to the pre-industrial. During the last deglaciation, it has been shown that the increase in the silica sinking flux and the decrease in $\delta^{13}\mathrm{C}$ and $\Delta^{14}\mathrm{C}$ in the intermediate Southern Ocean. This is thought to be due to the increase in nutrient supply from the deep ocean at that time by enhanced upwelling in the Southern Ocean, which flows old water mass isolated in the deep ocean into the upper ocean (*Anderson et al.*, 2009; *Marchitto et al.*, 2007; *Meckler et al.*, 2013). This supports the idea that regenerated carbon that was vertically transported by efficient biological pumps and stored for a long time in the Southern Ocean during the LGM released to the upper ocean during the deglaciation.

1.3 Objective of this study

In this study, the role of ocean carbon cycle on the glacial reduction of atmospheric $p\mathrm{CO_2}$ is discussed. Ice core records reveal that atmospheric $p\mathrm{CO_2}$ at the LGM was about $100\,\mathrm{ppm}$ lower than that at the pre-industrial, but previous modeling studies using OGCMs fail to reproduce the amplitude, and the obtained $p\mathrm{CO_2}$ change is about $40\,\mathrm{ppm}$. State-of-the-art models in the third phase of Paleoclimate Modelling Intercomparison Project do not adequately reproduce properties in the glacial deep Southern Ocean (*Adkins et al.*, 2002; *Skinner et al.*, 2010; *Burke and Robinson*, 2012) and the enhanced salinity stratification at that time (*IPCC*, 2013). In other words, the underestimation of the amplitude of the glacial reduction of atmospheric $p\mathrm{CO_2}$ in the previous OGCM simulations is possibly because these simulations have not sufficiently reproduced the enhanced stratification in the glacial Southern Ocean, which is a precondition for the Southern

Ocean hypothesis. For this reason, I first attempt to reproduce the glacial ocean state reconstructed from paleo-ocean proxy data (*Adkins et al.*, 2002; *Skinner et al.*, 2010; *Burke and Robinson*, 2012) by simulations using an OGCM. After that, the response of ocean carbon cycle to the physical fields, which reproduce the paleo-ocean reconstructions, is quantitatively evaluated. Furthermore, previous OGCM simulations that focused on the glacial atmospheric $p\mathrm{CO_2}$ change do not take into account the interaction between the ocean carbon cycle and ocean sediments. By using an ocean sediment model and coupling it to an OGCM, I evaluate the atmospheric $p\mathrm{CO_2}$ reduction by carbonate compensation process.

This paper is organized as follows. In Chapter 2, the impact of enhanced stratification in the Southern Ocean on the glacial atmospheric $p\mathrm{CO_2}$ decline is evaluated in a closed-system response of ocean carbon cycle. In Chapter 3, I perform numerical simulations using an OGCM coupled with a sediment model. I assess the impact of carbonate compensation process on the glacial reduction of atmospheric $p\mathrm{CO_2}$. In Chapter 4, I examine the glacial atmospheric $p\mathrm{CO_2}$ change by using an OGCM adapting versatile parameterizations of brine rejection and stratification-dependent vertical diffusivity. Finally, discussion and conclusion of this paper are shown in Chapter 5.

Note that the content of Chapter 2 has already been published in Paleoceanography (*Kobayashi et al.*, 2015).

Chapter 2

Role of Southern Ocean stratification in glacial atmospheric carbon dioxide reduction evaluated by a three-dimensional ocean general circulation model

Abstract

Atmospheric carbon dioxide concentration ($p\mathrm{CO_2}$) during glacial periods is known to be considerably lower than during interglacial periods. However, previous studies using an ocean general circulation model (OGCM) fail to reproduce this. Paleoclimate proxy data of the Last Glacial Maximum indicate high bottom-water salinity ($> 37.0\,\mathrm{psu}$) and long residence time of water masses ($> 3,000$ years) in the Southern Ocean, suggesting that salinity stratification was enhanced and more carbon was stored there. Reproducibility of salinity and water mass ages is considered insufficient in previous OGCMs, which might affect the reproducibility of atmospheric $p\mathrm{CO_2}$. This chapter investigate the role of increased stratification of the Southern Ocean in the glacial $p\mathrm{CO_2}$ variation using an OGCM. I find that deep-water formation in the East Antarctica is required to explain high bottom-water salinity in the South Atlantic. Saline deep Southern Ocean causes an increase in atmospheric $p\mathrm{CO_2}$ against previous estimates. This is partly due to the increased volume transport of Antarctic Bottom Water because of the increase in the density of deep water and the associated decrease in water mass ages of the deep Pacific Ocean. On the other hand, the weakening of vertical mixing contributes to the increase in the vertical gradient of dissolved inorganic carbon and decrease in atmospheric $p\mathrm{CO_2}$. However, I show that it is unable to explain all of the glacial $p\mathrm{CO_2}$ variations by the contribution of the Southern Ocean. My findings indicate that it might be crucial to appreciate the impact of enhanced stratification in the Southern Ocean on the Pacific Ocean to understand the mechanisms behind the glacial-interglacial ocean carbon cycle variations.

2.1 Introduction

Recent paleo-ocean proxy data support an idea that the deep Southern Ocean acts as a large carbon reservoir during glacial periods (*Fischer et al.*, 2010; *Sigman et al.*, 2010;

Skinner et al., 2010). *Adkins et al.* (2002) reconstruct bottom-water salinity and temperature during the Last Glacial Maximum (LGM) from chloride concentration and oxygen isotopic composition of pore water in marine sediments. These data show high salinity ($> 37.0\,\mathrm{psu}$) in the deep South Atlantic during the LGM, implying that salinity stratification was enhanced in the glacial deep Southern Ocean. In addition, analyses of radiocarbon isotopic ratios ($\Delta^{14}\mathrm{C}$) included in benthic foraminifera and deep-sea coral reveal that a very old water mass ($> 3,000$ years) isolated from the ocean surface occupied the South Atlantic during the LGM (*Skinner et al.*, 2010; *Burke and Robinson*, 2012). Therefore, it is expected that the isolated Southern Ocean stored more carbon during the LGM than at present (e.g. *Francois et al.*, 1997; *Toggweiler*, 1999).

Köhler et al. (2005) estimate the effect of enhanced stratification in the deep Southern Ocean on atmospheric carbon dioxide concentration ($p\mathrm{CO_2}$) using an ocean box model. They suggest that isolation of the deep ocean by enhanced stratification contributes to a reduction in atmospheric $p\mathrm{CO_2}$ of about $35\,\mathrm{ppm}$. *Bouttes et al.* (2011) conduct a numerical study using an earth system model including a two-dimensional ocean model. They report success in reproducing atmospheric $p\mathrm{CO_2}$ and oceanic distribution of carbon stable isotope ratios ($\delta^{13}\mathrm{C}$) during the LGM by introducing appropriate parameterization of oceanic mechanisms of brine-induced stratification, stratification-dependent diffusivity, and iron fertilization to their standard simulation of the LGM.

The spatial scale of the process of deep-water formation in the Southern Ocean is small and cannot be resolved directly by coarse-resolution OGCMs (*Heuzé et al.*, 2013). A large polynya was observed in the Weddell Sea during the 1974–1976 winters (*Gordon*, 1978). This is the last observed event of open-ocean deep convection in the Southern Ocean. However, such OGCMs tend to simulate the permanent open-ocean deep convection in winter (*Griffies et al.*, 2009), which leads to underestimations of the vertical gradient of salinity and the strength of stratification in the Southern Ocean. This is one of the reasons why the salinity data of *Adkins et al.* (2002) is not reproduced realistically

by previous OGCM studies (*Otto-Bliesner et al.*, 2007; *IPCC*, 2013). Furthermore, it is also expected to prevent accurate simulation of glacial atmospheric $p\mathrm{CO_2}$. The vertical diffusion coefficient of OGCMs for previous LGM simulations is unchanged from present-day simulations; however, *Gargett* (1984) suggests that the vertical diffusion coefficient is inversely proportional to the strength of ocean stratification. Assuming that this relation is true, the vertical diffusion coefficient in the glacial deep Southern Ocean would be expected to be smaller than the present because of the enhanced stratification. It is speculated that this is also related to the presence of very old water mass suggested at the LGM.

In this chapter, I perform numerical experiments using a three-dimensional OGCM to evaluate the impact of the enhanced stratification inferred from paleo-ocean proxy data (*Adkins et al.*, 2002; *Skinner et al.*, 2010; *Burke and Robinson*, 2012) on the low atmospheric $p\mathrm{CO_2}$ at the LGM. First, to reproduce the recorded salinity in the deep ocean, I apply salinity restoring toward high salinity reported in *Adkins et al.* (2002) at the bottom of the Southern Ocean. This enables me to reproduce saline bottom water in a coarse-resolution OGCM (*England*, 1993; *Nakata and Suginohara*, 1998). Furthermore, considering the weakening of vertical mixing caused by the enhanced stratification, I apply a small vertical diffusion coefficient in the Southern Ocean to reproduce the very old water mass of the glacial South Atlantic. Based on such treatments, the response of ocean carbon cycle and atmospheric $p\mathrm{CO_2}$ to the enhanced stratification in the Southern Ocean can be evaluated more realistically than in previous studies.

This chapter is organized as follows. Numerical models and experimental design are explained in Section 2.2. The effect of enhanced stratification in the glacial Southern Ocean on the glacial change in atmospheric $p\mathrm{CO_2}$ is described in Section 2.3. The discussion of simulation results and their significance is presented in Section 2.4, and Section 2.5 provides conclusions.

2.2 Methods

2.2.1 Ocean general circulation model

The OGCM used is COCO version 4.0 (*Hasumi*, 2006). It has a global computational domain with a horizontal resolution of about 1° and 43 vertical levels. Present-day ocean basin topography is used in both the pre-industrial (PI) and the LGM simulations.

Sea surface boundary conditions for the PI and LGM simulations are obtained from coupled model results of present-day and LGM simulations (*Oka et al.*, 2012) by MIROC 3.2 (*K-1 Model Developers*, 2004). Prescribed boundary conditions are monthly climatology from 30-year averages of horizontal wind stress, sea surface air temperature, sea surface specific humidity, sea surface short-wave radiation, sea surface long-wave radiation, freshwater flux, and sea surface wind speed. Sea surface sensible and latent heat fluxes are calculated using bulk formula as described in *Oka et al.* (2012).

Initial values of potential temperature and salinity are taken from the climatology of the Polar Science Center Hydrographic Climatology (*Steele et al.*, 2001). I perform a $3,000$-year integration and analyze the time average of the last 100 years.

2.2.2 Offline biogeochemical model

Steady-state ocean biogeochemical tracers are obtained by offline simulations for $3,000$ years using an offline tracer model. These simulations are conducted under the physical ocean fields calculated by the OGCM COCO (*Oka et al.*, 2008, 2011); horizontal velocity, vertical diffusion coefficient, sea level height, sea surface wind speed, sea ice concentration, and sea surface short-wave radiation are used in an offline tracer model. Note that only short-wave radiation is given the annual mean distribution. Tracer concentrations are

calculated by the following tracer equation (*Oka et al.*, 2011).

$$\frac{\partial C}{\partial t} = -\nu \cdot \nabla C + K_H \nabla_H^2 C + K_V \frac{\partial^2 C}{\partial z^2} + S_C, \tag{2.1}$$

where C is the concentration of each ocean biogeochemical tracer, ν is current velocity, K_H and K_V are horizontal and vertical diffusive coefficients, and S_C is a source/sink term related to ocean biogeochemical processes. The ocean biogeochemical model used in this study is based on that of *Parekh et al.* (2005) and the same as that used in *Oka et al.* (2011). The prognostic variables are phosphate, dissolved inorganic carbon (DIC), alkalinity, dissolved organic phosphate, dissolved oxygen, iron, and silicate. The uptake rate of phosphate by phytoplankton is determined from availability of light, phosphate, and iron. The iron flux is assumed to be 3.5 wt% of total dust deposition flux (*Fung et al.*, 2000). The initial distribution of ocean biogeochemical tracers is taken from the climatology of World Ocean Atlas 2001 (*Conkright et al.*, 2002; *Locarnini et al.*, 2002) and Global Ocean Data Analysis Project (*Key et al.*, 2004). The initial value of iron concentration is a constant value of $0.6\,\mathrm{nM}$. The model includes a well-mixed atmosphere box; atmospheric $p\mathrm{CO_2}$ is predicted by the gas exchange between the sea surface and atmosphere. In my glacial simulations, atmospheric $p\mathrm{CO_2}$ is not fixed and calculated from the same initial condition as the pre-industrial simulation to come into equilibrium by gas exchange. The export of calcium carbonate ($\mathrm{CaCO_3}$) and biogenic silica ($\mathrm{SiO_2}$) particles from the ocean surface is obtained from the organic carbon export multiplied by the rain ratio. The rain ratio of calcium carbonate to particulate organic carbon (POC) is set to a constant value of 0.08 (*Yamanaka and Tajika*, 1996). The rain ratio of silica to organic carbon is taken from the distribution of *Sarmiento et al.* (2004). The distribution of sinking particles from the upper ocean are calculated by empirical equations (*Martin*

et al., 1987; *Klaas and Archer*, 2002):

$$
\begin{aligned}
F_{\mathrm{POC}}(z) &= F_{\mathrm{POC}}(z_{ref})\left(\frac{z}{z_{ref}}\right)^{-b}, \\
F_{\mathrm{CaCO_3}}(z) &= F_{\mathrm{CaCO_3}}(z_{ref})\exp\left(\frac{z-z_{ref}}{z_{pc}}\right), \\
F_{\mathrm{SiO_2}}(z) &= F_{\mathrm{SiO_2}}(z_{ref})\exp\left(\frac{z-z_{ref}}{z_{ps}}\right),
\end{aligned}
\tag{2.2}
$$

where z_{ref} is the depth of euphotic zone and sets to $100\,\mathrm{m}$, and the exponent of organic carbon dissolution b is 0.858 (*Martin et al.*, 1987). z_{pc} and z_{ps} are the penetration depth of calcium carbonate and biogenic silica, respectively. The former is taken as $3,500\,\mathrm{m}$ (*Yamanaka and Tajika*, 1996), and the latter is $10,000\,\mathrm{m}$ (*Henderson et al.*, 1999). The dust deposition flux at the sea surface is taken from the simulation results of a global atmospheric aerosol transport-radiation model of SPRINTARS (*Takemura et al.*, 2005, 2009).

I also calculate a virtual age tracer that explicitly represents water mass ages of the model ocean. The age tracer is forced to be zero at the sea surface and to increase at a constant rate within the ocean. This indicates the length of time the water mass spends within the ocean after sinking from the sea surface (*Thiele and Sarmiento*, 1990; *Oka and Niwa*, 2013).

2.2.3 Experimental design

I perform three experiments: Control, Restoring, and Stratification experiment. The Control experiment is conducted under both the pre-industrial and LGM boundary conditions, whereas the Restoring and Stratification experiments are conducted under the LGM boundary conditions only. The Restoring experiment examines the response of ocean carbon cycle under the presence of high bottom-water salinity in the Southern Ocean. The Stratification experiment investigates the response of ocean carbon cycle to changes in the

vertical diffusion coefficient induced by enhanced ocean stratification.

In the Restoring experiment, salinity in the deepest layer is restored toward high salinity in specified regions in the Southern Ocean where deep-water formation occurs (*England*, 1993; *Nakata and Suginohara*, 1998). Salinity restoring at the deepest layer is introduced to incorporate the effects of entrainment and the associated salt transport induced by continental slope flow, which are unresolved in the Control experiment. This treatment enables me to reproduce the salinity distribution reported by *Adkins et al.* (2002). In the LGMsrst-rw simulation, the salinity restoring regions are the Weddell Sea (163° E–126° W, 73°–90° S) and Ross Sea (15°–64° W, 73°–90° S) (Figure 2.1a), which are the major present-day regions of deep-water formation. In the LGMsrst simulation, I additionally apply restoring in the East Antarctica (0°–45° E, 64°–90° S) (Figure 2.1b). This region has also been recognized as a present-day region of deep-water formation, in addition to the Ross and Weddell Seas, because of the large volume of sea ice production there (*Tamura et al.*, 2008). Moreover, *Kusahara et al.* (2015) show that there is a large amount of sea ice production, compared with the present, in the coastal region of the East Antarctica during the LGM. In the LGMsrst simulation, I evaluate the role of deep-water formation near the East Antarctica during the LGM. I choose 37.0 and $38.0\,\mathrm{psu}$ as the restoring values of salinity. The time constant of salinity restoring is $1\,\mathrm{year}^{-1}$.

In the Stratification experiment, the vertical diffusion coefficient in the Southern Ocean (30°–90° S) or global ocean is forced to be a constant value of $0.10\,\mathrm{cm}^2\,\mathrm{s}^{-1}$, which is of the order of observed value around the thermocline of the open ocean (*Gregg*, 1989; *Ledwell et al.*, 1993). The vertical diffusion coefficient of $0.10\,\mathrm{cm}^2\,\mathrm{s}^{-1}$ is almost the minimum value of vertical diffusion coefficient that can be taken in the ocean model. In other words, it corresponds to evaluate the response to the situation where the vertical mixing attenuates remarkably as a result of the enhanced stratification. Ocean stratification and vertical diffusivity are mutually related; the stronger stratification causes the smaller vertical diffusivity, and the smaller vertical diffusivity leads to the stronger stratification. Under the

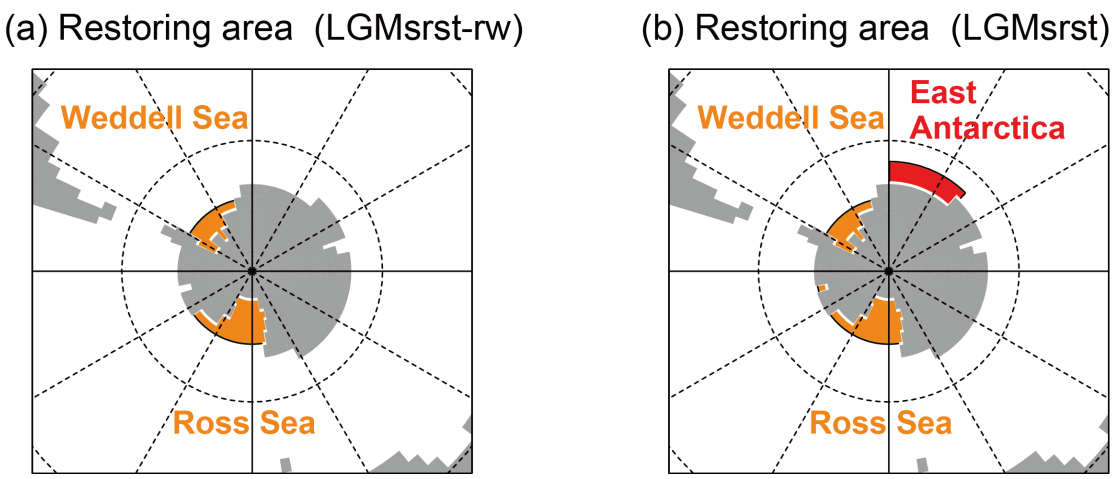

Figure 2.1: Salinity restored areas for the (a) LGMsrst-rw and (b) LGMsrst simulations, where salinity restoring toward 37.0 and $38.0\,\mathrm{psu}$ of salinity are shaded orange and red, respectively.

situation in which ocean stratification is stronger (such as the glacial Southern Ocean), it is reasonable to assume that the vertical diffusivity becomes weaker. Nevertheless, the vertical diffusivity has been assumed to be unchanged in previous OGCM studies. Therefore, in the LGMsrstS and LGMsrstG simulations, I attempt to evaluate the effects of weakened vertical diffusivity on atmospheric $p\mathrm{CO_2}$. On the other hand, from recent tide model simulations, more tidal energy dissipation at the LGM is reported (*Wilmes and Green*, 2014). Because the vertical diffusivity depends on both tidal energy dissipation and ocean stratification (*St. Laurent et al.*, 2002; *Oka and Niwa*, 2013), such change in tidal dissipation is also expected to affect the value of vertical diffusivity (more tidal energy dissipation leads to stronger vertical diffusivity). For example, a recent OGCM simulation suggests that enhanced tidal dissipation in glacial climate contributes to the strengthening of deep ocean circulation (*Schmittner et al.*, 2015). However, the detailed mechanism on changes in the vertical diffusivity is beyond the scope of this study, and I only focus on the stratification effect (i.e. the weaker vertical diffusivity at the LGM is assumed).

Table 2.1 summarizes the simulations conducted in this study.

Table 2.1: Experimental design of Chapter 2. The name of simulations is listed in the first and second columns. The restoring regions and the restoring value of salinity (psu) are shown in the third column (Body-forcing). The specified background vertical diffusivity is described in the fourth column: TSUJINO represents the formulation of vertical diffusion coefficient by case III of *Tsujino et al.* (2000).

Experiments	Simulations	Body-forcing		Vertical diffusivity
Control	PI	-		TSUJINO
	LGM	-		TSUJINO
Restoring	LGMsrst-rw	Ross and Weddell Seas	37.0	TSUJINO
	LGMsrst	Ross and Weddell Seas	37.0	TSUJINO
		East Antarctica	38.0	
Stratification	LGMsrstS	Ross and Weddell Seas	37.0	$0.10\,\mathrm{cm^2\,s^{-1}}$
		East Antarctica	38.0	(30°–90° S)
	LGMsrstG	Ross and Weddell Seas	37.0	$0.10\,\mathrm{cm^2\,s^{-1}}$
		East Antarctica	38.0	(global ocean)

2.3 Results

2.3.1 Control experiment

In the PI simulation, the simulated distribution of potential temperature and salinity reproduces the climatology of World Ocean Atlas 2001 well (Figures 2.2 and 2.3). In the LGM simulation, the globally averaged values of potential temperature and sea surface temperature (SST) are $1.92\,^{\circ}\mathrm{C}$ and $13.66\,^{\circ}\mathrm{C}$, respectively. These are lower than the PI simulation by about $1.4\,^{\circ}\mathrm{C}$ and $3.2\,^{\circ}\mathrm{C}$, respectively. Both results are consistent with the estimates of a previous study (*Sigman and Boyle*, 2000). The globally averaged values of salinity and sea surface salinity (SSS) in the LGM simulation are 34.72 and $34.13\,\mathrm{psu}$, respectively, which are almost the same as the PI simulation. Although the increase of average ocean salinity by about $1\,\mathrm{psu}$ is expected to arise from sea level change during the LGM, note that I do not explicitly consider this effect in the LGM simulation. Atlantic meridional overturning circulation (AMOC) in the LGM simulation is different from that in the PI simulation. Its maximum value is decreased by about $4\,\mathrm{Sv}$, and the depth of the border

between the North Atlantic Deep Water (NADW) and Antarctic Bottom Water (AABW) is shallower by about 300–$500\,\mathrm{m}$ (Figure 2.4; Table 2.2). Such features are consistent with $\delta^{13}\mathrm{C}$ distributions reported from proxy data (*Curry and Oppo*, 2005; *Lynch-Stieglitz et al.*, 2007). Figure 2.5 indicates the sea ice concentration in the Southern Ocean. Sea ice in the LGM simulation expands over the entire subantarctic region in the winter. During the summer, it expands to the same extent as in the winter of the PI simulation around the Weddell Sea. The LGM simulation reproduces the reconstructed sea ice concentration of *Gersonde et al.* (2005) well. However, the LGM simulation cannot sufficiently reproduce the glacial atmospheric $p\mathrm{CO_2}$, distribution of salinity, and water mass ages in the deep Southern Ocean.

Table 2.2: The maximum value of volume transport in the Atlantic and Pacific (Sv) is described in the second, third, and fourth column. The last two columns show the maximum value of virtual age tracer in the North Pacific and Southern Ocean (years). The abbreviations ATL, PAC, NP, and SO indicate the Atlantic, Pacific, North Pacific (110° E–280° W, 0°–60° N), and Southern Ocean (90°–40° S), respectively.

Simulations	NADW (ATL)	AABW (ATL)	AABW (PAC)	Age (NP)	Age (SO)
PI	15.99	7.71	11.86	1022	868
LGM	12.14	7.98	11.50	936	818
LGMsrst	10.84	9.62	14.49	898	807
LGMsrstS	8.84	9.52	14.27	881	816
LGMsrstG	13.05	3.97	4.73	1877	1640

Atmospheric $p\mathrm{CO_2}$ is $261.21\,\mathrm{ppm}$ in the LGM simulation and $299.87\,\mathrm{ppm}$ in the PI simulation (Table 2.3). The difference between these simulations is $38.66\,\mathrm{ppm}$, similar to that found in previous studies (*Oka et al.*, 2011; *Chikamoto et al.*, 2012), and it does not reproduce all the recorded variations of atmospheric $p\mathrm{CO_2}$ ($\sim\ 100\,\mathrm{ppm}$). Figure 2.6 displays the zonally averaged distribution of simulated DIC in the Atlantic and Pacific Oceans. Dissolved inorganic carbon in the LGM simulation decreases in the surface ocean, increases in the deep ocean, and the vertical gradient of DIC between the surface and deep ocean is greater than the PI simulation. This change contributes to the reduction

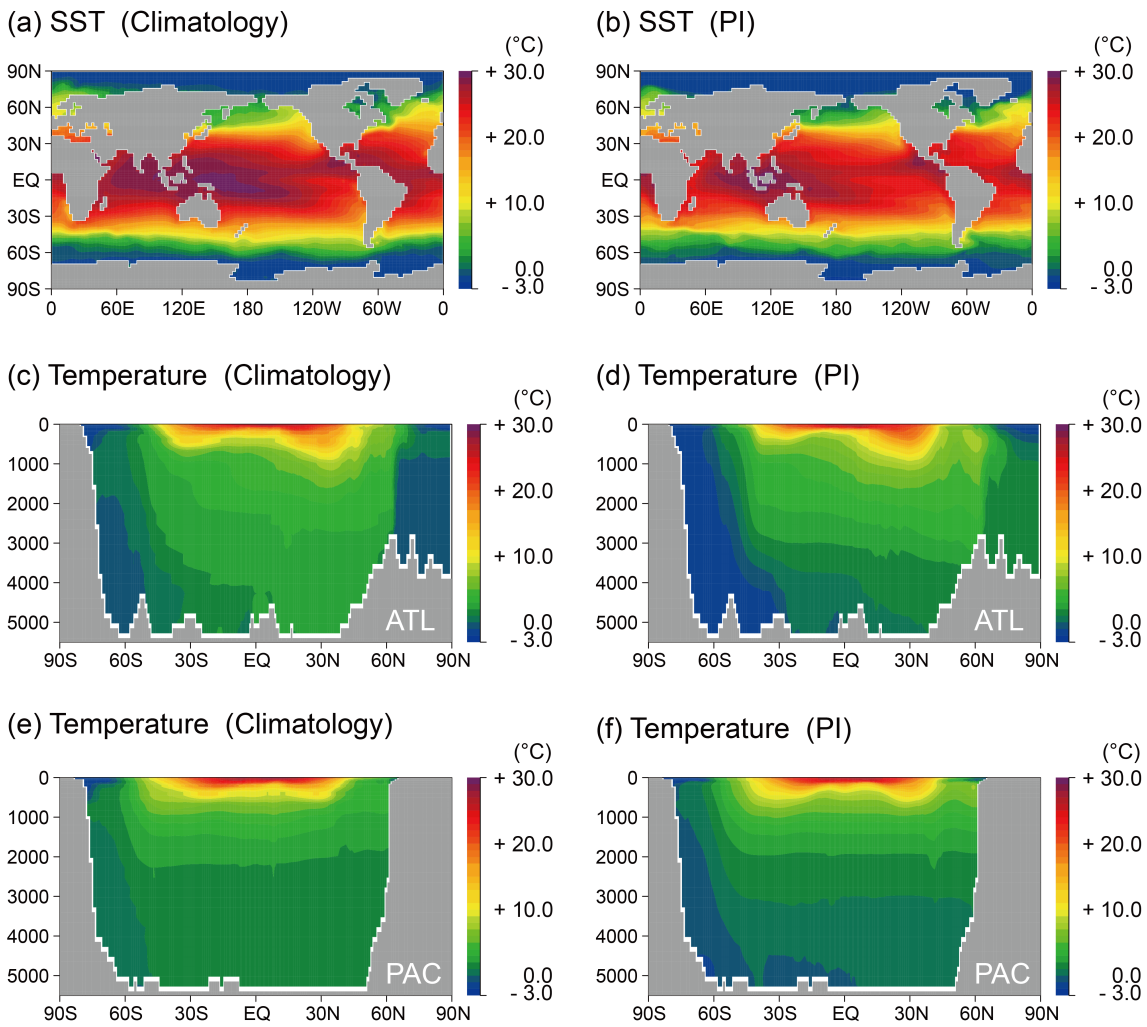

Figure 2.2: Annual mean temperature (°C) at the sea surface and zonally averaged distribution in the Atlantic and Pacific Oceans taken from the climatology of *Steele et al.* (2001) and the output of the PI simulation: (a) Sea surface of the climatology, (b) Sea surface in the PI simulation, (c) Atlantic of the climatology, (d) Atlantic in the PI simulation, (e) Pacific of the climatology, and (f) Pacific in the PI simulation.

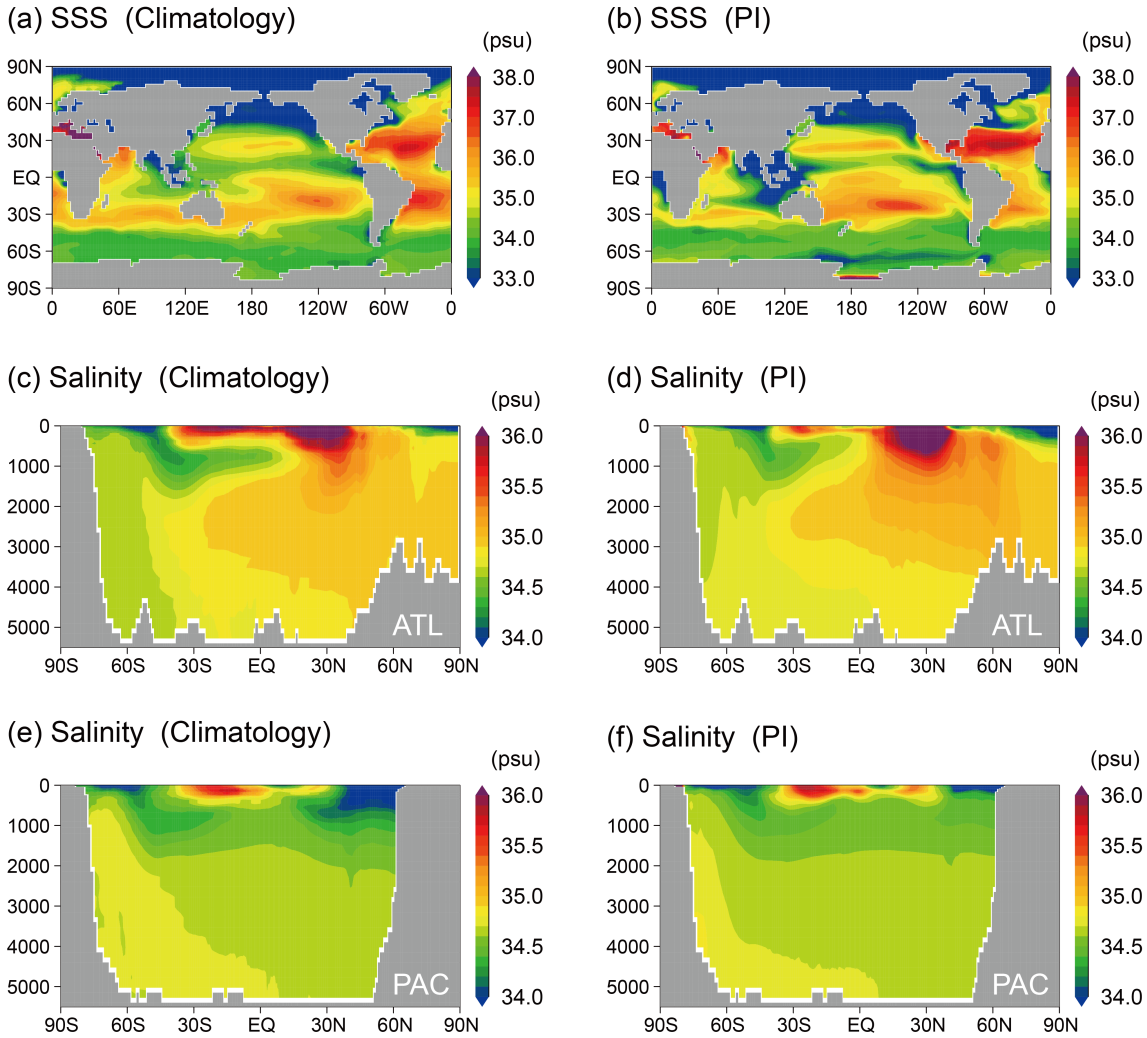

Figure 2.3: Annual mean salinity (psu) at the sea surface and zonally averaged distribution in the Atlantic and Pacific Oceans taken from the climatology of *Steele et al.* (2001) and the output of the PI simulation: (a) Sea surface of the climatology, (b) Sea surface in the PI simulation, (c) Atlantic of the climatology, (d) Atlantic in the PI simulation, (e) Pacific of the climatology, and (f) Pacific in the PI simulation.

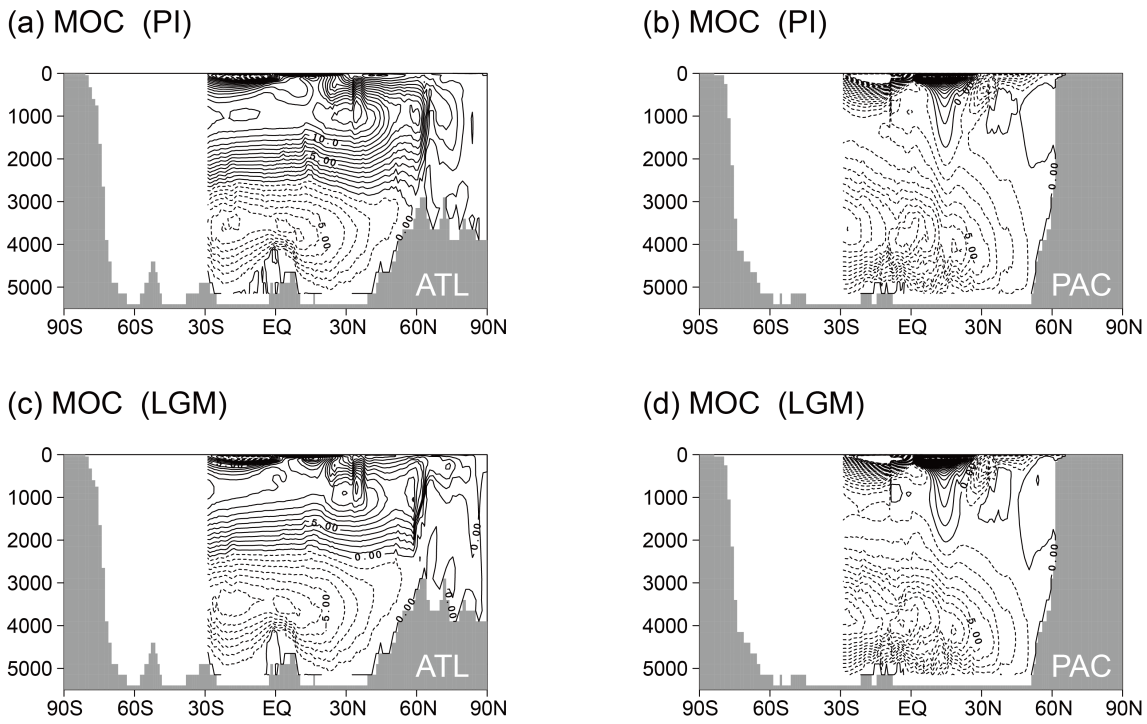

Figure 2.4: Meridional overturning circulation (Sv) in the Atlantic and Pacific Oceans in the Control experiment: (a) Atlantic in the PI simulation, (b) Pacific in the PI simulation, (c) Atlantic in the LGM simulation, and (d) Pacific in the LGM simulation. The contour interval is 1.0 Sv.

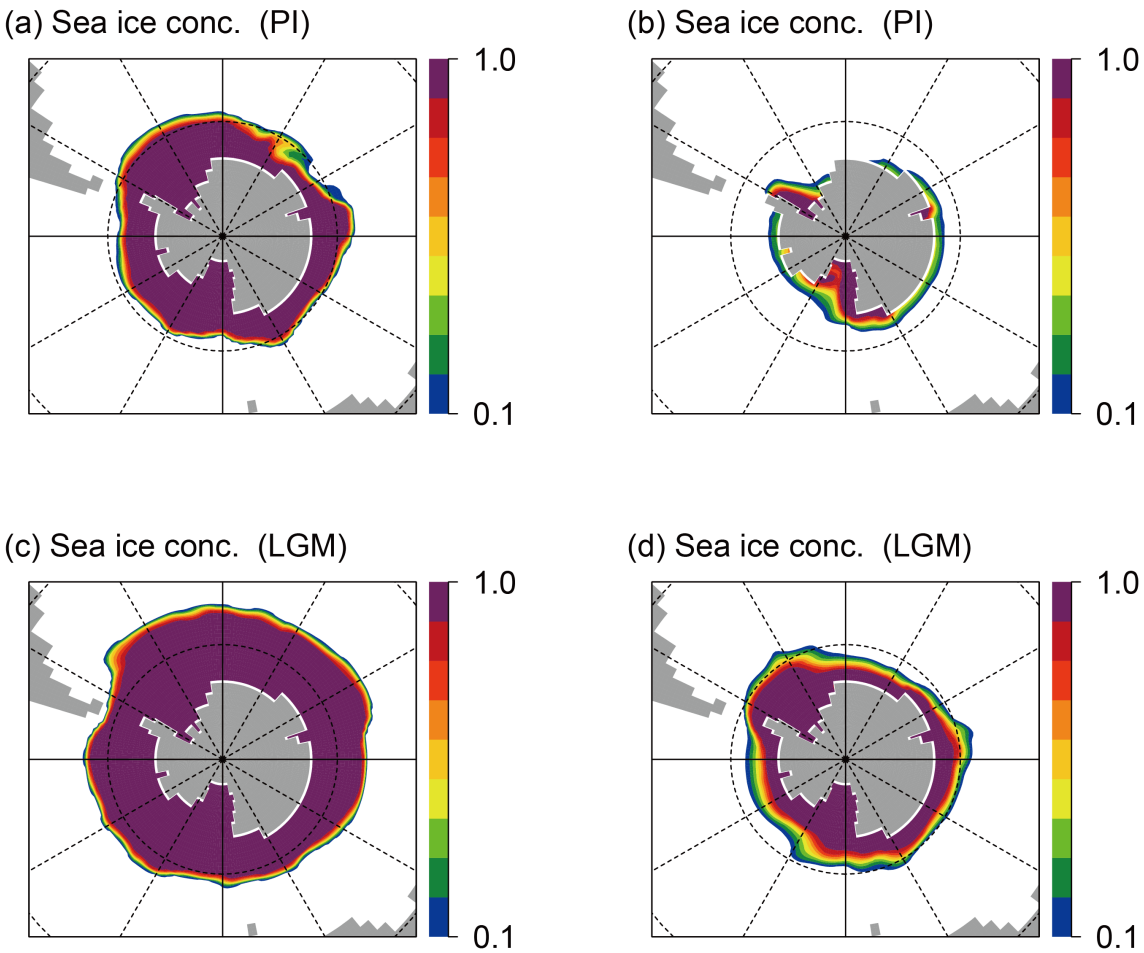

Figure 2.5: Sea ice concentration in the Southern Ocean in the Control experiment: (a) Winter in the PI simulation, (b) Summer in the PI simulation, (c) Winter in the LGM simulation, and (d) Summer in the LGM simulation. Winter represents average from August to October, and summer from February to April. The contour interval is 0.2.

of glacial atmospheric $p\mathrm{CO_2}$, but it is not large enough to reproduce the 100-ppm reduction of atmospheric $p\mathrm{CO_2}$. Figure 2.7 shows bottom-water salinity in the PI and LGM simulations together with the proxy data of *Adkins et al.* (2002). The PI simulation reproduces the reported data well and the difference is within $0.3\,\mathrm{psu}$. Conversely, even if I take into account the additional increase of globally averaged ocean salinity caused by sea level change, the LGM simulation underestimates the reported data by about $1\,\mathrm{psu}$ at a site in the deep South Atlantic (Ocean Drilling Program site 1093, Shona Rise, $49°58.588'\,\mathrm{S}$, $5°51.935'\,\mathrm{E}$, $3,626\,\mathrm{m}$) where the highest salinity is reconstructed in *Adkins et al.* (2002). Figure 2.8 presents the zonally averaged distribution of simulated virtual age tracer in the Atlantic and Pacific Oceans. In the Southern Ocean and the deep Pacific, water mass ages get younger in the LGM simulation than the PI simulation. The oldest water in the Southern Ocean is about 800 years old in the LGM simulation, which is younger than in the PI simulation by about 50 years, i.e., the very old water mass exceeding $3,000$ years reported in *Skinner et al.* (2010) and *Burke and Robinson* (2012) is not found in the LGM simulation.

Table 2.3: The partial pressure of carbon dioxide in the atmosphere ($p\mathrm{CO_2}^{atm}$) and in the surface ocean ($p\mathrm{CO_2}^{os}$) (ppm) is shown in the second and third columns. Difference from the LGM simulation is represented in parentheses. This difference is decomposed into two parts; $\Delta p\mathrm{CO_2}^{os}(TS)$ represents $p\mathrm{CO_2}^{os}$ change caused by changes in sea surface temperature and sea surface salinity, and $\Delta p\mathrm{CO_2}^{os}(CA)$ represents $p\mathrm{CO_2}^{os}$ change caused by changes in dissolved inorganic carbon and alkalinity (see text). SSS presents globally averaged sea surface salinity (psu). EP means globally integrated export production ($\mathrm{PgC\,yr^{-1}}$).

Simulations	$p\mathrm{CO_2}^{atm}$ (diff LGM)	$p\mathrm{CO_2}^{os}$ (diff LGM)	(TS)	(CA)	SSS	EP
PI	$299.87\,(+38.66)$	$303.95\,(+35.52)$	$+42.09$	-5.26	34.39	8.06
LGM	261.21	268.43			34.13	8.23
LGMsrst	$264.85\,(+3.64)$	$273.01\,(+4.58)$	$+7.39$	-2.67	35.03	7.99
LGMsrstS	$252.20\,(-9.01)$	$263.62\,(-4.81)$	$+4.05$	-9.41	34.81	7.75
LGMsrstG	$245.55\,(-15.66)$	$253.67\,(-14.76)$	-4.40	-10.69	33.53	6.66

The LGM simulation fails to reproduce the high-salinity and very old water mass in

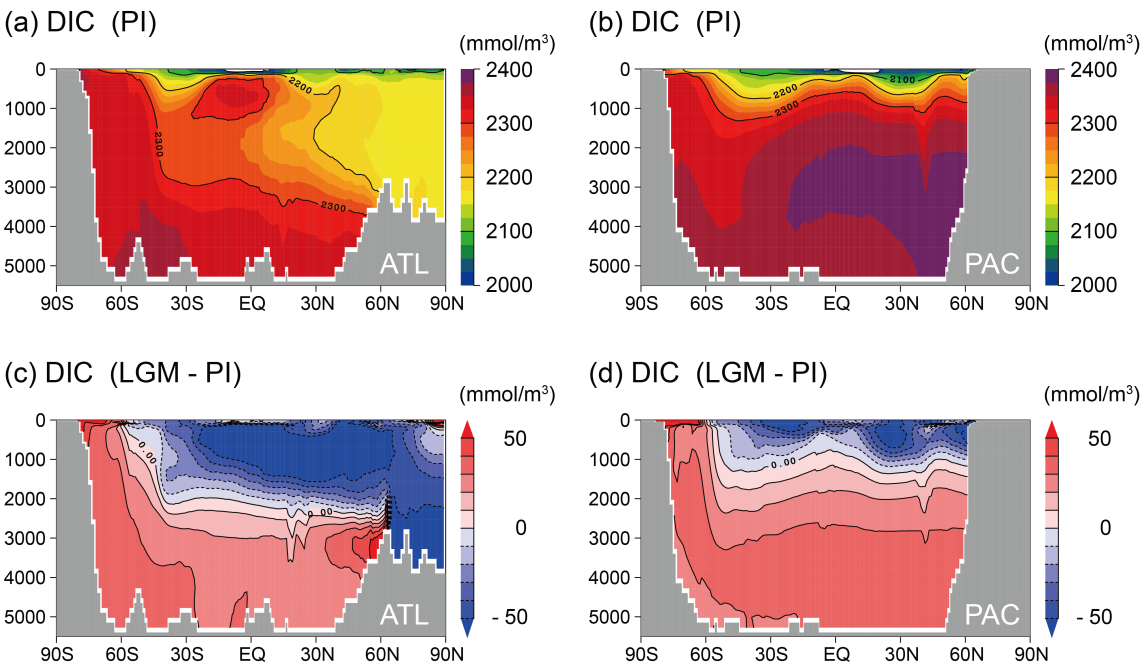

Figure 2.6: Zonally averaged distribution of annual mean dissolved inorganic carbon ($\mathrm{mmol\,m^{-3}}$) in the Atlantic and Pacific Oceans in the Control experiment: (a) Atlantic in the PI simulation, (b) Pacific in the PI simulation, (c) Atlantic in the LGM simulation (difference from the PI case), and (d) Pacific in the LGM simulation (difference from the PI case). The contour interval is $100\,\mathrm{mmol\,m^{-3}}$ in Figures 2.6a and 2.6b, and $10\,\mathrm{mmol\,m^{-3}}$ in Figures 2.6c and 2.6d.

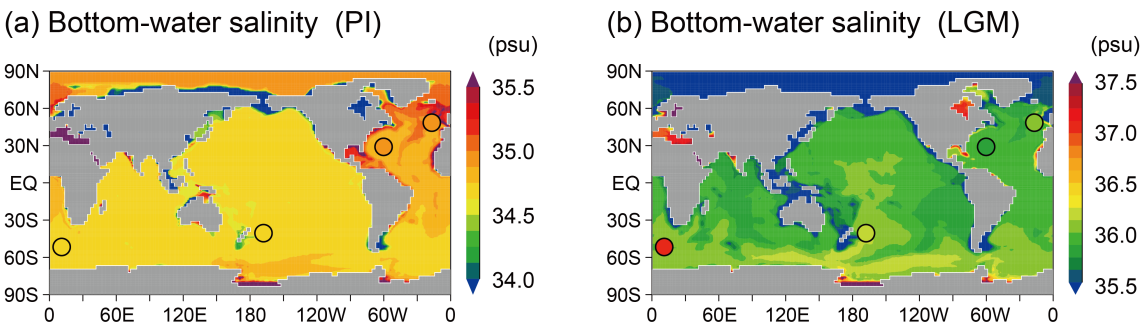

Figure 2.7: Annual mean bottom-water salinity (psu) of the (a) PI and (b) LGM simulations in the Control experiment. The four circles represent the reconstructed bottom-water salinity by *Adkins et al.* (2002).

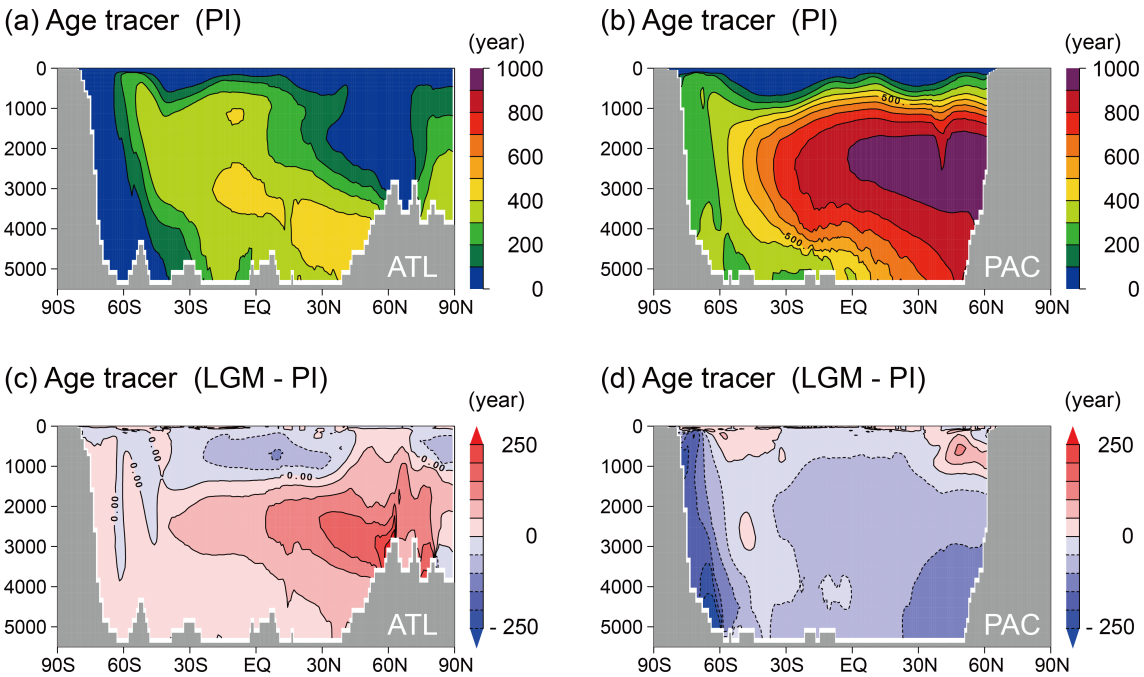

Figure 2.8: Zonally averaged distribution of annual mean virtual age tracer (years) in the Atlantic and Pacific Oceans in the Control experiment: (a) Atlantic in the PI simulation, (b) Pacific in the PI simulation, (c) Atlantic in the LGM simulation (difference from the PI case), and (d) Pacific in the LGM simulation (difference from the PI case). The contour interval is 100 years in Figures 2.8a and 2.8b, and 50 years in Figures 2.8c and 2.8d.

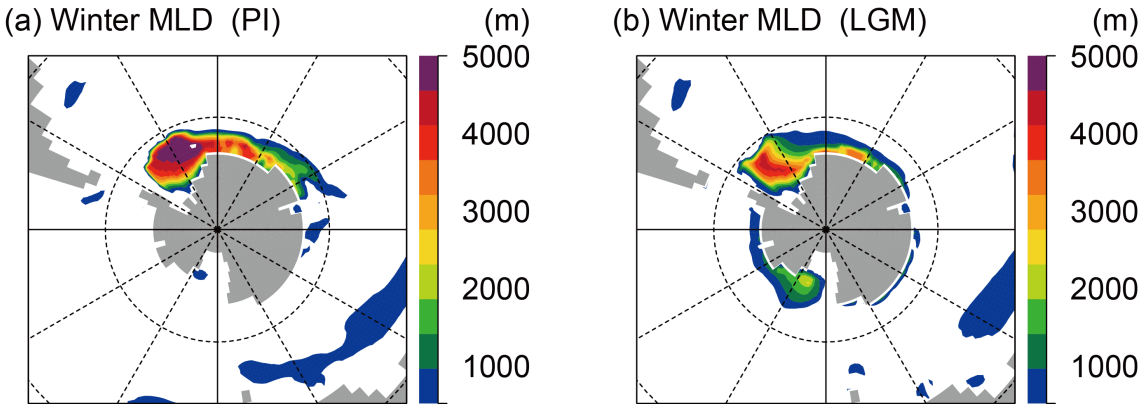

Figure 2.9: The winter mixed layer depth (m) in the Southern Ocean of the (a) PI and (b) LGM simulations in the Control experiment.

the glacial Southern Ocean, which means that the simulation underestimates the strength of ocean stratification in the Southern Ocean. This is considered as one of the reasons why the 100-ppm reduction of atmospheric $p\mathrm{CO}_2$ during the LGM cannot be reproduced in the Control experiment and previous OGCMs.

2.3.2 Restoring experiment

Figure 2.9 shows the mixed layer depth in the Southern Ocean for the PI and LGM simulations. In these simulations, deep water is formed by unrealistic open-ocean deep convection in the Southern Ocean. As a result, ocean stratification in the Southern Ocean is weakened. This is one possible reason why the recorded glacial distribution of salinity and water mass ages cannot be reproduced. In contrast, the Restoring experiment based on the proxy data of *Adkins et al.* (2002) is expected to reproduce saline bottom water in the Southern Ocean and suppress open-ocean deep convection.

Bottom-water salinity in the LGMsrst-rw and LGMsrst simulations are shown in Figures 2.10c and 2.10d, respectively. The LGMsrst-rw simulation still underestimates the reconstructed salinity in the deep South Atlantic of *Adkins et al.* (2002). On the other hand, the LGMsrst simulation successfully reproduces the very high bottom-water salinity. The horizontal distribution of salinity in the LGMsrst simulation is also consistent

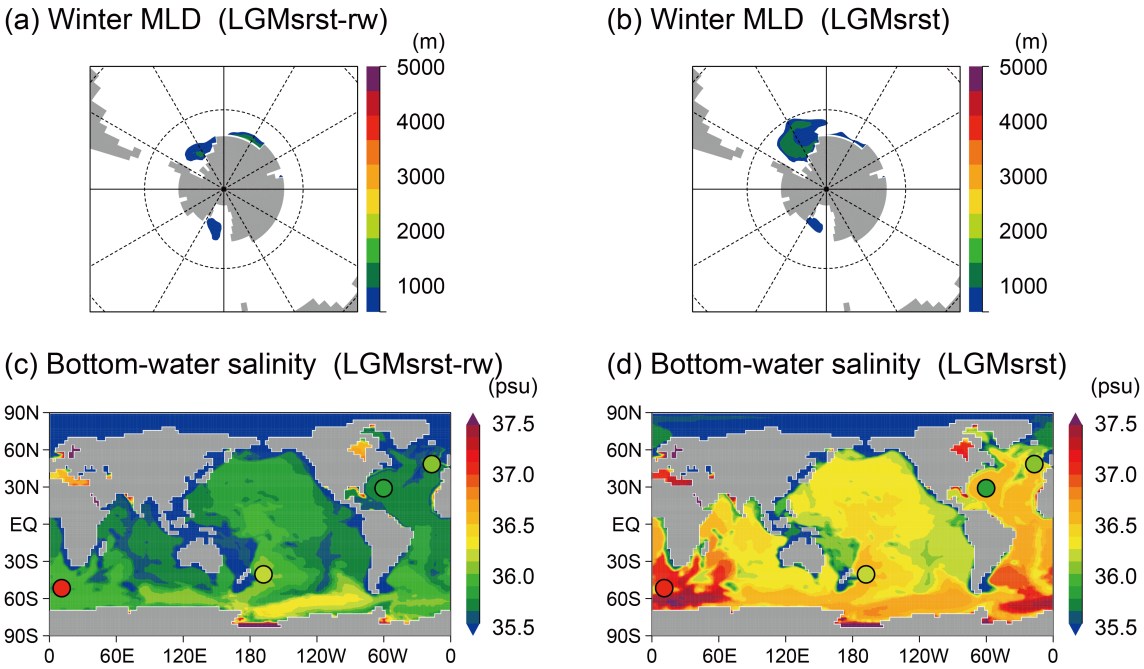

Figure 2.10: The winter mixed layer depth (m) around the Antarctica of the (a) LGMsrst-rw and (b) LGMsrst simulations in the Restoring experiment. Annual mean bottom-water salinity (psu) of the (c) LGMsrst-rw and (d) LGMsrst simulations in the Restoring experiment. The four circles represent the reconstructed bottom-water salinity by *Adkins et al.* (2002).

with the results of *Adkins et al.* (2002), where the maximum bottom-water salinity locates in the South Atlantic. Although open-ocean deep convection still exists in the LGMsrst-rw and LGMsrst simulations (Figures 2.10a and 2.10b), the depth of convection is suppressed compared with the LGM simulation.

Next, I focus on the response of atmospheric $p\mathrm{CO_2}$ and water mass ages of the LGMsrst simulation. In the LGMsrst simulation, although the reproducibility of salinity and convection is improved compared with the LGM simulation, the glacial atmospheric $p\mathrm{CO_2}$ and water mass ages are still not reproduced sufficiently. Atmospheric $p\mathrm{CO_2}$ increases by $3.64\,\mathrm{ppm}$ from the LGM simulation and reaches $264.85\,\mathrm{ppm}$ (Table 2.3). This response is opposite to my expectations and the findings of a previous study (*Bouttes et al.*, 2011). Water mass ages become older by about 100–200 years around the Antarctica, compared with the LGM simulation as a result of the enhanced stratification (Figures

2.11a and 2.11b). Interestingly, however, water mass ages in the North Pacific become younger than the LGM simulation. This change in the Pacific is explained by changes in ocean circulation as described below. The deep Southern Ocean in the LGMsrst simulation becomes saltier and denser, which causes an increase of the volume transport of the AABW flow by about 2–$3\,\mathrm{Sv}$ (Figures 2.4c, 2.4d, 2.11e, and 2.11f; Table 2.2). Thus, despite the older water mass ages around Antarctica, the residence time of carbon in the ocean is reduced, especially over the North Pacific Ocean (Figure 2.11b).

2.3.3 Stratification experiment

The Restoring experiment does not consider the effect of the weakening of vertical mixing arising from the enhanced salinity stratification. To evaluate this effect, I prescribe a small vertical diffusion coefficient caused by the enhanced stratification in the Stratification experiment.

In the LGMsrstS simulation, I apply a vertical diffusion coefficient of $0.10\,\mathrm{cm^2\,s^{-1}}$ over the south of $30^\circ\,\mathrm{S}$, where I assume that the stratification of the Southern Ocean is strengthened. The vertical gradient of DIC in the LGMsrstS simulation increases from the LGMsrst simulation (Figures 2.12c and 2.12d). As a consequence, atmospheric $p\mathrm{CO_2}$ in the LGMsrstS simulation decreases by $12.65\,\mathrm{ppm}$ compared with the LGMsrst simulation and it reaches a value of $252.20\,\mathrm{ppm}$ (Table 2.3). Water mass ages get older than the LGMsrst simulation around the deep Southern Ocean (Figures 2.12a and 2.12b), which contributes to the reduction of atmospheric $p\mathrm{CO_2}$. However, the ocean model still does not reproduce the very old glacial water mass reported by *Skinner et al.* (2010) and *Burke and Robinson* (2012).

The local change of ocean stratification in the Southern Ocean might be insufficient to explain the glacial atmospheric $p\mathrm{CO_2}$ and water mass ages. For this reason, the LGMsrstG simulation is performed, in which a vertical diffusion coefficient of $0.10\,\mathrm{cm^2\,s^{-1}}$ is applied to the global ocean. In this LGMsrstG simulation, I consider an ideal situation

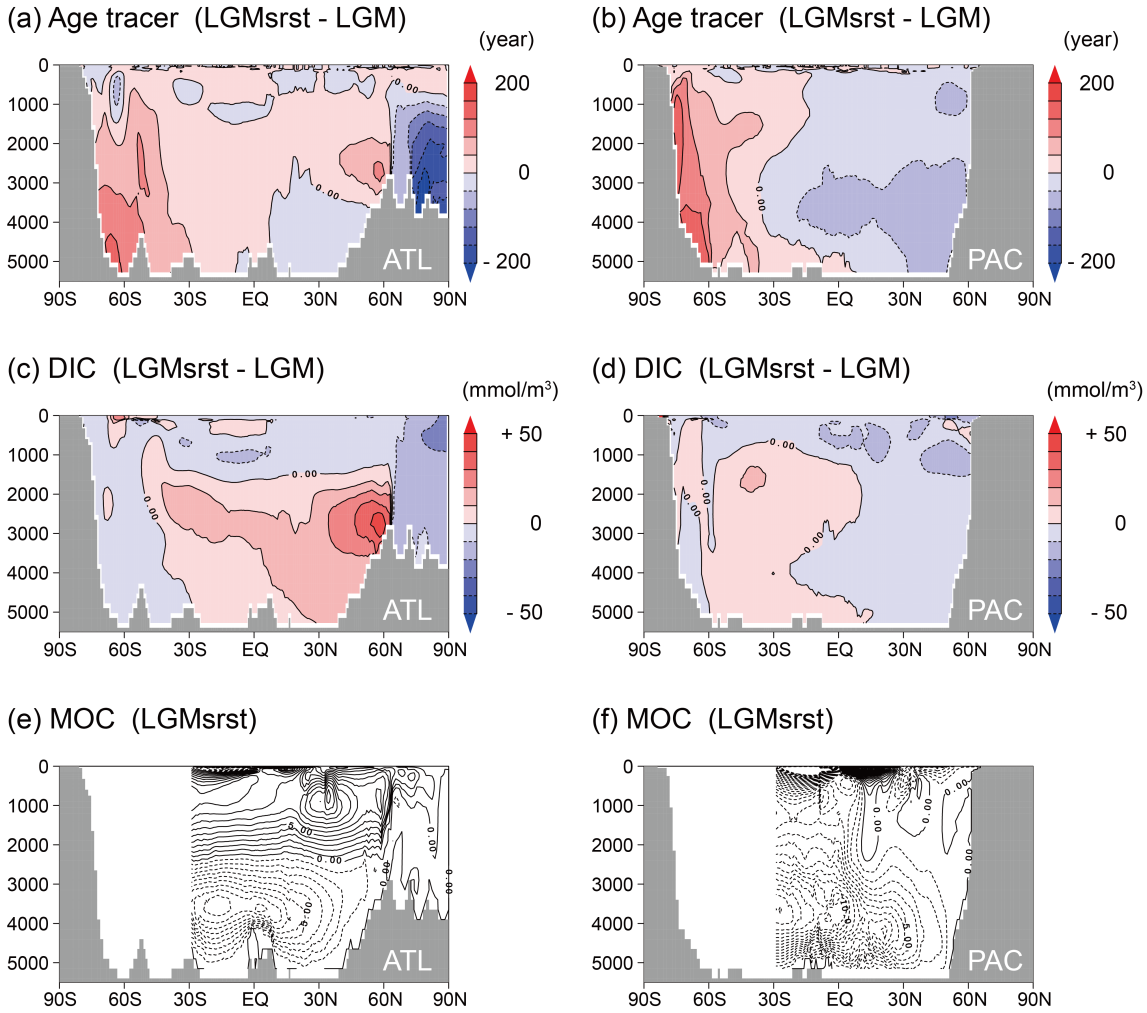

Figure 2.11: Results of the LGMsrst simulation (effects of stratification). Zonally averaged distribution of annual mean virtual age tracer (years) in the (a) Atlantic and (b) Pacific (difference from the LGM case). Zonally averaged distribution of annual mean dissolved inorganic carbon ($\mathrm{mmol\,m^{-3}}$) in the (c) Atlantic and (d) Pacific (difference from the LGM case). Meridional overturning circulation (Sv) in the (e) Atlantic and (f) Pacific. The contour interval is $40\,\mathrm{years}$ in Figures 2.11a and 2.11b, $10\,\mathrm{mmol\,m^{-3}}$ in Figures 2.11c and 2.11d, and $1.0\,\mathrm{Sv}$ in Figures 2.11e and 2.11f.

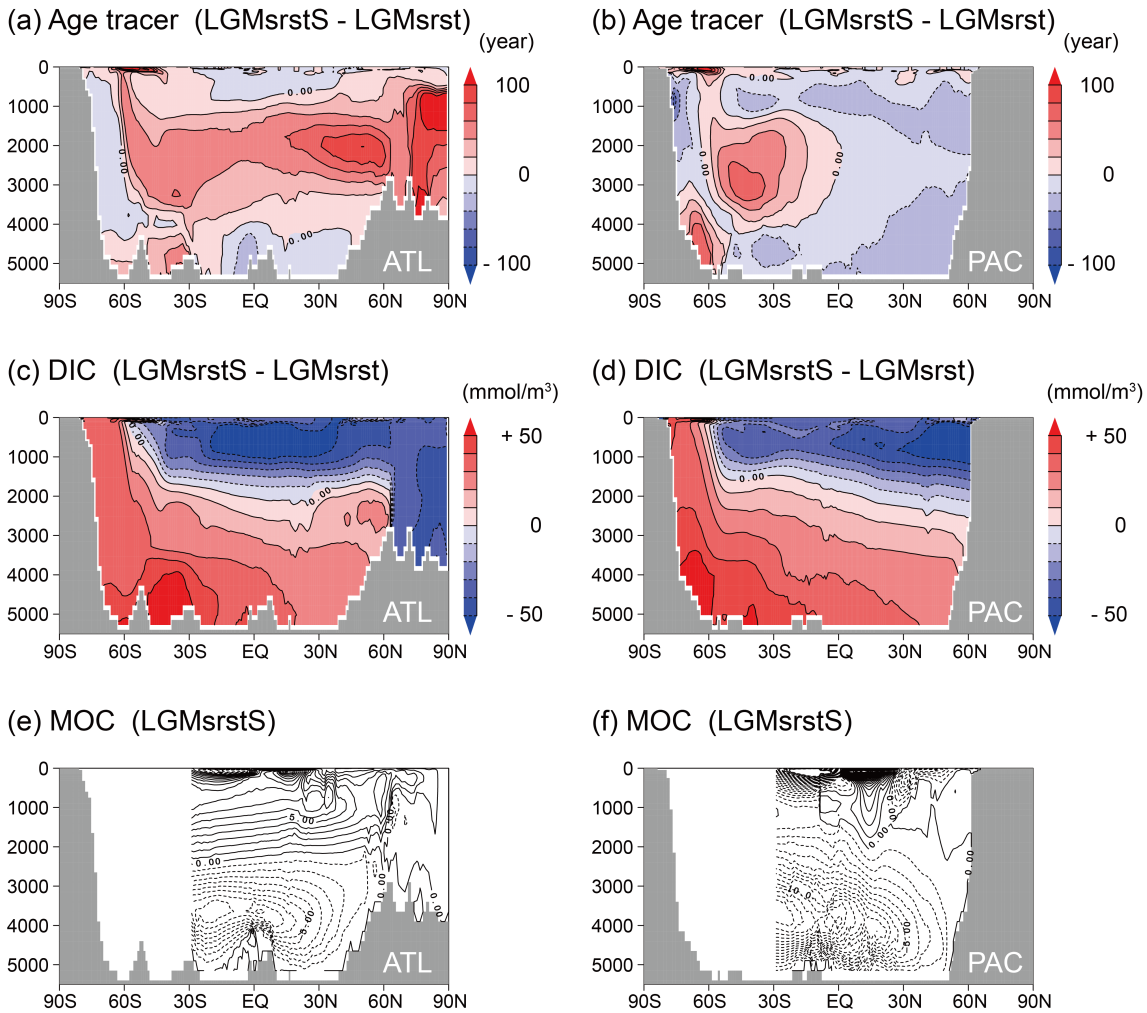

Figure 2.12: Results of the LGMsrstS simulation (effects of small vertical mixing in the Southern Ocean). Zonally averaged distribution of annual mean virtual age tracer (years) in the (a) Atlantic and (b) Pacific (difference from the LGMsrst case). Zonally averaged distribution of annual mean dissolved inorganic carbon ($\mathrm{mmol\,m^{-3}}$) in the (c) Atlantic and (d) Pacific (difference from the LGMsrst case). Meridional overturning circulation (Sv) in the (e) Atlantic and (f) Pacific. The contour interval is $20\,\mathrm{years}$ in Figures 2.12a and 2.12b, $10\,\mathrm{mmol\,m^{-3}}$ in Figures 2.12c and 2.12d, and $1.0\,\mathrm{Sv}$ in Figures 2.12e and 2.12f.

where the vertical mixing is very small in the global ocean. Atmospheric $p\mathrm{CO}_2$ in the LGMsrstG simulation decreases by $19.30\,\mathrm{ppm}$ compared with the LGMsrst simulation and reaches a value of $245.55\,\mathrm{ppm}$ (Table 2.3). The volume transport of the AABW flow in the LGMsrstG simulation reduces considerably (Figures 2.13e and 2.13f), to about half that of the LGMsrstS simulation (Figures 2.12e and 2.12f; Table 2.2). The depth of the NADW flow in the LGMsrstG simulation is about $2,000\,\mathrm{m}$, which is shallower than the LGMsrst simulation by about $500\,\mathrm{m}$ (Figure 2.13e). The deep layer is isolated more strongly from the shallow layer. Water mass ages in the deep ocean become older than in the LGMsrst simulation (Figures 2.13a and 2.13b); the oldest water in the Southern Ocean is $1,640$ years. The release of carbon from the abyssal sea is also suppressed compared with the LGMsrst simulation (Figures 2.13c and 2.13d). However, even the LGMsrstG simulation cannot reproduce the glacial atmospheric $p\mathrm{CO}_2$ and water mass ages suggested by *Burke and Robinson* (2012) sufficiently well.

2.4 Discussion

2.4.1 Glacial high bottom-water salinity and deep-water formation

Deep-water formation in the LGM simulation occurs in the form of unrealistic open-ocean deep convection (Figure 2.9b). In addition, the LGM simulation underestimates bottom-water salinity compared with *Adkins et al.* (2002) (Figure 2.7b). For the reasons stated above, I perform salinity restoring at the bottom layer to reproduce saline bottom water in the Southern Ocean in the Restoring experiment. The LGMsrst-rw simulation, in which salinity restoring is applied only in the Weddell and Ross Seas, is insufficient to explain the reported high bottom-water salinity in the South Atlantic of *Adkins et al.* (2002). By contrast, it is reproduced successfully in the LGMsrst simulation, in which I additionally apply salinity restoring near the East Antarctica. *Kusahara et al.* (2015) show that a large amount of sea ice is produced near the East Antarctica in their LGM simulation, which

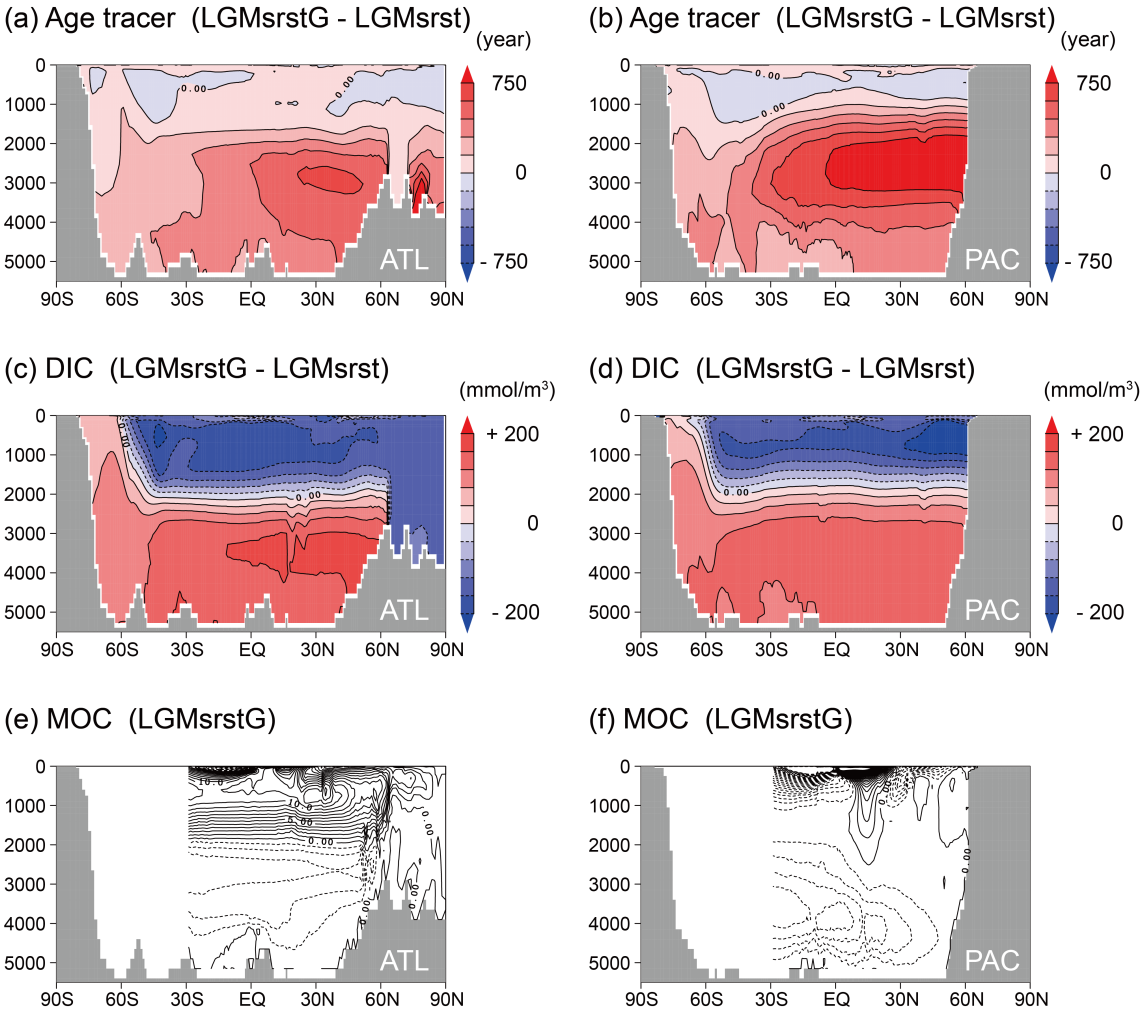

Figure 2.13: Results of the LGMsrstG simulation (effects of small vertical mixing in the global ocean). Zonally averaged distribution of annual mean virtual age tracer (years) in the (a) Atlantic and (b) Pacific (difference from the LGMsrst case). Zonally averaged distribution of annual mean DIC ($\mathrm{mmol\,m^{-3}}$) in the (c) Atlantic and (d) Pacific (difference from the LGMsrst case). Meridional overturning circulation (Sv) in the (e) Atlantic and (f) Pacific. The contour interval is $150\,\mathrm{years}$ in Figures 2.13a and 2.13b, $40\,\mathrm{mmol\,m^{-3}}$ in Figures 2.13c and 2.13d, and $1.0\,\mathrm{Sv}$ in Figures 2.13e and 2.13f.

suggests the possibility that deep-water formation occurs there at the LGM. Both their and my results suggest that the East Antarctica might be an important region for deep-water formation at the LGM.

2.4.2 Glacial water mass ages

In the LGM simulations of the Control and Restoring experiments, water mass ages in the Southern Ocean are younger than the PI simulation, contrary to the reconstructed very old glacial water mass in the Southern Ocean (*Skinner et al.*, 2010; *Burke and Robinson*, 2012). Enhanced stratification is expected to cause the weakening of vertical mixing, which might produce an isolated $^{14}\mathrm{C}$-depleted carbon reservoir in the deep ocean. However, such a change in vertical diffusivity is not considered in the Control and Restoring experiments.

In the Stratification experiment, I examine the impact of stratified Southern Ocean on water mass ages by providing very small vertical diffusivity of $0.10\,\mathrm{cm}^2\,\mathrm{s}^{-1}$ in addition to the salinity restoring. In the LGMsrstS simulation, water mass ages in the deep Southern Ocean become older compared with the LGMsrst simulation (Figures 2.12a and 2.12b) because of the weakening of vertical mixing. Nevertheless, the oldest water in the south of $40^\circ\,\mathrm{S}$ is only 816 years old, which is not old enough to satisfy the paleo-ocean reconstruction of *Skinner et al.* (2010). Water mass ages in the LGMsrstG simulation become older compared with the LGMsrst simulation (Figures 2.13a and 2.13b). This is related to the significant decrease of the volume transport of the AABW flow. The oldest water in the south of $40^\circ\,\mathrm{S}$ is $1,640$ years old, which is about twice that in the LGM simulation. However, even by applying an extremely small global vertical diffusion coefficient, I cannot reproduce the proxy data.

This discrepancy might arise partly because the simulated physical fields in this study still has a problem. Open-ocean deep convection in the Southern Ocean has not been completely eliminated in the glacial simulations (Figures 2.10a and 2.10b). Such open-

ocean deep convection increases surface ocean salinity; therefore, the glacial simulations still have a potential to underestimate the vertical gradient of glacial salinity and water mass ages. Another possibility is that water mass ages estimated from $\Delta^{14}\mathrm{C}$ might not correctly represent the actual residence time (*Broecker and Clark*, 2010; *De Pol-Holz et al.*, 2010; *Cléroux et al.*, 2011).

2.4.3 Mechanism of glacial changes in atmospheric carbon dioxide concentration

In the equilibrium state, atmospheric $p\mathrm{CO_2}$ becomes close to the surface ocean partial pressure of carbon dioxide (${p\mathrm{CO_2}}^{os}$) through gas exchange between the atmosphere and sea surface. Here, I investigate the mechanism of ${p\mathrm{CO_2}}^{os}$ differences between the simulations, by which I can discuss the mechanism of glacial atmospheric $p\mathrm{CO_2}$ change. According to inorganic carbon chemistry, ${p\mathrm{CO_2}}^{os}$ is controlled by DIC, alkalinity, temperature and salinity of surface water. It can be expressed symbolically as below:

$$ {p\mathrm{CO_2}}^{os} = f(\mathrm{DIC}, \mathrm{ALK}, \mathrm{SST}, \mathrm{SSS}), \tag{2.3} $$

where f represents a function determined from the inorganic chemistry of ocean carbon system (*Millero*, 1995; *Yoshikawa et al.*, 2008; *Oka et al.*, 2011b). I divide changes in ${p\mathrm{CO_2}}^{os}$ into two parts. First, effects of DIC and alkalinity changes, ΔDIC and ΔALK, on ${p\mathrm{CO_2}}^{os}$ changes are defined as

$$ \Delta {p\mathrm{CO_2}}^{os}(CA) = f(\mathrm{DIC} + \Delta\mathrm{DIC}, \mathrm{ALK} + \Delta\mathrm{ALK}, \mathrm{SST}, \mathrm{SSS}) - f(\mathrm{DIC}, \mathrm{ALK}, \mathrm{SST}, \mathrm{SSS}), \tag{2.4} $$

and next effects of SST and SSS changes, ΔSST and ΔSSS, on $p\mathrm{CO_2}^{os}$ changes as

$$\Delta p\mathrm{CO_2}^{os}(TS) = f(\mathrm{DIC}, \mathrm{ALK}, \mathrm{SST} + \Delta\mathrm{SST}, \mathrm{SSS} + \Delta\mathrm{SSS}) - f(\mathrm{DIC}, \mathrm{ALK}, \mathrm{SST}, \mathrm{SSS}). \tag{2.5}$$

In the Control experiment, the difference in atmospheric $p\mathrm{CO_2}$ between the PI and LGM simulations is $38.66\,\mathrm{ppm}$ and that in the globally averaged $p\mathrm{CO_2}^{os}$ is $35.52\,\mathrm{ppm}$ (Table 2.3). $\Delta p\mathrm{CO_2}^{os}(TS)$ is calculated as $+42.09\,\mathrm{ppm}$, which mainly results from the globally averaged SST cooling of about $3.3\,^{\circ}\mathrm{C}$. The vertical gradient of DIC in the LGM simulation increases compared with the PI simulation (Figure 2.6), which contributes to reduce $p\mathrm{CO_2}^{os}$. However, the decrease in surface alkalinity offsets most of it; therefore, $\Delta p\mathrm{CO_2}^{os}(CA)$ becomes $-5.26\,\mathrm{ppm}$.

In the LGMsrst simulation, atmospheric $p\mathrm{CO_2}$ and the globally averaged $p\mathrm{CO_2}^{os}$ increase from the LGM simulation by 3.64 and $4.58\,\mathrm{ppm}$, respectively (Table 2.3). The increase in SSS lowers the gas solubility of carbon dioxide and has a dominant impact on the atmospheric $p\mathrm{CO_2}$ change. The globally averaged SSS increases from the LGM simulation by $0.90\,\mathrm{psu}$, which results in $+7.39\,\mathrm{ppm}$ of $\Delta p\mathrm{CO_2}^{os}(TS)$ (Table 2.3). On the other hand, $\Delta p\mathrm{CO_2}^{os}(CA)$ only contributes $-2.67\,\mathrm{ppm}$. This response is smaller than my expectations and the simulation results of *Bouttes et al.* (2011). The increase in the volume transport of the AABW flow reduces water mass ages and DIC in the North Pacific (Figure 2.11; Table 2.2), which vents more carbon dioxide to the atmosphere. The change in the globally integrated export production is almost the same between the LGMsrst and LGM simulations and appears to have a little effect on the atmospheric $p\mathrm{CO_2}$ change (Table 2.3).

In the Stratification experiment, atmospheric $p\mathrm{CO_2}$ decreases from the LGM simulation by 9.01 and $15.66\,\mathrm{ppm}$ in the LGMsrstS and LGMsrstG simulations, respectively (Table 2.3). The globally averaged $p\mathrm{CO_2}^{os}$ is decreased in the LGMsrstS simulation from the LGMsrst simulation by $9.39\,\mathrm{ppm}$ (Table 2.3). The significant increase in DIC is found

around the deep Southern Ocean in the LGMsrstS simulation (Figures 2.12c and 2.12d), which is ascribable to the reduced vertical mixing caused by the enhanced stratification. Due to the associated increase in the vertical gradient of DIC, $\Delta p\mathrm{CO_2}^{os}(CA)$ contributes $-9.41\,\mathrm{ppm}$. This is the major reason for the reduction of $p\mathrm{CO_2}^{os}$ (Table 2.3). In the LGMsrstG simulation, the globally averaged $p\mathrm{CO_2}^{os}$ is decreased from the LGMsrstS simulation further by $9.95\,\mathrm{ppm}$. The vertical gradient of DIC is significantly increased from the LGMsrst and LGMsrstS simulations (Figures 2.13c and 2.13d), which results from the very sluggish AABW flow (Figures 2.13e and 2.13f; Table 2.2). However, the vertical gradient of alkalinity also increases (not illustrated), and resulting $\Delta p\mathrm{CO_2}^{os}(CA)$ becomes almost the same between the LGMsrstS and LGMsrstG simulations (Table 2.3). The increase in the vertical gradient of salinity causes $-4.40\,\mathrm{ppm}$ of $\Delta p\mathrm{CO_2}^{os}(TS)$, which further reduces $\Delta p\mathrm{CO_2}^{os}$ (Table 2.3). Export production is reduced in the Stratification experiment and contributes to reducing the vertical gradient of DIC and alkalinity. It is expected to partly cancel the stratification effects on $\Delta p\mathrm{CO_2}^{os}(CA)$ described above. I additionally perform new experiments with a fixed amount of the biological production of the LGM simulation to check the biological effects in each sensitivity simulation (not shown). Simulation results obtained in the new experiments are consistent to the above-mentioned interpretation.

Effects of expanded sea ice coverage in the glacial Southern Ocean on atmospheric $p\mathrm{CO_2}$ is also discussed in previous studies (*Stephens and Keeling*, 2000; *Kurahashi-Nakamura et al.*, 2007; *Sun and Matsumoto*, 2010). In the glacial simulations, I find that $\Delta p\mathrm{CO_2}^{os}(CA)$ contributed from changes in sea ice coverage is not so large compared with the other physical process by conducting additional experiments, in which sea ice distribution is fixed with the LGM simulation (not shown).

2.4.4 Comparison with previous studies and importance of Pacific Ocean

Bouttes et al. (2011) report that the glacial atmospheric $p\mathrm{CO_2}$ can be explained by focusing on processes within the Southern Ocean, especially brine rejection. They demonstrated that the high bottom-water salinity in the Southern Ocean due to brine rejection explains about 42-ppm decrease of atmospheric $p\mathrm{CO_2}$.

In the Restoring experiment, atmospheric $p\mathrm{CO_2}$ is increased in contrast to *Bouttes et al.* (2011) under the high bottom-water salinity in the Southern Ocean. Although changes in ocean circulation are not discussed explicitly in *Bouttes et al.* (2011), I expect that the volume transport of the AABW flow is decreased in their simulation, because the vertical gradient of $\delta^{13}\mathrm{C}$ becomes larger, suggesting that overturning circulation becomes more sluggish. This response of ocean circulation is the opposite to my LGMsrst simulation, where a three-dimensional OGCM is used and the distribution of bottom-water salinity of *Adkins et al.* (2002) is reproduced appropriately. I believe that this study reproduces a more realistic response compared with that of *Bouttes et al.* (2011). This implication proposes that the contribution of high bottom-water salinity in the glacial Southern Ocean to the low atmospheric $p\mathrm{CO_2}$ is considered less important than suggested by *Bouttes et al.* (2011).

The response of atmospheric $p\mathrm{CO_2}$ to changes in the vertical diffusion coefficient is almost the same as in *Bouttes et al.* (2011). Note that I assume an ideal situation in which very small vertical diffusivity is uniformly specified over the Southern Ocean or global oceans, whereas *Bouttes et al.* (2011) represent the vertical diffusion coefficient as a function of buoyancy frequency. A comparison of the LGMsrstG and LGMsrstS simulations shows that the reduced vertical mixing in the Pacific Ocean as well as in the Southern Ocean reduces atmospheric $p\mathrm{CO_2}$. Accordingly, if the glacial stratified Southern Ocean affects the stratification in the Pacific Ocean by any process, atmospheric $p\mathrm{CO_2}$ might be

reduced. Consequently, detailed understanding is required regarding the contribution of the Pacific Ocean in particular, to the glacial ocean carbon cycle.

2.5 Summary

Paleo-ocean proxy data indicate that the strengthening of ocean stratification in the Southern Ocean is important for the glacial-interglacial variation of atmospheric $p\mathrm{CO}_2$. In this chapter, I investigate the contribution of enhanced stratification in the Southern Ocean to changes in atmospheric $p\mathrm{CO}_2$ using a three-dimensional OGCM.

My Control experiment does not reproduce all the glacial atmospheric $p\mathrm{CO}_2$ variations, as in previous GCM studies; atmospheric $p\mathrm{CO}_2$ is $299.87\,\mathrm{ppm}$ in the pre-industrial simulation and $261.21\,\mathrm{ppm}$ in the LGM simulation ($\Delta p\mathrm{CO}_{2\,(\mathrm{LGM-PI})}^{atm} \sim -39\,\mathrm{ppm}$). The LGM simulation does not reproduce the high bottom-water salinity (*Adkins et al.*, 2002) and old water mass (*Skinner et al.*, 2010; *Burke and Robinson*, 2012) in the Southern Ocean, because it does not reproduce sufficiently well the process of deep-water formation in the Southern Ocean.

When salinity restoring is applied to the East Antarctica and the Ross and Weddell Seas (LGMsrst simulation), the LGM simulation approximately reproduces the salinity distribution reported by *Adkins et al.* (2002). Salinity restoring near the East Antarctica contributes significantly to its reproduction, which implies that the East Antarctica is an important area of deep-water formation at the LGM. Meanwhile, the residence time in the deep ocean becomes shorter because the overturning circulation associated with the AABW flow gets stronger due to the higher density in the deep Southern Ocean. As a result, atmospheric $p\mathrm{CO}_2$ increases from the LGM control simulation in contrast to previous studies (effect of high bottom-water salinity: $\Delta p\mathrm{CO}_{2\,(\mathrm{brine})}^{atm} \sim +4\,\mathrm{ppm}$).

To consider the reduced vertical mixing resulting from the enhanced stratification, small vertical diffusivity is prescribed in the Southern Ocean. As a result, atmospheric

$p\mathrm{CO_2}$ decreases by about $13\,\mathrm{ppm}$ (effect of reduced vertical diffusivity in the Southern Ocean: $\Delta p\mathrm{CO_2}^{atm}_{(\mathrm{K_V}0.1\mathrm{SO})} \sim -13\,\mathrm{ppm}$). This is attributed to the increase in the vertical gradient of DIC around the deep Southern Ocean. However, I cannot reproduce all of the glacial atmospheric $p\mathrm{CO_2}$ variation and the reported water mass ages. This result is unchanged even if I additionally consider the decrease of vertical diffusivity in the global oceans (effect of the reduced vertical diffusivity in the global Ocean: $\Delta p\mathrm{CO_2}^{atm}_{(\mathrm{K_V}0.1\mathrm{global})} \sim -19\,\mathrm{ppm}$).

I show that the contribution of enhanced stratification in the Southern Ocean to the variation of atmospheric $p\mathrm{CO_2}$ is smaller than reported by *Bouttes et al.* (2011). This is mainly because the response of ocean circulation to the enhanced stratification in the Southern Ocean is different from the previous study; the volume transport of the AABW flow increases in my glacial simulation, but decreases in *Bouttes et al.* (2011). I also show that the reduced vertical mixing in the Pacific Ocean as well as in the Southern Ocean significantly contributes to changes in atmospheric $p\mathrm{CO_2}$, because the reduced vertical mixing in the Pacific helps to accumulate carbon there. Accordingly, it might be important to assess the impact of strongly stratified Southern Ocean on the Pacific Ocean to clarify the mechanisms behind the variations of glacial-interglacial ocean carbon cycle.

Note that I do not consider carbonate compensation process in this chapter. *Bouttes et al.* (2011) estimated that about 40-ppm drawdown of atmospheric $p\mathrm{CO_2}$ is associated with this process. This may be a possible reason why glacial atmospheric $p\mathrm{CO_2}$ is not completely simulated. Therefore, the impact of considering carbonate compensation process will be discussed in Chapter 3.

Chapter 3

Response of atmospheric carbon dioxide to glacial changes in the Southern Ocean amplified by carbonate compensation process

本章については, 5 年以内に雑誌等で刊行予定のため, 非公開.

Chapter 4

Simulations of glacial ocean carbon cycle with parameterizations of brine rejection and stratification-dependent vertical diffusivity

本章については, 5 年以内に雑誌等で刊行予定のため, 非公開.

Chapter 5

General discussion and conclusion

Atmospheric carbon dioxide concentration ($p\mathrm{CO_2}$) at the Last Glacial Maximum (LGM) is about $100\,\mathrm{ppm}$ lower than that in the pre-industrial period. It is recognized that the ocean carbon cycle has a primary role on this glacial reduction of atmospheric $p\mathrm{CO_2}$. However, previous studies using ocean general circulation models (OGCMs) could not fully explain the 100-ppm reduction of glacial atmospheric $p\mathrm{CO_2}$. Paleo-ocean reconstructions using proxy data have shown that high-salinity and old water mass occupies the Southern Ocean at the LGM. From these reconstructions, a hypothesis, which suggests that carbon storage in the deep Southern Ocean increases as a result of the enhanced salinity stratification and a decrease in carbon supply to the surface ocean, is proposed. This study focuses on the Southern Ocean hypothesis to explain the mechanism of the low atmospheric $p\mathrm{CO_2}$ at the LGM by ocean biogeochemical modeling using an OGCM. Changes in atmospheric $p\mathrm{CO_2}$ are attributed to the following two causes. The first is redistribution of biogeochemical properties in the ocean interior ("closed-system" ocean carbon cycle response), and the second is changes in the whole ocean inventory of biogeochemical properties ("open-system" ocean carbon cycle response). The former response is discussed in detail in Chapter 2. The latter response is discussed in Chapter 3. In Chapter 4, I examine these responses by using an OGCM introducing parameterizations applicable to the glacial ocean state. In order to evaluate carbonate compensation process associated with the latter response, an ocean sediment model is created. Details of the sediment model is described in Appendix A. Technical information for introducing the parameterization of brine rejection to an OGCM is provided in Appendix B. What I clarified in each chapter, the novelty of this study, and future tasks are shown below. The process focused on this study is summarized in Figure 5.1.

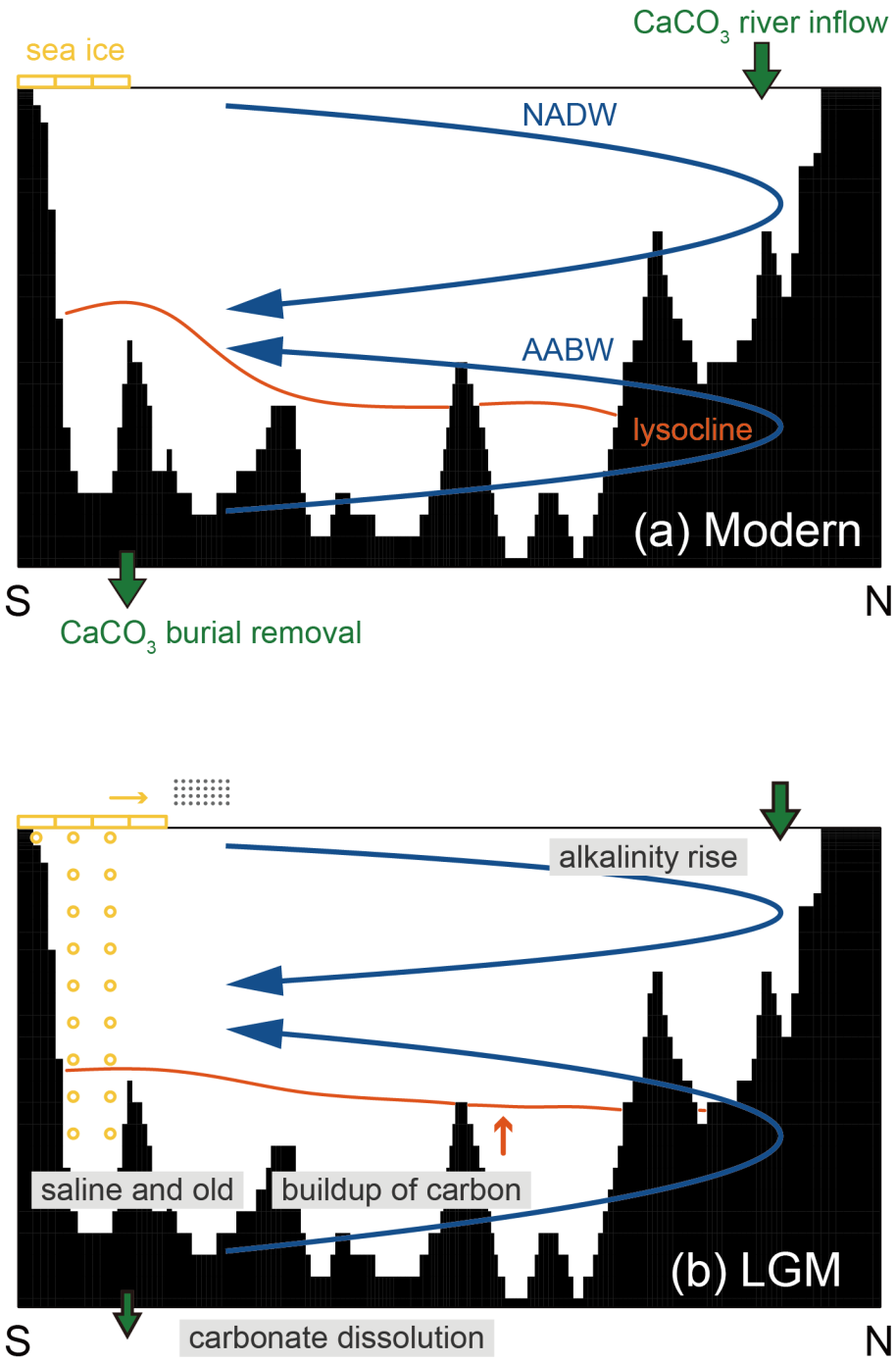

Figure 5.1: Schematic view summarizing the processes that focused on this study with respect to the (a) pre-industrial and (b) LGM.

Summary of simulation results of each chapter

Chapter 2: Role of Southern Ocean stratification in glacial atmospheric carbon dioxide reduction evaluated by a three-dimensional ocean general circulation model

Changes in atmospheric $p\mathrm{CO_2}$ caused by the redistribution of biogeochemical properties in the atmosphere and ocean system ("closed-system" carbon cycle response) is quantitatively investigated by using an OGCM with an ocean tracer model. In order to reproduce the distribution of reconstructed salinity and water mass ages at the LGM, bottom-water salinity is restored toward high salinity reported by proxy data around the Antarctica, and a small vertical diffusion coefficient is specified in the Southern Ocean.

- Atmospheric $p\mathrm{CO_2}$ is further reduced by $9.0\,\mathrm{ppm}$ in the above-mentioned LGM simulation compared with the LGM control simulation.
- Water mass ages around the Antarctica increase due to the enhanced salinity stratification in the Southern Ocean. As a result, the vertical gradient of dissolved inorganic carbon (DIC) from the LGM control simulation is increased; the decline in surface ocean DIC contributes to the most of the reduction of atmospheric $p\mathrm{CO_2}$.

Chapter 3: Response of atmospheric carbon dioxide to glacial changes in the Southern Ocean amplified by carbonate compensation process

The glacial atmospheric $p\mathrm{CO_2}$ reduction due to changes in the ocean carbon cycle including carbonate compensation process is quantitatively examined by using an OGCM with an ocean tracer model coupled with a newly created ocean sediment model.

- Carbonate compensation process amplifies the glacial reduction of atmospheric $p\mathrm{CO_2}$ as previous studies have suggested. Furthermore, this study newly finds that

the response of carbonate compensation is amplified by the enhanced stratification in the glacial Southern Ocean.

- Water mass ages get older around the Antarctica because of the enhanced stratification in the glacial Southern Ocean. This change results in an increase in DIC in the entire deep ocean. The increase in DIC expands the undersaturation of calcium carbonate ($\mathrm{CaCO_3}$) in the bottom water and reduces the burial of $\mathrm{CaCO_3}$. As a result, the imbalance between the river inflow and burial loss of $\mathrm{CaCO_3}$ becomes larger, and atmospheric $p\mathrm{CO_2}$ is decreased until this imbalance is relaxed via carbonate compensation process.

- Considering the "enhanced salinity stratification in the Southern Ocean" and "carbonate compensation process", the LGM simulation obtains a large decline in atmospheric $p\mathrm{CO_2}$ exceeding $70\,\mathrm{ppm}$ from the pre-industrial to LGM. This is the largest response which has not been obtained by previous OGCM studies.

Chapter 4: Simulations of glacial ocean carbon cycle with parameterizations of brine rejection and stratification-dependent vertical diffusivity

Simulations introducing parameterizations of brine rejection and stratification-dependent vertical diffusivity are conducted to reproduce LGM ocean properties suggested by paleo-ocean reconstructions.

- The LGM simulation introducing the parameterization of brine rejection during sea ice production successfully reproduces the glacial bottom-water salinity suggested by paleo-ocean proxy data. This is because a large glacial sea ice production contributes to producing a saline deep Southern Ocean.

- As water mass ages in the deep ocean get older from the pre-industrial simulation in the entire deep ocean, the glacial decline in atmospheric $p\mathrm{CO_2}$ is larger in the

LGM simulation with the parameterization of brine rejection compared with the LGM simulation with salinity restoring shown in Chapter 2.

- In the LGM simulation introducing the parameterization of stratification-dependent vertical diffusion coefficient in addition to the brine parameterization, the vertical gradient of DIC is further strengthened by the enhanced salinity stratification at the LGM. Considering all the effects, this study demonstrates that the simulated glacial reduction of atmospheric $p\mathrm{CO_2}$ gets very close to $100\,\mathrm{ppm}$ and successfully explains the amplitude inferred from ice core records.

Implication from this study

Saline and old water mass in the glacial deep Southern Ocean

Coarse-resolution OGCMs simulating the global ocean cannot reproduce the deep-water formation process in the Southern Ocean realistically. Deep water is formed by unrealistic open-ocean deep convection even in the latest fifth phase of Coupled Model Intercomparison Project models (*Heuzé et al.*, 2013). This is a critical problem not only for the reproducibility of the present day but also for glacial periods. Paleo-ocean proxy data indicate that saline and old water mass occupied the deep Southern Ocean at the LGM. However, it is known that such ocean properties are not properly reproduced in the previous OGCM studies focusing on glacial periods (*Otto-Bliesner et al.*, 2007; *IPCC*, 2013). The above-mentioned problem concerning the deep-water formation process is considered to be a possible reason. I confirmed that this problem is also remarkable in my LGM control simulation, and the open-ocean deep convection occurs around the Antarctica. In order to avoid this problem, in Chapter 2, a LGM simulation, in which bottom-water salinity is restored toward high salinity at the deep-water formation regions to mimic the deep-water formation process, is conducted (LGMsrstS simulation). Salinity stratification in the Southern Ocean is enhanced in the LGMsrstS simulation owing to the increase

in bottom-water salinity around the Antarctica compared with the LGM control simulation. The unrealistic deep convection is also suppressed in the LGMsrstS simulation; the exchange of ocean properties between the surface and deep ocean decreases, and water mass ages in the deep Southern Ocean become older than that in the LGM control simulation. In Chapter 4, instead of salinity restoring, I introduce the parameterization of brine rejection. It is shown that similar glacial changes in ocean properties can be reproduced by introducing this parameterization; massive glacial sea ice production in the Southern Ocean is a key process for reproducing saline and old water mass.

Mechanism of the glacial reduction of atmospheric carbon dioxide concentration

In the control experiment of Chapter 2, the glacial drawdown of atmospheric $p\mathrm{CO_2}$ from the pre-industrial is about $40\,\mathrm{ppm}$, which is comparable to that obtained in the previous modeling studies using OGCMs. The decrease in the globally averaged partial pressure of ocean carbon dioxide is mainly caused by changes in the gas solubility of carbon dioxide due to the cooling of sea surface temperature.

In Chapter 4, the glacial reduction of atmospheric $p\mathrm{CO_2}$ reaches almost $100\,\mathrm{ppm}$ in the LGMbrineON simulation, in which parameterizations of brine rejection and stratification-dependent vertical diffusivity are introduced and carbonate compensation process is considered. In the LGMbrineON simulation, water mass ages in the entire deep ocean get older from the pre-industrial simulation compared with the LGM control simulation due to the enhanced salinity stratification in the Southern Ocean and the accompanying changes in deep ocean circulation. This change in water mass ages leads to higher DIC concentration in the deep ocean and lower concentration in the surface ocean (redistribution of dissolved inorganic carbon). Furthermore, considering carbonate compensation process acts to increase the whole ocean alkalinity. These two processes lower the partial pressure of carbon dioxide at the ocean surface. Compared with previous GCM studies (e.g. *Archer et al.*, 2000; *Oka et al.*, 2011), it is possible to reproduce the expected changes in

the glacial ocean carbon cycle. Taking into account the enhanced salinity stratification in the glacial Southern Ocean and the accompanying enhanced response of carbonate compensation process are essential reasons why my LGM simulation successfully explains the glacial reduction of atmospheric $p\mathrm{CO_2}$ in this study.

There is a large variation in model-based estimates of the glacial reduction of atmospheric $p\mathrm{CO_2}$ caused by carbonate compensation process. The response of carbonate compensation process is also different between the LGM simulations of this study. It is about $15\,\mathrm{ppm}$ in the LGM control simulation, whereas it is about $35\,\mathrm{ppm}$ in the LGMsrstS and LGMbrineON simulation; this is because the enhanced stratification in the Southern Ocean increases the response of carbonate compensation process. Because my LGMsrstS and LGMbrineON simulations reproduce the glacial Southern Ocean more realistically than previous studies (e.g. *Brovkin et al.*, 2007; *Bouttes et al.*, 2011), I believe that my estimate of the response of carbonate compensation process (about $35\,\mathrm{ppm}$) is the best among existing studies.

Future works

Brine parameterization

As mentioned above, one of the reasons why the saline and old glacial deep Southern Ocean cannot be reproduced sufficiently in OGCMs comes from the difficulty in representing the realistic deep-water formation process in the Southern Ocean. In this study, a LGM simulation introducing the parameterization of brine rejection shows that the active sea ice production at the LGM rises bottom-water salinity and suppresses the unrealistic open-ocean deep convection. However, concerning the brine parameterization, there remains some problems in that it is applied to the entire Southern Ocean including the open ocean, and that a brine parameter bf is different between the pre-industrial and LGM simulations. In the future, I try to extend the parameterization that can be applied to both the

pre-industrial and glacial simulations, for example, by changing the brine parameter bf according to a sea ice production rate.

Transient response of carbon cycle in the glacial-interglacial climate change

The required spin-up time to obtain a steady state of ocean carbon cycle including carbonate compensation process is about $500,000$ years, which is longer than the actual glacial-interglacial cycles (about $100,000$ years). I confirmed that most of the changes caused by carbonate compensation occurred in the first $100,000$ years in my simulations, and therefore, simulation results are considered to be sufficiently meaningful for discussing changes in atmospheric $p\mathrm{CO_2}$ in an actual glacial period. However, the transient response of ocean carbon cycle including carbonate compensation process will be investigated in the future.

Changes in dominant species of phytoplankton in the surface ocean

In the LGM, it is pointed out that the dominant species of phytoplankton in the surface ocean changes as the dust-derived iron supply increases, and biological productivity by organisms forming $\mathrm{CaCO_3}$ shells decreases (*Matsumoto et al.*, 2002). The formation of $\mathrm{CaCO_3}$ shells of plankton in the surface ocean and its dissolution in water columns create a vertical gradient of alkalinity in the ocean interior. Therefore, changes in the dominant species weaken the vertical gradient of alkalinity and decrease the particle flux of $\mathrm{CaCO_3}$ reaching the ocean floor. Both of these changes decrease the $\mathrm{CaCO_3}$ burial into ocean sediments. Consequently, it is expected that the glacial reduction in atmospheric $p\mathrm{CO_2}$ due to carbonate compensation process becomes larger by considering this process.

Concluding Remarks

Focusing on the "Southern Ocean hypothesis", I evaluate the impact of enhanced salinity stratification in the Southern Ocean during the LGM on the glacial atmospheric $p\mathrm{CO_2}$ re-

duction by OGCM simulations. In the LGM simulation that reproduces the reconstructed LGM bottom-water salinity, the difference of atmospheric $p\mathrm{CO_2}$ between the LGM and pre-industrial reaches about $63\,\mathrm{ppm}$ in the "closed-system" response of ocean carbon cycle, and about $96\,\mathrm{ppm}$ in the "open-system" response of ocean carbon cycle including carbonate compensation process. It is newly found that the enhanced stratification in the Southern Ocean amplify the response of carbonate compensation process. Under the constraints of paleo-ocean proxy data, this study demonstrates that the Southern Ocean stratification and carbonate compensation process are important for explaining atmospheric $p\mathrm{CO_2}$ reduction during glacial times.

Appendix A

Description of a sediment model

There are many previous studies using one-dimensional sediment models. It has been confirmed that the distribution of calcium carbonate and silica is reproduced consistent with observational data (*Rabouille and Gaillard*, 1990; *Archer*, 1991). In addition, responses of ocean sediments to changes in ocean circulation or organic carbon and calcium carbonate flux reaching the ocean floor have been investigated by combining ocean general circulation models (OGCMs) and sediment models (*Archer and Maier-Reimer*, 1994; *Heinze et al.*, 1999). In this study, I create a new one-dimensional simple sediment model based on previous studies (*Archer*, 1991; *Archer et al.*, 2002; *Chikamoto and Yamanaka*, 2005; *Chikamoto et al.*, 2009) to evaluate the impact of carbonate compensation process on the glacial reduction of atmospheric carbon dioxide concentration.

The processes involved are particle deposition at the sea bottom, vertical advection, bioturbation, dissolution and diffusion in the pore water, and interaction between the bottom water and the pore water. The schematic view of the process considered in the sediment model is shown in Figure A.1. The prognostic variables are four solid particles (clay, organic carbon, calcium carbonate, and biogenic silica) and five dissolved materials (phosphate, dissolved inorganic carbon, alkalinity, oxygen, and silicate) in the sediment pore water. A long-term numerical simulation is performed by imposing a two-dimensional distribution of the benthic particles flux and bottom water concentration of

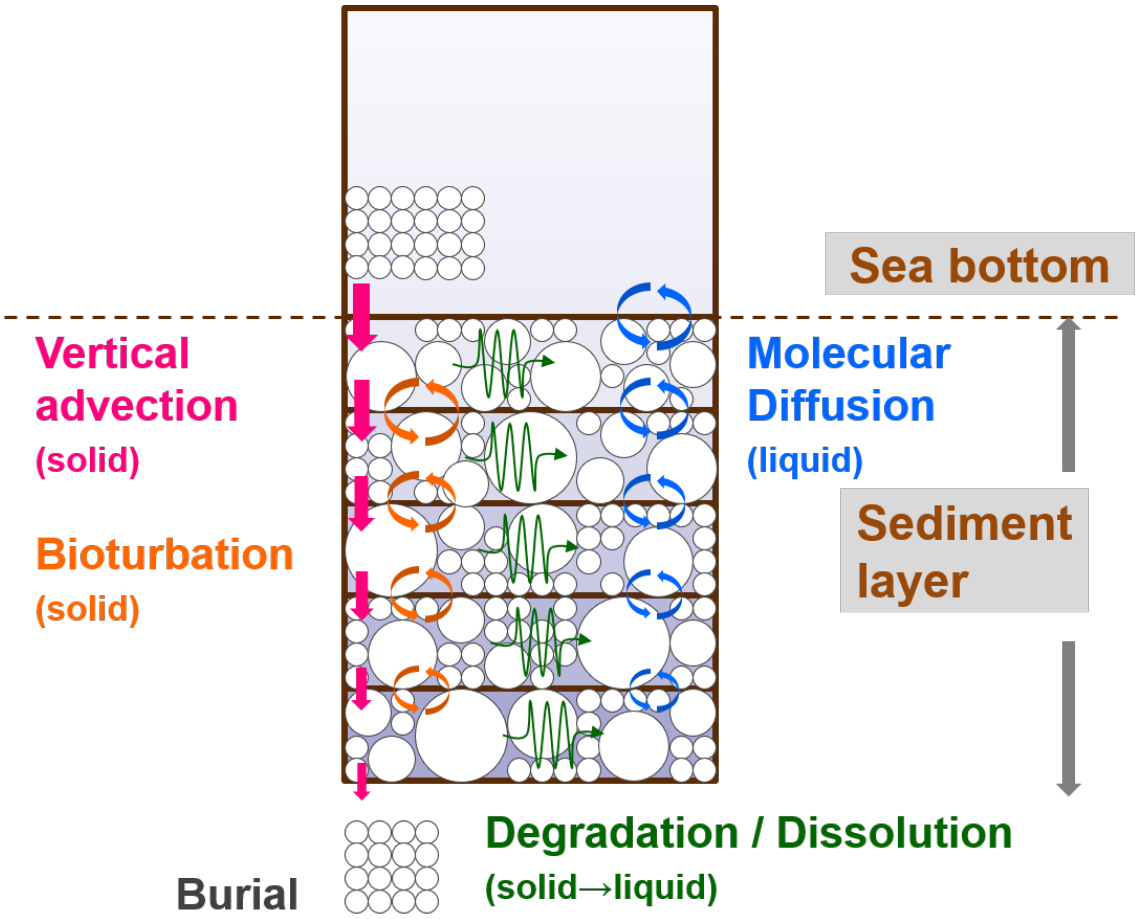

Figure A.1: Schematic view of the sediment model.

dissolved properties at the sediment-water interface.

A.1 Equations

Equations for each sediment tracer are as follows:

$$
\begin{aligned}
\frac{\partial}{\partial t}\{(1-\phi)S_{\mathrm{Clay}}\} &= \frac{\partial}{\partial z}\left\{(1-\phi)wS_{\mathrm{Clay}}\right\} + \frac{\partial}{\partial z}\left\{(1-\phi)D_B\frac{\partial S_{\mathrm{Clay}}}{\partial z}\right\} \\
\frac{\partial}{\partial t}\{(1-\phi)S_{\mathrm{POC}}\} &= \frac{\partial}{\partial z}\left\{(1-\phi)wS_{\mathrm{POC}}\right\} + \frac{\partial}{\partial z}\left\{(1-\phi)D_B\frac{\partial S_{\mathrm{POC}}}{\partial z}\right\} - (1-\phi)R_{\mathrm{POC}}S_{\mathrm{POC}} \\
\frac{\partial}{\partial t}\{(1-\phi)S_{\mathrm{CaCO_3}}\} &= \frac{\partial}{\partial z}\left\{(1-\phi)wS_{\mathrm{CaCO_3}}\right\} + \frac{\partial}{\partial z}\left\{(1-\phi)D_B\frac{\partial S_{\mathrm{CaCO_3}}}{\partial z}\right\} - (1-\phi)R_{\mathrm{CaCO_3}}S_{\mathrm{CaCO_3}} \\
\frac{\partial}{\partial t}\{(1-\phi)S_{\mathrm{SiO_2}}\} &= \frac{\partial}{\partial z}\left\{(1-\phi)wS_{\mathrm{SiO_2}}\right\} + \frac{\partial}{\partial z}\left\{(1-\phi)D_B\frac{\partial S_{\mathrm{SiO_2}}}{\partial z}\right\} - (1-\phi)R_{\mathrm{SiO_2}}S_{\mathrm{SiO_2}} \\
\frac{\partial}{\partial t}\{\phi C_{\mathrm{PO_4}}\} &= \frac{\partial}{\partial z}\left\{\phi D_E\frac{\partial C_{\mathrm{PO_4}}}{\partial z}\right\} + \mathcal{R}_{\mathrm{PO_4}}/\mathcal{R}_{\mathrm{C}}\cdot(1-\phi)R_{\mathrm{POC}}S_{\mathrm{POC}} \\
\frac{\partial}{\partial t}\{\phi C_{\mathrm{DIC}}\} &= \frac{\partial}{\partial z}\left\{\phi D_E\frac{\partial C_{\mathrm{DIC}}}{\partial z}\right\} + (1-\phi)R_{\mathrm{POC}}S_{\mathrm{POC}} + (1-\phi)R_{\mathrm{CaCO_3}}S_{\mathrm{CaCO_3}} \\
\frac{\partial}{\partial t}\{\phi C_{\mathrm{Alk}}\} &= \frac{\partial}{\partial z}\left\{\phi D_E\frac{\partial C_{\mathrm{Alk}}}{\partial z}\right\} - (1-\phi)R_{\mathrm{POC}}S_{\mathrm{POC}} + 2\cdot(1-\phi)R_{\mathrm{CaCO_3}}S_{\mathrm{CaCO_3}} \\
\frac{\partial}{\partial t}\{\phi C_{\mathrm{O_2}}\} &= \frac{\partial}{\partial z}\left\{\phi D_E\frac{\partial C_{\mathrm{O_2}}}{\partial z}\right\} - \mathcal{R}_{\mathrm{O_2}}/\mathcal{R}_{\mathrm{C}}\cdot(1-\phi)R_{\mathrm{POC}}S_{\mathrm{POC}} \\
\frac{\partial}{\partial t}\{\phi C_{\mathrm{Si(OH)_4}}\} &= \frac{\partial}{\partial z}\left\{\phi D_E\frac{\partial C_{\mathrm{Si(OH)_4}}}{\partial z}\right\} + (1-\phi)R_{\mathrm{SiO_2}}S_{\mathrm{SiO_2}},
\end{aligned}
\tag{A.1}
$$

where S is the concentration of solid particles, C is the concentration of dissolved materials, ϕ is porosity, w is the vertical advection velocity of solid particles, D_B is the vertical diffusivity for bioturbation, D_E is the vertical diffusivity for pore water diffusion, R is the dissolution rate, and $\mathcal{R}$ are redfield ratios. Porosity is the fraction of liquid water to the total sediment volume. The vertical distribution of porosity is set as

$$\phi(z) = \phi_0 \cdot \exp(-z/z_0), \tag{A.2}$$

where ϕ_0 is set to 0.90 at the sediment-water interface and z_0 is $1.823\,\mathrm{m}$ (*Berner*, 1980). From the balance of the total amount of solid particles in the sediment layer, the sedimen-

tation rate w is determined as

$$\frac{\partial}{\partial z}\{(1-\phi)w\} = -(1-\phi)(R_{\mathrm{POC}}S_{\mathrm{POC}} + R_{\mathrm{CaCO_3}}S_{\mathrm{CaCO_3}} + R_{\mathrm{SiO_2}}S_{\mathrm{SiO_2}}). \tag{A.3}$$

Bioturbation is expressed as vertical mixing in the solids. The depth-dependent mixing coefficient of bioturbation provided in *Berner* (1980) is used here.

$$D_B(z) = \frac{D_{B0}}{1+\exp\{2(z-z_B)\}} \quad \left(D_{B0} = 0.3\ \mathrm{cm}^2\ \mathrm{yr}^{-1},\ z_B = 10\ \mathrm{cm}\right). \tag{A.4}$$

The effective diffusivity D_E depends on molecular diffusivity (D_{DM}) and formation factor (F) as $D_E(z) = D_{\mathrm{DM}}/F(z)$ (*Archer et al.*, 2002). The formation factor $F(z)$ is defined as

$$F(z) = \frac{1}{\phi(z)^m}, \tag{A.5}$$

where factor m is set to 3 (*Ullman and Aller*, 1982; *Archer et al.*, 2002). The molecular diffusivity D_{DM} of each dissolved material and other model parameter values are shown in Table A.1.

A.2 Boundary conditions

Boundary conditions at the sediment-water interface are written as

$$\begin{aligned}
(1-\phi)w|_{z=0} &= F^{os}_{\mathrm{Clay}}/\rho_{\mathrm{Clay}} + F^{os}_{\mathrm{POC}}/(\rho_{\mathrm{POC}}\cdot M^{-1}_{\mathrm{POC}}) \\
&+ F^{os}_{\mathrm{CaCO_3}}/(\rho_{\mathrm{CaCO_3}}\cdot M^{-1}_{\mathrm{CaCO_3}}) + F^{os}_{\mathrm{SiO_2}}/(\rho_{\mathrm{SiO_2}}\cdot M^{-1}_{\mathrm{SiO_2}}), \\
(1-\phi)wS_{\mathrm{SP}}|_{z=0} &= F^{os}_{\mathrm{SP}\ (\mathrm{SP=Clay,\,POC,\,CaCO_3,\,SiO_2})}, \\
C_{\mathrm{DM}}\big|_{z=0} &= C^{BW}_{\mathrm{DM}\ (\mathrm{DM=PO_4,\,DIC,\,Alk,\,O_2,\,Si(OH)_4})}, \\
\text{and} & \\
\left.\frac{\partial C_{\mathrm{DM}}}{\partial z}\right|_{z=z_{\mathrm{Bottom}}} &= 0,
\end{aligned} \tag{A.6}$$

Table A.1: Parameters and references used in the sediment model.

Symbol	Parameter	Value	Reference
ρ	Density of solid sediment components	$2.6\,\mathrm{g\,cm^{-3}}$	(*Heinze et al.*, 1999)
M_{POC}	Molar weight of POC	$32.74\,\mathrm{g\,mol^{-1}}$	(*Heinze et al.*, 1999)
$M_{\mathrm{CaCO_3}}$	Molar weight of $\mathrm{CaCO_3}$	$100.0\,\mathrm{g\,mol^{-1}}$	(*Heinze et al.*, 1999)
M_{Silica}	Molar weight of Silica	$67.2\,\mathrm{g\,mol^{-1}}$	(*Heinze et al.*, 1999)
ϕ_0	Porosity ($z = 0$)	0.90	(*Berner*, 1980)
z_0	Porosity e-folding depth	$182.3\,\mathrm{cm}$	(*Berner*, 1980)
D_{B0}	Bioturbation diffusion coefficient ($z = 0$)	$3 \times 10^{-1}\,\mathrm{cm^2\,yr^{-1}}$	(*Berner*, 1980)
z_B	Bioturbation diffusion e-folding depth	$10.0\,\mathrm{cm}$	(*Berner*, 1980)
$D_{\mathrm{PO_4}}$	Pore water diffusion coefficient	$5.00 \times 10^{-10}\,\mathrm{cm^2\,s^{-1}}$	(*Archer et al.*, 2002)
D_{DIC}	Pore water diffusion coefficient	$6.40 \times 10^{-10}\,\mathrm{cm^2\,s^{-1}}$	(*Archer et al.*, 2002)
D_{Alk}	Pore water diffusion coefficient	$6.40 \times 10^{-10}\,\mathrm{cm^2\,s^{-1}}$	(*Archer et al.*, 2002)
$D_{\mathrm{O_2}}$	Pore water diffusion coefficient	$1.20 \times 10^{-9}\,\mathrm{cm^2\,s^{-1}}$	(*Archer et al.*, 2002)
$D_{\mathrm{Si(OH)_4}}$	Pore water diffusion coefficient	$5.00 \times 10^{-10}\,\mathrm{cm^2\,s^{-1}}$	(*Archer et al.*, 2002)
r_{Silica}	Rate constant for Silica redissolution	$5.0 \times 10^{-6}\,\mathrm{cm^3\,mol^{-1}\,s^{-1}}$	(*Archer et al.*, 1993)
r_{POC}	Rate constant for POC oxic redissolution	$2.0 \times 10^{-9}\,\mathrm{s^{-1}}$	(*Archer*, 1991)
r_{POC}	Rate constant for POC anoxic redissolution	$7.9 \times 10^{-11}\,\mathrm{s^{-1}}$	(*Berner*, 1980)
$r_{\mathrm{CaCO_3}}$	Rate constant for $\mathrm{CaCO_3}$ redissolution	$1.0\,\mathrm{day^{-1}}$	(*Archer*, 1991)
$\mathcal{R}_{\mathrm{PO_4}}$	Redfield coefficient for phosphate	1	(*Anderson and Sarmiento*, 1995)
$\mathcal{R}_{\mathrm{O_2}}$	Redfield coefficient for oxygen	170	(*Anderson and Sarmiento*, 1995)
$\mathcal{R}_{\mathrm{C}}$	Redfield coefficient for carbon	16	(*Anderson and Sarmiento*, 1995)

where F^{os}_{SP} is the particle deposition flux, C^{BW}_{DM} is the bottom water concentration of each dissolved material, M is the molar weight of each solid particle, and ρ is the density of each solid particle.

A.3 Dissolution terms

The remineralization rate of POC depends on the concentration of oxygen in the pore water because POC is efficiently decomposed under oxic conditions. The remineralization

rate of POC (R_{POC}) represented in *Chikamoto et al.* (2009) is used here.

$$R_{\mathrm{POC}} = \begin{cases} k_{\mathrm{OX}} & if\ [C_{\mathrm{O_2}}] > 0 \\ k_{\mathrm{AX}}, & if\ [C_{\mathrm{O_2}}] = 0 \end{cases} \tag{A.7}$$

where $k_{\mathrm{OX}} = 2 \times 10^{-9}\,\mathrm{s}^{-1}$ (*Archer*, 1991), and $k_{\mathrm{AX}} = 7.9 \times 10^{-11}\,\mathrm{s}^{-1}$ (*Berner*, 1980). Brackets indicate the concentration of dissolved materials.

The dissolution of $\mathrm{CaCO_3}$ depends on the undersaturation. Following *Chikamoto et al.* (2009), the dissolution rate of $\mathrm{CaCO_3}$ ($R_{\mathrm{CaCO_3}}$) is

$$R_{\mathrm{CaCO_3}} = \begin{cases} r_{\mathrm{CaCO_3}} \cdot \left(\dfrac{[C_{\mathrm{CO_3^{2-}}}]^{(sat)} - [C_{\mathrm{CO_3^{2-}}}]}{[C_{\mathrm{CO_3^{2-}}}]^{(sat)}} \right)^n & if\ [C_{\mathrm{CO_3^{2-}}}] < [C_{\mathrm{CO_3^{2-}}}]^{(sat)} \\ 0, & if\ [C_{\mathrm{CO_3^{2-}}}] \geq [C_{\mathrm{CO_3^{2-}}}]^{(sat)} \end{cases} \tag{A.8}$$

where $r_{\mathrm{CaCO_3}} = 1.0\,\mathrm{day}^{-1}$ (*Archer*, 1991), and $n = 4.5$ (*Keir*, 1980). The concentration of carbonate ion is determined by the carbon chemistry in the pore water.

The dissolution of silica also depends on the undersaturation. The dissolution rate of silica ($R_{\mathrm{SiO_2}}$) presented in *Archer et al.* (1993) is used here.

$$R_{\mathrm{SiO_2}} = \begin{cases} r_{\mathrm{SiO_2}} \cdot \left([C_{\mathrm{Si(OH)_4}}]^{(sat)} - [C_{\mathrm{Si(OH)_4}}] \right) & if\ [C_{\mathrm{Si(OH)_4}}] < [C_{\mathrm{Si(OH)_4}}]^{(sat)} \\ 0, & if\ [C_{\mathrm{Si(OH)_4}}] \geq [C_{\mathrm{Si(OH)_4}}]^{(sat)} \end{cases} \tag{A.9}$$

where $r_{\mathrm{SiO_2}} = 5.0 \times 10^{-6}\,\mathrm{cm}^3\,\mathrm{mol}^{-1}\,\mathrm{s}^{-1}$. The saturation concentration of silicate is

$$[C_{\mathrm{Si(OH)_4}}]^{(sat)} = \gamma_{\mathrm{Al}} 10^{\left(6.44 - \frac{968}{T}\right)}, \tag{A.10}$$

where T is temperature in the pore water, which is assumed to be the same as the ocean bottom water temperature in the ocean model. γ_{Al} represents the presence of aluminum

in the clay because the saturation concentration of silicate depends on it as

$$\gamma_{\mathrm{Al}} = \begin{cases} 0.2 & if\ \dfrac{P_{\mathrm{Clay}}}{P_{\mathrm{SiO_2}}} > 15 \\ 1.0 - \left(0.045 \dfrac{P_{\mathrm{Clay}}}{P_{\mathrm{SiO_2}}}\right)^{0.58}, & if\ \dfrac{P_{\mathrm{Clay}}}{P_{\mathrm{SiO_2}}} \leq 15 \end{cases} \tag{A.11}$$

where P_{Clay} and $P_{\mathrm{SiO_2}}$ are weight percentages of dry clay and silica, respectively.

Appendix B

Parameterization of brine rejection

I describe in detail how to introduce the parameterization of brine rejection to the ocean general circulation model COCO version 4.0 (*Hasumi*, 2006). A detailed description of sea ice model coupled to COCO is shown in *Hasumi* (2006).

Sea surface salinity flux F_S is related to the salt trapped in sea ice. It is positive when sea ice is formed and negative when sea ice melts. The virtual fresh water flux associated with sea ice production F_W is calculated from F_S as

$$F_W = F_S / S_I, \tag{B.1}$$

where S_I is the salinity contained in sea ice, and is assumed to be a constant value. Then, the brine flux F_S^{brine} is calculated from the virtual fresh water flux F_W as

$$F_S^{brine} = bf\ F_W\ S_1, \tag{B.2}$$

where bf is the brine parameter, which can take a range from 0 to 1, S_1 is the salinity of top layer in the ocean model. the brine flux F_S^{brine} is distributed from the ocean top layer to the ocean bottom layer according to the parameters. Changes in salinity due to this

brine flux is presented as

$$\frac{\Delta S_1}{\Delta t} = -\frac{S^{brine}}{\Delta z_1}, \tag{B.3}$$

where ΔS_1 is the change in salinity of the top layer, Δt is the time step, Δz_1 is the thickness of the top layer. Since similar salinity change occurs in the bottom layer, whole ocean salinity is preserved in this parameterization.

References

Adkins, J. F., K. McIntyre, and D. P. Schrag (2002), The Salinity, Temperature, and $\delta^{18}O$ of the Glacial Deep Ocean, *Science*, *298*(5599), 1769–1773, doi:10.1126/science.1076252.

Adkins, J. F. (2013), The role of deep ocean circulation in setting glacial climates, *Paleoceanography*, *28*(3), 539–561, doi:10.1002/palo.20046.

Annan J. D., and J. C. Hargreaves (2013), A new global reconstruction of temperature changes at the Last Glacial Maximum, *Clim. Past*, *9*(1), 367–376, doi:10.5194/cp-9-367-2013.

Anderson, L. A., and J. L. Sarmiento (1995), Global ocean phosphate and oxygen simulations, *Glob. Biogeochem. Cycles*, *9*(4), 621–636, doi:10.1029/95GB01902.

Anderson, R. F., S. Ali, L. I. Bradtmiller, S. H. H. Nielsen, M. Q. Fleisher, B. E. Anderson, and L. H. Burckle (2009), Wind-Driven Upwelling in the Southern Ocean and the Deglacial Rise in Atmospheric CO_2, *Science*, *323*(5920), 1443–1448, doi:10.1126/science.1167441.

Archer, D. (1991), Modeling the calcite lysocline, *J. Geophys. Res.*, *96*(C9), 17037–17050, doi:10.1029/91JC01812.

Archer, D., M. Lyle, K. Rodgers, and P. Froelich (1993), What Controls Opal

Preservation in Tropical Deep-Sea Sediments?, *Paleoceanography*, *8*(1), 7–21, doi:10.1029/92PA02803.

Archer, D., and E. Maier-Reimer (1994), Effect of deep-sea sedimentary calcite preservation on atmospheric CO_2 concentration, *Nature*, *367*(6460), 260–263, doi:10.1038/367260a0.

Archer, D. E. (1996a), An atlas of the distribution of calcium carbonate in sediments of the deep sea, *Glob. Biogeochem. Cycles*, *10*(1), 159–174, doi:10.1029/95GB03016.

Archer, D. (1996b), A data-driven model of the global calcite lysocline, *Glob. Biogeochem. Cycles*, *10*(3), 511–526, doi:10.1029/96GB01521.

Archer, D., H. Kheshgi, and E. Maier-Reimer (1997), Multiple timescales for neutralization of fossil fuel CO_2, *Geophys. Res. Lett.*, *24*(4), 405–408, doi:10.1029/97GL00168.

Archer, D., A. Winguth, D. Lea, and N. Mahowald (2000), What caused the glacial/interglacial atmospheric pCO_2 cycles?, *Rev. Geophys.*, *38*(2), 159–189, doi:10.1029/1999RG000066.

Archer, D. E., J. L. Morford, and S. R. Emerson (2002), A model of suboxic sedimentary diagenesis suitable for automatic tuning and gridded global domains, *Glob. Biogeochem. Cycles*, *16*(1), doi:10.1029/2000GB001288.

Bartlein, P. J., S. P. Harrison, S. Brewer, S. Connor, B. A. S. Davis, K. Gajewski, J. Guiot, T. I. Harrison-Prentice, A. Henderson, O. Peyron, I. C. Prentice, M. Scholze, H. Seppä, B. Shuman, S. Sugita, R. S. Thompson, A. E. Viau, J. Williams, and H. Wu (2011), Pollen-based continental climate reconstructions at 6 and 21 ka: a global synthesis, *Clim. Dyn.*, *37*(3–4), 775–802, doi:10.1007/s00382-010-0904-1.

Bereiter, B., S. Shackleton, D. Baggenstos, K. Kawamura, and J. Severinghaus (2018),

Mean global ocean temperatures during the last glacial transition, *Nature*, *553*(7686), 39–44, doi:10.1038/nature25152.

Berner, R. A. (1980), *Early Diagenesis: A Theoretical Approach*, 241 pp., Princeton University Press, Princeton, N. J.

Berner, E. K., and R. A. Berner (2012), *Global environment: water, air and geochemical cycles*, 2nd ed., 488 pp., Princeton University Press, Princeton, N. J.

Bird, M. I., J. Lloyd, and G. D. Farquhar (1994), Terrestrial carbon storage at the LGM, *Nature*, *371*(6498), 566, doi:10.1038/371566a0.

Bopp, L., K. E. Kohfeld, C. Le Quéré, and O. Aumont (2003), Dust impact on marine biota and atmospheric CO_2 during glacial periods, *Paleoceanography*, *18*(2), 1046, doi:10.1029/2002PA000810.

Bouttes, N., D. Paillard, and D. M. Roche, (2010), Impact of brine-induced stratification on the glacial carbon cycle, *Clim. Past*, *6*(5), 575–589, doi:10.5194/cp-6-575-2010.

Bouttes, N., D. Paillard, D. M. Roche, V. Brovkin, and L. Bopp (2011), Last Glacial Maximum CO_2 and $\delta^{13}C$ successfully reconciled, *Geophys. Res. Lett.*, *38*(2), L02705, doi:10.1029/2010GL044499.

Boyle, E. A., and L. Keigwin (1987), North Atlantic thermohaline circulation during the past 20,000 years linked to high-latitude surface temperature, *Nature*, *330*(6143), 35–40, doi:10.1038/330035a0.

Boyle, E. A. (1988), The role of vertical chemical fractionation in controlling late Quaternary atmospheric carbon dioxide, *J. Geophys. Res.*, *93*(C12), 15701–15714, doi:10.1029/JC093iC12p15701.

Broecker, W. S., and T. Takahashi (1977), Neutralization of fossil fuel CO_2 by marine calcium carbonate, in *The Fate of Fossil Fuel CO_2 in the Oceans*, edited by N. R. Andersen and A. Malahoff, pp. 213–241, Plenum Press, New York.

Broecker, W. S., and T. -H. Peng (1982), *Tracers in the Sea*, 690 pp., Eldigio Press, Palisades, New York.

Broecker, W. S. (1982), Glacial to interglacial changes in ocean chemistry, *Prog. Oceanogr.*, *11*(2), 151–197, doi:10.1016/0079-6611(82)90007-6.

Broecker, W. S., and T. -H. Peng (1987), The role of $CaCO_3$ compensation in the glacial to interglacial atmospheric CO_2 change, *Glob. Biogeochem. cycles*, *1*(1), 15–29, doi:10.1029/GB001i001p00015.

Broecker, W., and E. Clark (2010), Search for a glacial-age ^{14}C-depleted ocean reservoir, *Geophys. Res. Lett.*, *37*(13), L13606, doi:10.1029/2010GL043969.

Brovkin, V., A. Ganopolski, D. Archer, and S. Rahmstorf (2007), Lowering of glacial atmospheric CO_2 in response to changes in oceanic circulation and marine biogeochemistry, *Paleoceanography*, *22*(4), PA4202, doi:10.1029/2006PA001380.

Brovkin, V., A. Ganopolski, D. Archer, and G. Munhoven (2012), Glacial CO_2 cycle as a succession of key physical and biogeochemical processes, *Clim. Past*, *8*(1), 251–264, doi:10.5194/cp-8-251-2012.

Bryan, F. (1987), Parameter Sensitivity of Primitive Equation Ocean General Circulation Models, *J. Phys. Oceanogr.*, *17*(7), 970–985, doi:10.1175/1520-0485(1987)017¡0970:PSOPEO¿2.0.CO;2.

Burke, A., and L. F. Robinson (2012), The Southern Ocean's Role in Carbon Exchange During the Last Deglaciation, *Science*, *335*(6068), 557–561, doi:10.1126/science.1208163.

Caldeira, K., and P. B. Duffy (1998), Sensitivity of simulated CFC-11 distributions in a global ocean model to the treatment of salt rejected during sea-ice formation, *Geophys. Res. Lett.*, *25*(7), 1003–1006, doi:10.1029/98GL00336.

Catubig, N. R., D. E. Archer, R. Francois, P. deMenocal, W. Howard, and E. -F. Yu (1998), Global deep-sea burial rate of calcium carbonate during the Last Glacial Maximum, *Paleoceanography*, *13*(3), 298–310, doi:10.1029/98PA00609.

Chikamoto, M. O., and Y. Yamanaka (2005), Sedimentary Responses to an Abrupt Change of Biogenic Silica Flux by a Sediment Model for Long Timescale Simulations, *J. Oceanogr.*, *61*(4), 733–746, doi:10.1007/s10872-005-0080-9.

Chikamoto, M. O., K. Matsumoto, and Y. Yamanaka (2009), Influence of export rain ratio changes on atmospheric CO_2 and sedimentary calcite preservation, *J. Oceanogr.*, *65*(2), 209–221, doi:10.1007/s10872-009-0020-1.

Chikamoto, M. O., A. Abe-Ouchi, A. Oka, R. Ohgaito, and A. Timmermann (2012), Quantifying the ocean's role in glacial CO_2 reductions, *Clim. Past*, *8*(2), 545–563, doi:10.5194/cp-8-545-2012.

Ciais, P., A. Tagliabue, M. Cuntz, L. Bopp, M. Scholze, G. Hoffmann, A. Lourantou, S. P. Harrison, I. C. Prentice, D. I. Kelley, C. Koven, and S. L. Piao (2012), Large inert carbon pool in the terrestrial biosphere during the Last Glacial Maximum, *Nat. Geosci.*, *5*(1), 74–79, doi:10.1038/ngeo1324.

Ciais, P., C. Sabine, G. Bala, L. Bopp, V. Brovkin, J. Canadell, A. Chhabra, R. DeFries, J. Galloway, M. Heimann, C. Jones, C. Le Quéré, R. B. Myneni, S. Piao, and P. Thornton (2013), Carbon and Other Biogeochemical Cycles, in *Climate Change 2013: The Physical Science Basis. Contribution of Working Group I to the Fifth Assessment Report of the Intergovernmental Panel on Climate Change*, edited by T. F. Stocker, D. Qin, G. -K. Plattner, M. Tignor, S. K. Allen, J. Boschung, A. Nauels, Y. Xia, V. Bex, and P. M.

Midgley, pp. 465–570, Cambridge University Press, Cambridge, United Kingdom and New York, NY, USA., doi:10.1017/CBO9781107415324.015.

Clark, P. U., A. S. Dyke, J. D. Shakun, A. E. Carlson, J. Clark, B. Wohlfarth, J. X. Mitrovica, S. W. Hostetler, and A. M. McCabe (2009), The Last Glacial Maximum, *Science*, *325*(5941), 710–714, doi:10.1126/science.1172873.

Cléroux, C., P. deMenocal, and T. Guilderson (2011), Deglacial radiocarbon history of tropical Atlantic thermocline waters: absence of CO_2 reservoir purging signal, *Quaternary Sci. Rev.*, *30*(15–16), 1875–1882, doi:10.1016/j.quascirev.2011.04.015.

Conkright, M. E., H. E. Garcia, T. D. O'Brien, R. A. Locarnini, T. P. Boyer, C. Stephens, and J. I. Antonov (2002), *World Ocean Atlas 2001*, vol. 4, *Nutrients*, *NOAA Atlas NESDIS*, vol. 52, edited by S. Levitus, 392 pp., NOAA, Silver Spring, Md.

Crowley, T. J. (1995), Ice Age terrestrial carbon changes revisited, *Glob. Biogeochem. Cycles*, *9*(3), 379–389, doi:10.1029/95GB01107.

Cummins, P. F., G. Holloway, and E. Gargett （1990), Sensitivity of the GFDL Ocean General Circulation Model to a Parameterization of Vertical Diffusion, *J. Phys. Oceanogr.*, *20*(6), 817–830. doi:10.1175/1520-0485(1990)020¡0817:SOTGOG¿2.0.CO;2.

Curry, W. B., and D. W. Oppo (2005), Glacial water mass geometry and the distribution of $\delta^{13}C$ of $\sum CO_2$ in the western Atlantic Ocean, *Paleoceanography*, *20*(1), PA1017, doi:10.1029/2004PA001021.

De Pol-Holz, R., L. Keigwin, J. Southon, D. Hebbeln, and M. Mohtadi (2010), No signature of abyssal carbon in intermediate waters off Chile during deglaciation, *Nat. Geosci.*, *3*(3), 192–195, doi:10.1038/ngeo745.

Duffy, P. B., and K. Caldeira (1997), Sensitivity of simulated salinity in a three-dimensional ocean model to upper ocean transport of salt from sea-ice formation, *Geophys. Res. Lett.*, *24*(11), 1323–1326, doi:10.1029/97GL01294.

Dunne, J. P., J. L. Sarmiento, and A. Gnanadesikan (2007), A synthesis of global particle export from the surface ocean and cycling through the ocean interior and on the seafloor, *Glob. Biogeochem Cycles*, *21*(4), GB4006, doi:10.1029/2006GB002907.

Duplessy, J. C., N. J. Shackleton, R. G. Fairbanks, L. Labeyrie, D. Oppo, and N. Kallel (1988), Deepwater source variations during the last climatic cycle and their impact on the global deepwater circulation, *Paleoceanography*, *3*(3), 343–360, doi:10.1029/PA003i003p00343.

Duplessy, J. -C., L. Labeyrie, and C. Waelbroeck (2002), Constraints on the ocean oxygen isotopic enrichment between the Last Glacial Maximum and the Holocene: Paleoceanographic implications, *Quaternary Sci. Rev.*, *21*(1–3), 315–330, doi:10.1016/S0277-3791(01)00107-X.

Elderfield, H., P. Ferretti, M. Greaves, S. Crowhurst, I. N. McCave, D. Hodell, and A. M. Piotrowski (2012), Evolution of Ocean Temperature and Ice Volume Through the Mid-Pleistocene Climate Transition, *Science*, *337*(6095), 704–709, doi:10.1126/science.1221294.

Emerson, S., and D. Archer (1992), Glacial carbonate dissolution cycles and atmospheric $p\mathrm{CO_2}$: A view from the ocean bottom, *Paleoceanography*, *7*(3), 319–331, doi:10.1029/92PA00773.

England, M. H. (1993), Representing the Global-Scale Water Masses in Ocean General Circulation Models, *J. Phys. Oceanogr.*, *23*(7), 1523–1552, doi:10.1175/1520-0485(1993)023¡1523:RTGSWM¿2.0.CO;2.

Farrell, J. W., and W. L. Prell (1989), Climatic change and $CaCO_3$ preservation: An 800,000 year bathymetric Reconstruction from the central equatorial Pacific Ocean, *Paleoceanography*, *4*(4), 447–466, doi:10.1029/PA004i004p00447.

Fischer, H., F. Fundela, U. Rutha, B. Twarloha, A. Wegnera, R. Udistib, S. Becaglib, E. Castellanob, A. Morgantib, M. Severib, E. Wolffc, and G. Littotc, (2007), Reconstruction of millennial changes in dust emission, transport and regional sea ice coverage using the deep EPICA ice cores from the Atlantic and Indian Ocean sector of Antarctica, *Earth Planet. Sci. Lett.*, *260*(1–2), 340–354, doi:10.1016/j.epsl.2007.06.014.

Fischer, H., J. Schmitt, D. Lüthi, T. F. Stocker, T. Tschumi, P. Parekh, F. Joos, P. Köhler, C. Völker, R. Gersonde, C. Barbante, M. Le Floch, D. Raynaud, and E. Wolff (2010), The role of Southern Ocean processes in orbital and millennial CO_2 variations - A synthesis, *Quaternary Sci. Rev.*, *29*(1–2), 193–205, doi:10.1016/j.quascirev.2009.06.007.

Francois, R., M. A. Altabet, E. -F. Yu, D. M. Sigman, M. P. Bacon, M. Frank, G. Bohrmann, G. Bareille, and L. D. Labeyrie (1997), Contribution of Southern Ocean surface-water stratification to low atmospheric CO_2 concentrations during the last glacial period, *Nature*, *38*(6654), 929–935, doi:10.1038/40073.

Fung, I. Y., S. K. Meyn, I. Tegen, S. C. Doney, J. G. John, and J. K. B. Bishop (2000), Iron supply and demand in the upper ocean, *Glob. Biogeochem. Cycles*, *14*(1), 281–295, doi:10.1029/1999GB900059.

Galbraith, E. D., S. L. Jaccard, T. F. Pedersen, D. M. Sigman, G. H. Haug, M. Cook, J. R. Southon, and R. Francois, (2007), Carbon dioxide release from the North Pacific abyss during the last deglaciation, *Nature*, *449*(7164), 890–893, doi:10.1038/nature06227.

Gargett, A. E. (1984), Vertical eddy diffusivity in the ocean interior, *J. Mar. Res.*, *42*(2), 359–393, doi:10.1357/002224084788502756.

Gaspari, V., C. Barbante, G. Cozzi, P. Cescon, C. F. Boutron, P. Gabrielli, G. Capodaglio, C. Ferrari, J. R. Petit, and B. Delmonte (2006), Atmospheric iron fluxes over the last deglaciation: Climatic implications, *Geophys. Res. Lett.*, *33*(3), L03704, doi:10.1029/2005GL024352.

Gehlen, M., L. Bopp, N. Emprin, O. Aumont, C. Heinze, and O. Ragueneau (2006), Reconciling surface ocean productivity, export fluxes and sediment composition in a global biogeochemical ocean model, *Biogeosciences*, *3*(4), 521–537, doi:10.5194/bg-3-521-2006.

Gersonde, R., X. Crosta, A. Abelmann, and L. Armand (2005), Sea-surface temperature and sea ice distribution of the Southern Ocean at the EPILOG Last Glacial Maximum—a circum-Antarctic view based on siliceous microfossil records, *Quaternary Sci. Rev.*, *24*(7-9), 869–896, doi:10.1016/j.quascirev.2004.07.015.

Gordon, A. L. (1978), Deep Antarctic Convection West of Maud Rise, *J. Phys. Oceanogr.*, *8*(4), 600–612, doi:10.1175/1520-0485(1978)008¡0600:DACWOM¿2.0.CO;2.

Gordon, A. L. (1998), Western Weddell Sea Thermohaline Stratification, in *Ocean, Ice, and Atmosphere: Interactions at the Antarctic Continental Margin*, edited by S. S. Jacobs and R. F. Weiss, pp. 215–240, American Geophysical Union, Washington, D. C., doi:10.1029/AR075p0215.

Gregg, M. C. (1989), Scaling turbulent dissipation in the thermocline, *J. Geophys. Res.*, *94*(C7), 9686–9698, doi:10.1029/JC094iC07p09686.

Griffies, S. M., A. Biastoch, C. Böning, F. Bryan, G. Danabasoglu, E. P. Chassignet, M. H. England, R. Gerdes, H. Haak, R. W. Hallberg, W. Hazeleger, J. Jungclaus, W. G. Large, G. Madec, A. Pirani, B. L. Samuels, M. Scheinert, A. S. Gupta, C. A. Severijns, H. L. Simmons, A. M. Treguier, M. Winton, S. Yeager, and J. Yin (2009), Co-

ordinated Ocean-ice Reference Experiments (COREs), *Ocean Modell.*, *26*(1–2), 1–46, doi:10.1016/j.ocemod.2008.08.007.

Hain, M. P., D. M. Sigman, and G. H. Haug (2010), Carbon dioxide effects of Antarctic stratification, North Atlantic Intermediate Water formation, and subantarctic nutrient drawdown during the last ice age: Diagnosis and synthesis in a geochemical box model, *Glob. Biogeochem. Cycles*, *24*(4), GB4023, doi:10.1029/2010GB003790.

Hasumi, H., and N. Suginohara （1999）, Atlantic deep circulation controlled by heating in the Southern Ocean, *Geophys. Res. Lett.*, *26*(13), 1873–1876, doi:10.1029/1999GL900420.

Hasumi, H. (2006), CCSR Ocean Component Model (COCO) Version 4.0, *CCSR Rep. 25*, 103 pp., Center for Climate System Research, Univ. of Tokyo, Japan.

Heinze, C., E. Maier-Reimer, A. M. E. Winguth, and D. Archer (1999), A global oceanic sediment model for long-term climate studies, *Glob. Biogeochem. Cycles*, *13*(1), 221–250, doi:10.1029/98GB02812.

Henderson, G. M., C. Heinze, R. F. Anderson, and A. M. E. Winguth (1999), Global distribution of the $^{230}\mathrm{Th}$ flux to ocean sediments constrained by GCM modelling, *Deep-Sea Res.*, *46*(11), 1861–1893, 10.1016/S0967-0637(99)00030-8.

Heuzé, C., K. J. Heywood, D. P. Stevens, and J. K. Ridley (2013), Southern Ocean bottom water characteristics in CMIP5 models, *Geophys. Res. Lett.*, *40*(7), 1409–1414, doi:10.1002/grl.50287.

Hodell D. A., C. D. Charles, and F. J. Sierro (2001), Late Pleistocene evolution of the ocean's carbonate system, *Earth Planet. Sci. Lett.*, *192*(2), 109–124, doi:10.1016/S0012-821X(01)00430-7.

Hodell, D. A., K. A. Venz, C. D. Charles, and U. S. Ninnemann (2003), Pleistocene vertical carbon isotope and carbonate gradients in the South Atlantic sector of the Southern Ocean, *Geochem. Geophys. Geosyst.*, *4*(1), 1–19, doi:10.1029/2002GC000367.

Insua, T. L., A. J. Spivack, D. Graham, S. D'Hondt, and K. Moran (2014), Reconstruction of Pacific Ocean bottom water salinity during the Last Glacial Maximum, *Geophys. Res. Lett.*, *41*(8), 2914–2920, doi:10.1002/2014GL059575.

IPCC, (2013) *Climate Change 2013: The Physical Science Basis. Contribution of Working Group I to the Fifth Assessment Report of the Intergovernmental Panel on Climate Change*, edited by T. F. Stocker, D. Qin, G. -K. Plattner, M. Tignor, S. K. Allen, J. Boschung, A. Nauels, Y. Xia, V. Bex, and P. M. Midgley, 1535 pp. Cambridge University Press, Cambridge, United Kingdom and New York, NY, USA.

Ito, T., and M. J. Follows (2011), Preformed phosphate, soft tissue pump and atmospheric CO_2, *J. Mar. Res.*, *63*(4), 813–839, doi:10.1357/0022240054663231.

Jaccard S. L., E. D. Galbraith, D. M. Sigman, G. H. Haug, R. Francois, T. F. Pedersen, P. Dulski, and H. R. Thierstein (2009), Subarctic Pacific evidence for a glacial deepening of the oceanic respired carbon pool, *Earth Planet. Sci. Lett.*, *277*(1–2), 156–165, doi:10.1016/j.epsl.2008.10.017.

Jouzel, J., V. Masson-Delmotte, O. Cattani, G. Dreyfus, S. Falourd, G. Hoffmann, B. Minster, J. Nouet, J. M. Barnola, J. Chappellaz, H. Fischer, J. C. Gallet, S. Johnsen, M. Leuenberger, L. Loulergue, D. Luethi, H. Oerter, F. Parrenin, G. Raisbeck, D. Raynaud, A. Schilt, J. Schwander, E. Selmo, R. Souchez, R. Spahni, B. Stauffer, J. P. Steffensen, B. Stenni, T. F. Stocker, J. L. Tison, M. Werner, and E. W. Wolff (2007), Orbital and Millennial Antarctic Climate Variability over the Past 800,000 Years, *Science*, *317*(5839), 793–796, doi:10.1126/science.1141038.

K-1 Model Developers (2004), K-1 Coupled GCM (MIROC) Description, *K-1 Tech. Rep.*

1, edited by H. Hasumi and S. Emori, 34 pp., Center for Climate System Research, Univ. of Tokyo., Japan.

Key, R. M., A. Kozyr, C. L. Sabine, K. Lee, R. Wanninkhof, J. L. Bullister, R. A. Feely, F. J. Millero, C. Mordy, and T. -H. Peng (2004), A global ocean carbon climatology: Results from Global Data Analysis Project (GLODAP), *Glob. Biogeochem. Cycles*, *18*(4), GB4031, doi:10.1029/2004GB002247.

Klaas, C., and D. E. Archer (2002), Association of sinking organic matter with various types of mineral ballast in the deep sea: Implications for the rain ratio, *Glob. Biogeochem. Cycles*, *16*(4), 1116, doi:10.1029/2001GB001765.

Keir, R. S. (1980), The dissolution kinetics of biogenic calcium carbonates in seawater, *Geochim. Cosmochim. Acta.*, *44*(2), 241–252, doi:10.1016/0016-7037(80)90135-0.

Knox, F., and M. B. McElroy (1984), Changes in atmospheric CO_2: Influence of the marine biota at high latitude *J. Geophys. Res.*, *89*(D3), 4629–4637, doi:10.1029/JD089iD03p04629.

Kobayashi, H., A. Abe-Ouchi, and A. Oka (2015), Role of Southern Ocean stratification in glacial atmospheric CO_2 reduction evaluated by a three-dimensional ocean general circulation model, *Paleoceanography*, *30*(9), 1202–1216, doi:10.1002/2015PA002786.

Kohfeld, K. E., and S. P. Harrison (2001), DIRTMAP: the geological record of dust, *Earth Sci. Rev.*, *54*(1–3), 81–114, doi:10.1016/S0012-8252(01)00042-3.

Kohfeld, K. E., C. Le Quéré, S. P. Harrison, and R. F. Anderson (2005), Role of Marine Biology in Glacial-Interglacial CO_2 Cycles, *Science*, *308*(5718), 74–78, doi:10.1126/science.1105375.

Kohfeld, K. E., and A. Ridgwell (2009), Glacial-Interglacial Variability in Atmospheric CO_2, in *Surface Ocean-Lower Atmosphere Processes*, edited by C. Le Quéré and

E. S. Saltzman, pp. 251–286, American Geophysical Union, Washington, D. C., doi:10.1029/2008GM000845.

Köhler, P., H. Fischer, G. Munhoven, and R. E. Zeebe (2005), Quantitative interpretation of atmospheric carbon records over the last glacial termination, *Glob. Biogeochem. Cycles*, *19*(4), GB4020, doi:10.1029/2004GB002345.

Kurahashi-Nakamura, T., A. Abe-Ouchi, Y. Yamanaka, and K. Misumi (2007), Compound effects of Antarctic sea ice on atmospheric $p\mathrm{CO}_2$ change during glacial-interglacial cycle, *Geophys. Res. Lett.*, *34*(20), L20708, doi:10.1029/2007GL030898.

Kusahara, K., T. Sato, A. Oka, T. Obase, R. Greve, A. Abe-Ouchi, and H. Hasumi (2015), Modeling Antarctic marine cryosphere at the Last Glacial Maximum, *Ann. Glaciol.*, *56*(69), 425–435, doi:10.3189/2015AoG69A792.

Kwon, E. Y., F. Primeau, and J. L. Sarmiento (2009), The impact of remineralization depth on the air-sea carbon balance, *Nat. Geosci.*, *2*(9), 630–635, doi:10.1038/ngeo612.

Lambert, F., B. Delmonte, J. R. Petit, M. Bigler, P. R. Kaufmann, M. A. Hutterli, T. F. Stocker, U. Ruth, J. P. Steffensen, and V. Maggi (2008), Dust-climate couplings over the past 800,000 years from the EPICA Dome C ice core, *Nature*, *452*(7187), 616–619, doi:10.1038/nature06763.

Lambert, F., A. Tagliabue, G. Shaffer, F. Lamy, G. Winckler, L. Farias, L. Gallardo, and R. De Pol-Holz (2015), Dust fluxes and iron fertilization in Holocene and Last Glacial Maximum climates, *Geophys. Res. Lett.*, *42*(14), 6014–6023, doi:10.1002/2015GL064250.

Lamy F., H. W. Arz, R. Kilian, C. B. Lange, L. Lembke-Jene, M. Wengler, J. Kaiser, O. Baeza-Urrea, I. R. Hall, N. Harada, and R. Tiedemann (2015), Glacial reduction and millennial-scale variations in Drake Passage throughflow, *Proc. Natl. Acad. Sci. USA*, *112*(44), 13496–13501, doi:10.1073/pnas.1509203112.

Ledwell, J. R., A. J. Watson, and C. S. Law (1993), Evidence for slow mixing across the pycnocline from an open-ocean tracer-release experiment, *Nature*, *364*(6439), 701–703, doi:10.1038/364701a0.

Locarnini, R. A., T. D. O'Brien, H. E. Garcia, J. I. Antonov, T. P. Boyer, M. E. Conkright, and C. Stephens (2002), *World Ocean Atlas 2001*, vol. 3, *Oxygen*, *NOAA Atlas NESDIS*, vol. 51, edited by S. Levitus, 286 pp., NOAA, Silver Spring, Md.

Lumpkin, R., and K. Speer (2007), Global Ocean Meridional Overturning *J. Phys. Oceanogr.*, *37*(10), 2550–2562, doi:10.1175/JPO3130.1.

Lüthi, D., M. Le Floch, B. Bereiter, T. Blunier, J. -M. Barnola, U. Siegenthaler, D. Raynaud, J. Jouzel, H. Fischer, K. Kawamura, and T. F. Stocker (2008), High-resolution carbon dioxide concentration record 650,000–800,000 years before present, *Nature*, *453*(7193), 379–382, doi:10.1038/nature06949.

Lynch-Stieglitz, J., J. F. Adkins, W. B. Curry, T. Dokken, I. R. Hall, J. C. Herguera, J. J. M. Hirschi, E. V. Ivanova, C. Kissel, O. Marchal, T. M. Marchitto, I. N. McCave, J. F. McManus, S. Mulitza, U. Ninnemann, F. Peeters, E. -F. Yu, and R. Zahn (2007), Atlantic Meridional Overturning Circulation During the Last Glacial Maximum, *Science*, *316*(5821), 66–69, doi:10.1126/science.1137127.

Maher, B. A., J. M. Prospero, D. Mackie, D. Gaiero, P. P. Hesse, and Y. Balkanski (2010), Global connections between aeolian dust, climate and ocean biogeochemistry at the present day and at the last glacial maximum, *Earth Sci. Rev.*, *99*(1–2), 61–97, doi:10.1016/j.earscirev.2009.12.001.

Marchitto, T. M., and W. S. Broecker (2006), Deep water mass geometry in the glacial Atlantic Ocean: A review of constraints from the paleonutrient proxy Cd/Ca, *Geochem. Geophys. Geosyst.*, *7*(12), Q12003, doi:10.1029/2006GC001323.

Marchitto, T. M., S. J. Lehman, K. D. Ortiz, J. Flückiger, and A. van Geen (2007), Marine Radiocarbon Evidence for the Mechanism of Deglacial Atmospheric CO_2 Rise, *Science*, *316*(5830), 1456–1459, doi:10.1126/science.1138679.

MARGO Project Members (2009), Constraints on the magnitude and patterns of ocean cooling at the Last Glacial Maximum, *Nat. Geosci.*, *2*(2), 127–132, doi:10.1038/ngeo411.

Marinov, I., A. Gnanadesikan, J. L. Sarmiento, J. R. Toggweiler, M. J. Follows, and B. K. Mignone (2008), Impact of oceanic circulation on biological carbon storage in the ocean and atmospheric $p\mathrm{CO}_2$, *Glob. Biogeochem. Cycles*, *22*(3), GB3007, doi:10.1029/2007GB002958.

Marotzke, J. (1997), Boundary Mixing and the Dynamics of Three-Dimensional Thermohaline Circulations, *J. Phys. Oceanogr.*, *27*(8), 1713–1728, doi:10.1175/1520-0485(1997)027¡1713:BMATDO¿2.0.CO;2.

Martin, J. H., G. A. Knauer, D. M. Karl, and W. W. Broenkow (1987), VERTEX: carbon cycling in the northeast Pacific, *Deep-Sea Res.*, *34*(2), 267–285, doi:10.1016/0198-0149(87)90086-0.

Martin, J. H. (1990), Glacial-interglacial CO_2 change: The iron hypothesis, *Paleoceanography*, *5*(1), 1–13, doi:10.1029/PA005i001p00001.

Martínez-Garcia, A., A. Rosell-Melé, W. Geibert, R. Gersonde, P. Masqué, V. Gaspari, and C. Barbante (2009), Links between iron supply, marine productivity, sea surface temperature, and CO_2 over the last 1.1 Ma, *Paleoceanography*, *24*(1), PA1207, doi:10.1029/2008PA001657.

Matsumoto, K., J. L. Sarmiento, and M. A. Brzezinski (2002), Silicic acid leakage from the Southern Ocean: A possible explanation for glacial atmospheric $p\mathrm{CO}_2$, *Glob. Biogeochem. Cycles*, *16*(3), 5-1–5-23, doi:10.1029/2001GB001442.

Matsumoto, K., T. Hashioka, and Y. Yamanaka (2007), Effect of temperature-dependent organic carbon decay on atmospheric $p\mathrm{CO}_2$, *J. Geophys. Res.*, *112*(G2), G02007, doi:10.1029/2006JG000187.

Mazaud, A., E. Michel, F. Dewilde, and J. L. Turon (2010), Variations of the Antarctic Circumpolar Current intensity during the past 500 ka, *Geochem. Geophys. Geosyst.*, *11*(8), Q08007, doi:10.1029/2010GC003033.

McCave, I. N., S. J. Crowhurst, G. Kuhn, C -D. Hillenbrand, and M. P. Meredith (2014), Minimal change in Antarctic Circumpolar Current flow speed between the last glacial and Holocene, *Nat. Geosci.*, *7*(2), 113–116, doi:10.1038/NGEO2037.

Meckler, A. N., D. M. Sigman, K. A. Gibson, R. Francois, A. Martínez-García, S. L. Jaccard, U. Röhl, L. C. Peterson, R. Tiedemann, and G. H. Haug (2013), Deglacial pulses of deep-ocean silicate into the subtropical North Atlantic Ocean, *Nature*, *495*(7442), 495–498, doi:10.1038/nature12006.

Menviel, L., A. Timmermann, A. Mouchet, and O. Timm (2008), Climate and marine carbon cycle response to changes in the strength of the Southern Hemispheric westerlies, *Paleoceanography*, *23*(4), PA4201, doi:10.1029/2008PA001604.

Menviel, L., A. Timmermann, O. Elison Timm, A. Mouchet, A. Abe-Ouchi, M. O. Chikamoto, N. Harada, R. Ohgaito, and Y. Okazaki (2012), Removing the North Pacific halocline: Effects on global climate, ocean circulation and the carbon cycle, *Deep-Sea Res.*, *61–64*, 106–113, doi:10.1016/j.dsr2.2011.03.005.

Millero, F. J. (1995), Thermodynamics of the carbon dioxide system in the oceans, *Geochim. Cosmochim. Acta.*, *59*(4), 661–677, doi:10.1016/0016-7037(94)00354-O.

Milliman, J. D., and A. W. Droxler (1996), Neritic and pelagic carbonate sedimentation in the marine environment: ignorance is not bliss, *Geol. Rund.*, *85*(3), 496–504, doi:10.1007/BF02369004.

Nakata, M., and N. Suginohara (1998), Role of deep stratification in transporting deep water from the Atlantic to the Pacific, *J. Geophys. Res.*, *103*(C1), 1067–1086, doi:10.1029/97JC02547.

Negre, C., R. Zahn, A. L. Thomas, P. Masqué, G. M. Henderson, G. Martínez-Méndez, I. R. Hall, and J. L. Mas (2010), Reversed flow of Atlantic deep water during the Last Glacial Maximum, *Nature*, *468*(7320), 84–88, doi:10.1038/nature09508.

Nikurashin, M., and G. Vallis (2011), A Theory of Deep Stratification and Overturning Circulation in the Ocean, *J. Phys. Oceanogr.*, *41*(3), 485–502, doi:10.1175/2010JPO4529.1.

Niwa, Y., and T. Hibiya (2011), Estimation of baroclinic tide energy available for deep ocean mixing based on three-dimensional global numerical simulations, *J. Oceanogr.*, *67*(4), 493–502, doi:10.1007/s10872-011-0052-1.

Oka, A., S. Kato, and H. Hasumi (2008), Evaluating effect of ballast mineral on deep-ocean nutrient concentration by using an ocean general circulation model, *Glob. Biogeochem. Cycles*, *22*(3), GB3004, doi:10.1029/2007GB003067.

Oka, A., A. Abe-Ouchi, M. O. Chikamoto, and T. Ide (2011a), Mechanisms controlling export production at the LGM: Effects of changes in oceanic physical fields and atmospheric dust deposition, *Glob. Biogeochem. Cycles*, *25*(2), GB2009, doi:10.1029/2009GB003628.

Oka, A., E. Tajika, A. Abe-Ouchi, and K. Kubota (2011b), Role of the ocean in controlling atmospheric CO_2 concentration in the course of global glaciations, *Clim. Dyn.*, *37*(9–10), 1755–1770, doi:10.1007/s00382-010-0959-z.

Oka, A., H. Hasumi, and A. Abe-Ouchi (2012), The thermal threshold of the Atlantic meridional overturning circulation and its control by wind stress forcing during glacial climate, *Geophys. Res. Lett.*, *39*(9), L09709, doi:10.1029/2012GL051421.

Oka, A., and Y. Niwa (2013), Pacific deep circulation and ventilation controlled by tidal mixing away from the sea bottom, *Nat. Commun.*, *4*(2419), doi:10.1038/ncomms3419.

Orsi, A. H., G. C. Johnson, and J. L. Bullister (1999), Circulation, mixing, and production of Antarctic Bottom Water, *Prog. Oceanogr.*, *43*(1), 55–109, doi:10.1016/S0079-6611(99)00004-X.

Otto-Bliesner, B. L., C. D. Hewitt, T. M. Marchitto, E. Brady, A. Abe-Ouchi, M. Crucifix, S. Murakami, and S. L. Weber (2007), Last Glacial Maximum ocean thermohaline circulation: PMIP2 model intercomparisons and data constraints, *Geophys. Res. Lett.*, *34*(12), L12706, doi:10.1029/2007GL029475.

Parekh, P., M. J. Follows, and E. A. Boyle (2005), Decoupling of iron and phosphate in the global ocean, *Glob. Biogeochem. Cycles*, *19*(2), GB2020, doi:10.1029/2004GB002280.

Peacock, S., E. Lane, and J. M. Restrepo (2006), A possible sequence of events for the generalized glacial-interglacial cycle, *Glob. Biogeochem. Cycles*, *20*(2), GB2010, doi:10.1029/2005GB002448.

Peterson, C. D., L. E. Lisiecki, and J. V. Stern (2014), Deglacial whole-ocean $\delta^{13}\mathrm{C}$ change estimated from 480 benthic foraminiferal records, *Paleoceanography*, *29*(6), 549–563, doi:10.1002/2013PA002552.

Petit, J. R., J. Jouzel, D. Raynaud, N. I. Barkov, J. -M. Barnola, I. Basile, M. Bender, J. Chappellaz, M. Davis, G. Delaygue, M. Delmotte, V. M. Kotlyakov, M. Legrand, V. Y. Lipenkov, C. Lorius, L. Pépin, C. Ritz, E. Saltzman, and M. Stievenard (1999), Climate and atmospheric history of the past 420,000 years from the Vostok ice core, Antarctica, *Nature*, *399*(6735), 429–436, doi:10.1038/20859.

Rabouille, C., and J. -F. Gaillard (1990), The validity of steady-state flux calculations in early diagenesis: a computer simulation of deep-sea silica diagenesis, *Deep-Sea Res.*, *37*(4), 625–646, doi:10.1016/0198-0149(90)90094-C.

Redfield, A. C., B. H. Ketchum, and F. A. Richards (1963), The influence of organisms on the composition of sea water, in *The Sea*, vol. 2, edited by M. N. Hill, pp. 26–77, Wiley Interscience, New York.

Rintoul, S. R. (1998), On the origin and influence of Adelie Land bottom water, in *Ocean, Ice, and Atmosphere: Interactions at the Antarctic Continental Margin*, Antarct. Res. Ser., vol. 75, edited by S. S. Jacobs and R. F. Weiss, pp. 151–171, American Geophysical Union, Washington, D. C.

Robinson, L. F., J. F. Adkins, L. D. Keigwin, J. Southon, D. P. Fernandez, S. -L. Wang, D. S. Scheirer (2005), Radiocarbon Variability in the Western North Atlantic During the Last Deglaciation, *Science*, *310*(5753), 1469–1473, doi:10.1126/science.1114832.

Rojas, M., P. Moreno, M. Kageyama, M. Crucifix, C. Hewitt, A. Abe-Ouchi, R. Ohgaito, E. C. Brady, and P. Hope (2009), The Southern Westerlies during the last glacial maximum in PMIP2 simulations, *Clim. Dyn.*, *32*(4), 525–548, doi:10.1007/s00382-008-0421-7.

Roth, R., S. P. Ritz, and F. Joos (2014), Burial-nutrient feedbacks amplify the sensitivity of atmospheric carbon dioxide to changes in organic matter remineralisation, *Earth Syst. Dynam.*, *5*(2), 321–343, doi:10.5194/esd-5-321-2014.

Sarmiento, J. L., and J. R. Toggweiler (1984), A new model for the role of the oceans in determining atmospheric $\mathrm{PCO_2}$, *Nature*, *308*(5960), 621–624, doi:10.1038/308621a0.

Sarmiento, J. L., J. Dunne, A. Gnanadesikan, R. M. Key, K. Matsumoto, and R. Slater (2002), A new estimate of the $\mathrm{CaCO_3}$ to organic carbon export ratio, *Glob. Biogeochem. Cycles*, *16*(4), 1107, doi:10.1029/2002GB001919.

Sarmiento, J. L., N. Gruber, M. A. Brzezinski, and J. P. Dunne (2004), High-latitude controls of thermocline nutrients and low latitude biological productivity, *Nature*, *427*(6969), 56–60, doi:10.1038/nature02127.

Sarmiento, J. L., and N. Gruber, (2006), Ocean Biogeochemical Cycles, 526 pp., Prinston Univ. Press, Prinston, N. J.

Schmittner, A., and E. D. Galbraith (2008), Glacial greenhouse-gas fluctuations controlled by ocean circulation changes, *Nature*, *456*(7220), 373–376, doi:10.1038/nature07531.

Schmittner, A., J. A. M. Green, and S. -B. Wilmes (2015), Glacial ocean overturning intensified by tidal mixing in a global circulation model, *Geophys. Res. Lett.*, *42*(10), 4014–4022, doi:10.1002/2015GL063561.

Schmitz Jr., W. J. (1995), On the interbasin-scale thermohaline circulation, *Rev. Geophys.*, *33*(2), 151–173, doi:10.1029/95RG00879.

Schrag, D. P., J. F. Adkins, K. McIntyre, J. L. Alexander, D. A. Hodell, C. D. Charles, and J. F. McManus (2002), The oxygen isotopic composition of seawater during the Last Glacial Maximum, *Quaternary Sci. Rev.*, *21*(1–3), 331–342, doi:10.1016/S0277-3791(01)00110-X.

Seiter, K., C. Hensen, J. Schröter, and M. Zabel (2004), Organic carbon content in surface sediments—defining regional provinces, *Deep-Sea Res.*, *51*(12), 2001–2026, doi:10.1016/j.dsr.2004.06.014.

Shakun, J. D., P. U. Clark, F. He, S. A. Marcott, A. C. Mix, Z. Liu, B. Otto-Bliesner, A. Schmittner, and E. Bard (2012), Global warming preceded by increasing carbon dioxide concentrations during the last deglaciation, *Nature*, *484*(7392), 49–54, doi:10.1038/nature10915.

Siegenthaler, U., and Th. Wenk (1984), Rapid atmospheric CO_2 variations and ocean circulation, *Nature*, *308*(5960), 624–626, doi:10.1038/308624a0.

Siegenthaler, U., T. F. Stocker, E. Monnin, D. Lüthi, J. Schwander, B. Stauffer, D. Raynaud, J. -M. Barnola, H. Fischer, V. Masson-Delmotte, and J. Jouzel (2005), Stable

Carbon Cycle–Climate Relationship During the Late Pleistocene, *Science*, *310*(5752), 1313–1317, doi:10.1126/science.1120130.

Sigman, D. M., and E. A. Boyle (2000), Glacial/interglacial variations in atmospheric carbon dioxide, *Nature*, *407*(6806), 859–869, doi:10.1038/35038000.

Sigman, D. M., M. P. Hain, and G. H. Haug (2010), The polar ocean and glacial cycles in atmospheric CO_2 concentration, *Nature*, *466*(7302), 47–55, doi:10.1038/nature09149.

Skinner, L. C., S. Fallon, C. Waelbroeck, E. Michel, and S. Barker (2010), Ventilation of the Deep Southern Ocean and Deglacial CO_2 Rise, *Science*, *328*(5982), 1147–1151, doi:10.1126/science.1183627.

Steele, M., R. Morley, and W. Ermold, (2001), PHC: A Global Ocean Hydrography with a High-Quality Arctic Ocean, *J. Climate*, *14*(9), 2079–2087, doi:10.1175/1520-0442(2001)014¡2079:PAGOHW¿2.0.CO;2.

Stephens, B. B., and R. F. Keeling (2000), The influence of Antarctic sea ice on glacial-interglacial CO_2 variations, *Nature*, *404*(6774), 171–174, doi:10.1038/35004556.

St. Laurent, L. C., H. L. Simmons, and S. R. Jayne (2002), Estimating tidally driven mixing in the deep ocean, *Geophys. Res. Lett.*, *29*(23), 2106, doi:10.1029/2002GL015633.

Sun, X., and K. Matsumoto (2010), Effects of sea ice on atmospheric $p\mathrm{CO}_2$: A revised view and implications for glacial and future climates, *J. Geophys. Res.*, *115*(G2), G02015, doi:10.1029/2009JG001023.

Sun, S., I. Eisenman, and A. L. Stewart (2016), The influence of Southern Ocean surface buoyancy forcing on glacial-interglacial changes in the global deep ocean stratification, *Geophys. Res. Lett.*, *43*(15), 8124–8132, doi:10.1002/2016GL070058.

Sundquist, E. T. (1991), Steady- and non-steady-state carbonate-silicate controls on atmosphere CO_2, *Quaternary Sci. Rev.*, *10*(2–3), 283–296, doi:10.1016/0277-3791(91)90026-Q.

Tagliabue, A., L. Bopp, D. M. Roche, N. Bouttes, J. -C. Dutay, R. Alkama, M. Kageyama, E. Michel, and D. Paillard (2009), Quantifying the roles of ocean circulation and biogeochemistry in governing ocean carbon-13 and atmospheric carbon dioxide at the last glacial maximum, *Clim. Past*, *5*(4), 695–706, doi:10.5194/cp-5-695-2009.

Takahashi, T., S. C. Sutherland, R. Wanninkhof, C. Sweeney, R. A. Feely, D. W. Chipman, B. Hales, G. Friederich, F. Chavez, C. Sabine, A. Watson, D. C. E. Bakker, U. Schuster, N. Metzl, H. Yoshikawa-Inoue, M. Ishii, T. Midorikawa, Y. Nojiri, A. Krtzinger, T. Steinhoff, M. Hoppema, J. Olafsson, T. S. Arnarson, B. Tilbrook, T. Johannessen, A. Olsen, R. Bellerby, C. S. Wong, B. Delille, N. R. Bates, and H. J. W. de Baar (2009), Climatological mean and decadal change in surface ocean $p\mathrm{CO_2}$, and net sea-air CO_2 flux over the global oceans, *Deep-Sea Res.*, *56*(8–10), 554–577, doi:10.1016/j.dsr2.2008.12.009.

Takemura, T., T. Nozawa, S. Emori, T. Y. Nakajima, and T. Nakajima (2005), Simulation of climate response to aerosol direct and indirect effects with aerosol transport-radiation model, *J. Geophys. Res.*, *110*(D2), D02202, doi:10.1029/2004JD005029.

Takemura, T., M. Egashira, K. Matsuzawa, H. Ichijo, R. O'ishi, and A. Abe-Ouchi (2009), A simulation of the global distribution and radiative forcing of soil dust aerosols at the Last Glacial Maximum, *Atmos. Chem. Phys.*, *9*(9), 3061–3073, doi:10.5194/acp-9-3061-2009.

Talley, L. D. (2013), Closure of the global overturning circulation through the Indian, Pacific, and Southern Oceans: Schematics and transports, *Oceanography*, *26*(1), 80–97, doi:10.5670/oceanog.2013.07.

Tamura, T., K. I. Ohshima, and S. Nihashi (2008), Mapping of sea ice production for Antarctic coastal polynyas, *Geophys. Res. Lett.*, *35*(7), L07606, doi:10.1029/2007GL032903.

Thiele, G., and J. L. Sarmiento (1990), Tracer dating and ocean ventilation, *J. Geophys. Res.*, *95*(C6), 9377–9391, doi:10.1029/JC095iC06p09377.

Toggweiler, J. R. (1999), Variation of atmospheric CO_2 by ventilation of the ocean's deepest water, *Paleoceanography*, *14*(5), 571–588, doi:10.1029/1999PA900033.

Toggweiler, J. R., J. L. Russell, and S. R. Carson (2006), Midlatitude westerlies, atmospheric CO_2, and climate change during the ice ages, *Paleoceanography*, *21*(2), PA2005, doi:10.1029/2005PA001154.

Tschumi, T., F. Joos, and P. Parekh (2008), How important are Southern Hemisphere wind changes for low glacial carbon dioxide? A model study, *Paleoceanography*, *23*(4), PA4208, doi:10.1029/2008PA001592.

Tschumi, T., F. Joos, M. Gehlen, and C. Heinze (2011), Deep ocean ventilation, carbon isotopes, marine sedimentation and the deglacial CO_2 rise, *Clim. Past*, *7*(3), 771–800, doi:10.5194/cp-7-771-2011.

Tsujino, H., H. Hasumi, and N. Suginohara (2000), Deep Pacific Circulation Controlled by Vertical Diffusivity at the Lower Thermocline Depths, *J. Phys. Oceanogr.*, *30*(11), 2853–2865, doi:10.1175/1520-0485(2001)031¡2853:DPCCBV¿2.0.CO;2.

Ullman, W. J., and R. C. Aller (1982), Diffusion coefficients in nearshore marine sediments, *Limnol. Oceanogr.*, *27*(3), 552–556, doi:10.4319/lo.1982.27.3.0552.

Volk, T., and M. I. Hoffert (1985), Ocean Carbon Pumps: Analysis of Relative Strengths and Efficiencies in Ocean-Driven Atmospheric CO_2 Changes, in *The Carbon Cycle and Atmospheric* CO_2*: Natural Variations Archean to Present*, edited by E. T. Sundquist

and W. S. Broecker, pp. 99–110, American Geophysical Union, Washington, D. C., doi:10.1029/GM032p0099.

Völker, C., and P. Köhler (2013), Responses of ocean circulation and carbon cycle to changes in the position of the Southern Hemisphere westerlies at Last Glacial Maximum, *Paleoceanography*, *28*(4), 726–739, doi:10.1002/2013PA002556.

Waelbroeck, C., L. Labeyrie, E. Michel, J. C. Duplessy, J. F. McManus, K. Lambeck, E. Balbon, and M. Labracherie (2002), Sea-level and deep water temperature changes derived from benthic foraminifera isotopic records, *Quaternary Sci. Rev.*, *21*(1–3), 295–305, doi:10.1016/S0277-3791(01)00101-9.

Watson, A. J., D. C. E. Bakker, A. J. Ridgwell, P. W. Boyd, and C. S. Law (2000), Effect of iron supply on Southern Ocean CO_2 uptake and implications for glacial atmospheric CO_2, *Nature*, *407*(6805), 730–733, doi:10.1038/35037561.

Watson, A. J., and A. C. N. Garabato (2006), The role of Southern Ocean mixing and upwelling in glacial-interglacial atmospheric CO_2 change, *Tellus B*, *58*(1), 73–87, doi:10.1111/j.1600-0889.2005.00167.x.

Watson, A. J., G. K. Vallis, and M. Nikurashin (2015), Southern Ocean buoyancy forcing of ocean ventilation and glacial atmospheric CO_2, *Glob. Biogeochem. Cycles*, *8*(11), 861–864, doi:10.1038/ngeo2538.

Wilmes, S. -B., and J. A. M. Green (2014), The evolution of tides and tidal dissipation over the past 21,000 years, *J. Geophys. Res.*, *119*(7), 4083–4100, doi:10.1002/2013JC009605.

Yamanaka, Y., and E. Tajika (1996), The role of the vertical fluxes of particulate organic matter and calcite in the oceanic carbon cycle: Studies using an ocean biogeochemical general circulation model, *Glob. Biogeochem. Cycles*, *10*(2), 361–382, doi:10.1029/96GB00634.

Yokoyama, Y., K. Lambeck, P. De Deckker, P. Johnston, and L. K. Fifield (2000), Timing of the Last Glacial Maximum from observed sea-level minima, *Nature*, *406*(6797), 713–716, doi:10.1038/35021035.

Yokoyama, Y., P. De Deckker, K. Lambeck, P. Johnston, and L. K. Fifield (2001), Sea-level at the Last Glacial Maximum: evidence from northwestern Australia to constrain ice volumes for oxygen isotope stage 2, *Palaeogeogr. Palaeoclim. Palaeoecol. 165*(3–4), 281–297, doi:10.1016/S0031-0182(00)00164-4.

Yoshikawa, C., M. Kawamiya, T. Kato, Y. Yamanaka, and T. Matsuno (2008), Geographical distribution of the feedback between future climate change and the carbon cycle, *J. Geophys. Res.*, *113*(G3), G03002, doi:10.1029/2007JG000570.